



HAL
open science

A new artificial spin system: the dipolar 4-state Potts model

Damien Louis

► **To cite this version:**

Damien Louis. A new artificial spin system: the dipolar 4-state Potts model. Quantum Physics [quant-ph]. Université de Lorraine, 2016. English. NNT : 2016LORR0154 . tel-01498449

HAL Id: tel-01498449

<https://theses.hal.science/tel-01498449>

Submitted on 30 Mar 2017

HAL is a multi-disciplinary open access archive for the deposit and dissemination of scientific research documents, whether they are published or not. The documents may come from teaching and research institutions in France or abroad, or from public or private research centers.

L'archive ouverte pluridisciplinaire **HAL**, est destinée au dépôt et à la diffusion de documents scientifiques de niveau recherche, publiés ou non, émanant des établissements d'enseignement et de recherche français ou étrangers, des laboratoires publics ou privés.



AVERTISSEMENT

Ce document est le fruit d'un long travail approuvé par le jury de soutenance et mis à disposition de l'ensemble de la communauté universitaire élargie.

Il est soumis à la propriété intellectuelle de l'auteur. Ceci implique une obligation de citation et de référencement lors de l'utilisation de ce document.

D'autre part, toute contrefaçon, plagiat, reproduction illicite encourt une poursuite pénale.

Contact : ddoc-theses-contact@univ-lorraine.fr

LIENS

Code de la Propriété Intellectuelle. articles L 122. 4

Code de la Propriété Intellectuelle. articles L 335.2- L 335.10

http://www.cfcopies.com/V2/leg/leg_droi.php

<http://www.culture.gouv.fr/culture/infos-pratiques/droits/protection.htm>

THÈSE

Pour l'obtention du titre de :

DOCTEUR de L'UNIVERSITÉ DE LORRAINE

Spécialité: Physique

Présentée par :

Damien LOUIS

A new artificial spin system: the dipolar 4-state Potts model

Thèse soutenue publiquement le 28 Octobre 2016 à Nancy devant le jury composé de :

O. FRUCHART	Directeur de recherche	SPINTEC - Grenoble	Rapporteur
J. CARREY	Maître de conférences	LPCNO – Toulouse	Rapporteur
A. THIAVILLE	Directeur de recherche	LPS – Orsay	Examineur
N. ROUGEMAILLE	Chargé de recherche	Institut Néel - Grenoble	Examineur
F. MONTAIGNE	Professeur	IJL – Nancy	Directeur de thèse
T. HAUET	Maître de Conférences	IJL – Nancy	Invité

Je souhaiterais remercier mes parents Nathalie et Daniel, sans qui ce travail n'aurait jamais pu voir le jour !!!!

Un grand merci à vous pour m'avoir soutenue durant toutes mes années d'études.

Remerciements

Déjà trois ans de passés et une belle histoire qui se termine...

Ce travail n'aurait pas été possible sans de nombreuses personnes et il me paraît nécessaire de les remercier.

Je souhaite tout d'abord remercier les membres du jury, Olivier Fruchart, Julian Carrey, André Thiaville et Nicolas Rougemaille d'avoir accepté d'évaluer ce travail.

Ce travail a été réalisé à l'institut Jean Lamour au sein de l'équipe nanomagnétisme et électroniques de spins. Je souhaite remercier mes encadrants de thèse, François Montaigne et Thomas Hauet pour m'avoir apporté leur soutien et surtout leur confiance. A certains moments les résultats ne sont pas à la hauteur des espérances mais grâce à votre enthousiasme ces difficultés se sont effacées rapidement. Je tiens également à vous remercier d'avoir toujours trouvé du temps pour répondre à mes questions et partager vos idées avec moi.

Je tiens également à remercier Michel Hehn, Daniel Lacour et Sébastien Petit-Watelot pour leurs questions et remarques pertinentes qui ont permis de faire avancer ce travail. Je remercie particulièrement Daniel qui m'a permis de comprendre au mieux le fonctionnement du MFM mais qui m'a également transmis son goût artistique associé à la science. Merci d'avoir passé du temps sur certaines figures dans le but de les rendre les plus agréables possibles !! J'ai également une pensée particulière pour Sébastien et sa femme, Amélie Boutinot, qui au fil de cette thèse sont devenus bien plus que des collègues, au point d'entrer dans la famille par l'intermédiaire du petit Ethan !! Evidemment cette thèse n'aurait pas pu se faire sans l'intégralité de l'équipe 101 que je souhaite remercier ici.

Je remercie également mes collègues thésards, Sarah Xing, Christopher Vautrin, Florent Hild, Mohammed El Hadri, Vincent Polewczyk, Marion Lavanant, Sébastien Geiskopf, Pierre Valobra, qui ont apporté une super ambiance pendant ces trois ans. Je remercie également mon co-bureau Arnaud Hillon qui a réussi à me supporter pendant ces années.

Je remercie mes amis et en particulier Gautier, Max, Amélie et Floriant avec qui j'ai passé de super moments durant mon séjour à Nancy.

Et ces remerciements ne seraient pas complets sans mentionner un soutien de poids :
MA FAMILLE !!! Merci d'avoir cru en moi et de m'avoir encouragé durant mes
longues années d'études.

Résumé

Dans les années 1920, de nombreux modèles de spin ont été décrits et en particulier deux modèles bien connus qui sont le modèle d'Ising [1] et le modèle de Potts [2]. Plus tard, des modèles de spin que l'on peut qualifier d'exotiques ont été étudiés, faisant notamment apparaître un nouveau concept : la frustration géométrique. Ce concept traduit l'incapacité pour un système de satisfaire simultanément toutes ses interactions, et amène comme conséquence une grande dégénérescence du niveau fondamental. Ces modèles ont suscité un large intérêt dans le domaine de la matière condensée, lorsque cette frustration géométrique a pu être mise en évidence dans un système magnétique : le réseau pyrochlore de $\text{Dy}_2\text{Ti}_2\text{O}_7$ [3]. Ces réseaux de spins étudiés au sein de matériaux bulk présentent des propriétés intéressantes (transitions de phases...) mais présentent certaines contraintes. Tout d'abord l'étude de ces systèmes n'est possible qu'à travers l'observation de grandeurs thermodynamiques (chaleur spécifique,...) ou à travers des techniques (diffraction de neutron, ...) qui permettent de sonder les systèmes dans l'espace réciproque. Une contrainte supplémentaire intervient sur la topographie des systèmes. Pour l'étude de réseaux de spins dans des matériaux bulk, la topologie des réseaux est imposée par la cristallographie du matériau. Dans le but de passer outre ces contraintes, des nouveaux systèmes rendus possibles grâce à l'avancée technologique dans le domaine de la nano-fabrication ont été élaborés. En effet il a été montré par Wang et al [4] qu'il est possible de réaliser des réseaux de nano-aimants présentant les mêmes propriétés que certains modèles de spin et qu'il est possible d'avoir accès dans l'espace direct à l'état de chaque spin. Suite à cette expérience, les réseaux de spins artificiels ont été massivement étudiés, essentiellement pour observer et comprendre les effets de la frustration.

Jusqu'à présent les nano-aimants réalisés présentent un comportement analogue aux spins d'Ising, où l'aimantation (dans le plan ou hors du plan) possède deux directions préférentielles. Cette particularité est l'une des principales motivations de la thèse, où l'idée est de réaliser en jouant sur l'anisotropie (de forme et magnéto-cristalline) un nouveau système où le nano-aimant ne représente plus un spin à 2 états mais un spin à 4 états. Ainsi plutôt que de modifier la topologie du système, comme d'autres groupes l'ont fait par le passé dans la communauté des réseaux de spins artificiels, c'est le spin lui-même qui est utilisé comme terrain de jeu. De cette manière le nouveau système de spins artificiels, décrit dans la thèse, n'est plus lié au modèle d'Ising mais à un modèle plus général qui est le modèle de Potts. Expérimentalement il existe quelques subtilités par rapport au modèle de Potts standard. Tout d'abord le nombre d'états possibles pour le spin est limité, et il est fixé pour notre étude à 4 états. Ensuite, dans le cas standard du modèle de Potts, les interactions entre les spins sont des interactions d'échanges, or dans nos réseaux expérimentaux les interactions entre nano-aimants sont de nature dipolaire. C'est pourquoi le modèle décrit par nos réseaux de spins artificiels n'est pas le modèle de Potts standard mais un modèle que l'on appelle le modèle de Potts dipolaire à 4 états.

Dans ce contexte, le modèle de Potts a été décrit en prenant en compte des spins avec 4 états confinés dans un plan, et en interaction via le couplage dipolaire. Premièrement le cas de deux spins d'Ising en interaction dipolaire a été décrit puis l'étude a été élargie au cas de deux spins à 4 états (appelés spins de Potts). Pour les deux modèles (Ising et Potts), les niveaux d'énergies évoluent en fonction de l'angle entre les spins et l'axe entre les deux spins (angle alpha), et souligne le caractère anisotrope du couplage dipolaire. En revanche l'étude montre que le fait d'insérer 2 états supplémentaires pour le spin, élargit le nombre de configurations possibles faisant passer le nombre de niveaux d'énergies de 2 (spins d'Ising) à 6 (spins de Potts). Suite à cette étude, le cas d'une chaîne

infinie composée de spins de Potts a été étudié. A travers l'observation des énergies dipolaires associées à différentes configurations, ces énergies révèlent que le fondamental d'un tel système présente des propriétés différentes selon l'angle entre le spin et l'axe de la chaîne (comportement similaire au cas de deux spins). Pour finir l'étude théorique sur les énergies dipolaires un réseau carré 2D de spins de Potts a été étudié, tout d'abord considéré infini puis fini (30x30 spins). Le principal objectif de cette étude est de déterminer le fondamental du réseau carré et de confirmer ou non une dépendance angulaire des propriétés associées à ce fondamental. Pour le réseau infini, la détermination de l'état fondamental s'est déroulée en plusieurs étapes. Premièrement des configurations simples: état ferromagnétique, état antiferromagnétique et état boucle, ont été observées dans le but d'entrevoir la dépendance du fondamental avec l'angle formé entre les spins et l'axe du réseau (angle alpha). Les résultats sont montrés dans la figure 1.

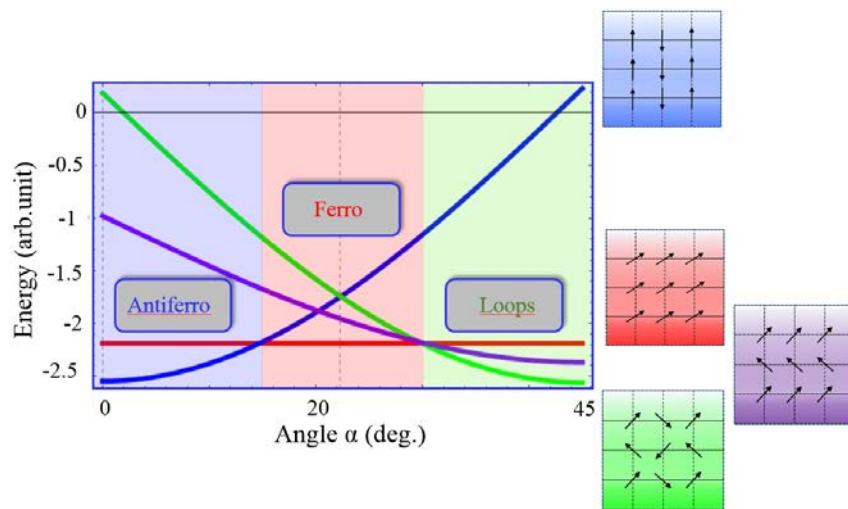


Figure 1_ Energies dipolaire correspondants à 4 configurations simples en fonction de l'angle alpha (angle entre le spin et l'axe du réseau) pour un réseau infini. Les configurations simples sont définies à partir d'une maille élémentaire composée de 2x2 spins et répétée une infinité de fois. Les courbes bleues, vertes, rouges, violettes représentent l'énergie dipolaire associée respectivement à la configuration antiferromagnétique, boucle, ferromagnétique et vague.

En considérant uniquement ces 4 configurations simples, la configuration du fondamental dépend fortement de l'angle alpha, du fait qu'il présente une configuration antiferromagnétique (direction des spins proches de la direction du réseau), une configuration boucle (direction des spins proche de 45° par rapport à l'axe du réseau) et une configuration ferromagnétique (direction du spin intermédiaire). A travers ces 4 configurations une idée générale des propriétés du fondamental est dévoilée mais ceci ne suffit pas à établir précisément la configuration de l'état fondamental. Pour aller plus loin dans l'investigation du fondamental, les 256 configurations possibles ainsi que les énergies dipolaires associées, pour un réseau infini formé à partir d'une maille élémentaire (composée de 2x2 spins de Potts), ont été déterminées. Il en résulte que les trois configurations simples représentées dans la figure 1 sont celles de plus basses énergies. Pour vérifier ce résultat, des simulations Monte Carlo ont été réalisées et celles-ci confirment que le fondamental d'un réseau infini de spins de Potts est le même que celui déterminé à travers l'observation de configurations simples présenté dans la figure 1. Cette étude démontre qu'un réseau composé de spins de Potts est un système très riche, comme une simple rotation entre les spins et l'axe du réseau donne lieu à des propriétés différentes pour le fondamental. De plus l'apparition d'un ordre ferromagnétique dans un système dirigé par les interactions dipolaires est une propriété non commune et présente une motivation supplémentaire pour la réalisation expérimentale de ce système. Avant d'entreprendre la réalisation expérimentale, il est nécessaire de s'interroger sur le

comportement de ce modèle pour un réseau fini (influence des bords). Il est évident qu'expérimentalement le réseau infini n'est pas envisageable et une taille de réseau de 30x30 spins a été sélectionnée. Ce choix a été motivé par des tests préalables qui révèlent un bon compromis entre le temps de mesure pour l'observation et la précision des mesures pour ce système. L'étude théorique de ce réseau fini révèle que les bords n'influencent pas les configurations du fondamental déterminées précédemment pour les angles 0 et 45°. En revanche pour la plage d'angle où l'état ferromagnétique était le plus bas en énergie, un état d'encore plus basse énergie apparaît composé de domaines ferromagnétiques suivant les bords du réseau (état de Landau). Toutefois il est à noter ici que la différence (en termes d'énergie) observée entre l'état ferromagnétique et l'état de Landau peut être vue comme minime par rapport aux autres niveaux d'énergies.

Motivé par les propriétés démontrées à travers l'étude théorique décrite précédemment, la possibilité de réaliser expérimentalement ce système a été étudié. Pour ce faire des simulations micro-magnétiques menées à l'aide du logiciel Mumax3 [5] ont servi de base pour déterminer les conditions requises à la réalisation expérimentale. Jusqu'à présent dans les réseaux de spins artificiels, les nano-aimants réalisés présentaient une anisotropie de forme uniaxiale imposant deux directions préférentielles pour l'aimantation et reproduisant ainsi le comportement d'un spin d'Ising [4, 6, 7]. Cette anisotropie de forme n'est pas adaptée pour notre modèle et d'autres anisotropies de formes ont dû être trouvées. De ce fait, deux formes respectant la symétrie quadratique ont été étudiées pour représenter les nano-aimants : le carré et le disque. Pour s'assurer que l'aimantation sera bien uniforme dans les nano-aimants, une anisotropie magnéto-cristalline est ajoutée par l'intermédiaire du matériau magnétique sélectionné : une couche de fer avec une anisotropie quadratique. La position relative des axes d'anisotropies magnéto-cristallines par rapport au nano-aimant présente une importance pour le cas de la forme carré. Deux configurations ont été discutées dans cette thèse, l'une où les axes d'anisotropies sont alignés avec les diagonales du carré (carré 0°) et l'autre où les axes d'anisotropies sont parallèles aux côtés du carré (carré 45°). Le premier objectif de ces simulations micro-magnétiques était de déterminer sous quelles conditions l'aimantation présente une configuration monodomaine uniforme. Pour cela la stabilisation de cette configuration a été testée en fonction des dimensions des formes (longueur pour le carré et diamètre pour le disque) et de l'épaisseur du matériau magnétique (fer). Les résultats sont présentés dans la figure 2.

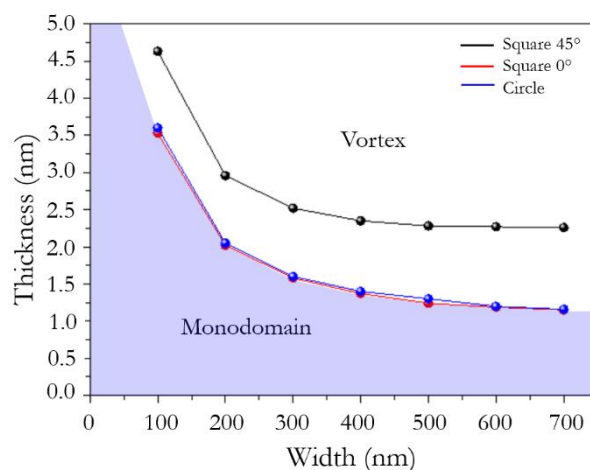


Figure 2_ Diagramme de phase en énergie pour deux configurations magnétiques (monodomaine et vortex). Il est représenté la comparaison entre les énergies associées à l'état monodomaine et à l'état vortex en fonction de l'épaisseur du fer combiné avec la taille de la forme. Les lignes (noire, rouge et bleue) représentent les régions où les deux configurations possèdent les mêmes énergies (respectivement pour le carré 45°, le carré 0° et le disque). En dessous de ces lignes l'état monodomaine est celui de plus basse énergie.

Cette étude démontre que pour favoriser la stabilisation d'un état monodomaine, il est nécessaire de travailler avec une couche de fer présentant une épaisseur inférieure à 2.5 nanomètres pour le carré 45° et inférieure à 1.5 nanomètres pour les deux autres formes. Après une étude détaillée des configurations micro-magnétiques, la forme carré avec les axes d'anisotropie alignés dans les diagonales apparait comme la plus adaptée pour notre modèle. En effet cette forme ne révèle que 4 degrés de liberté pour l'aimantation (monodomaine avec 4 directions préférentielles) contrairement aux autres formes. Finalement un dernier point a été testé via ces simulations: la validité de l'approximation dipolaire. Il s'avère que l'énergie entre deux nano-aimants présente le même comportement que celui entre deux spins et donc que l'approximation dipolaire est justifiée.

Les simulations micro-magnétiques montrent qu'un carré réalisé dans un film mince épitaxié de fer présente un comportement analogue à un spin de Potts. Suite à cette observation, il est nécessaire de déterminer quelle composition d'échantillon permet d'obtenir un film mince de fer présentant une bonne qualité cristalline donnant lieu uniquement à une anisotropie quadratique. Dans le but d'obtenir la meilleure qualité cristalline pour le film mince de fer, nous avons utilisé une méthode d'épitaxie par jet moléculaire sous ultra-vide. Basé sur des précédents travaux menés dans notre équipe [8], un matériau composé de MgO/V/Fe/V/Au a été élaboré. Une étude magnétométrique prouve que cet échantillon présente uniquement une anisotropie quadratique (voir figure 3) et nous avons également démontré que les interfaces ne fournissent aucune anisotropie magnétique de surface pour le fer [9].

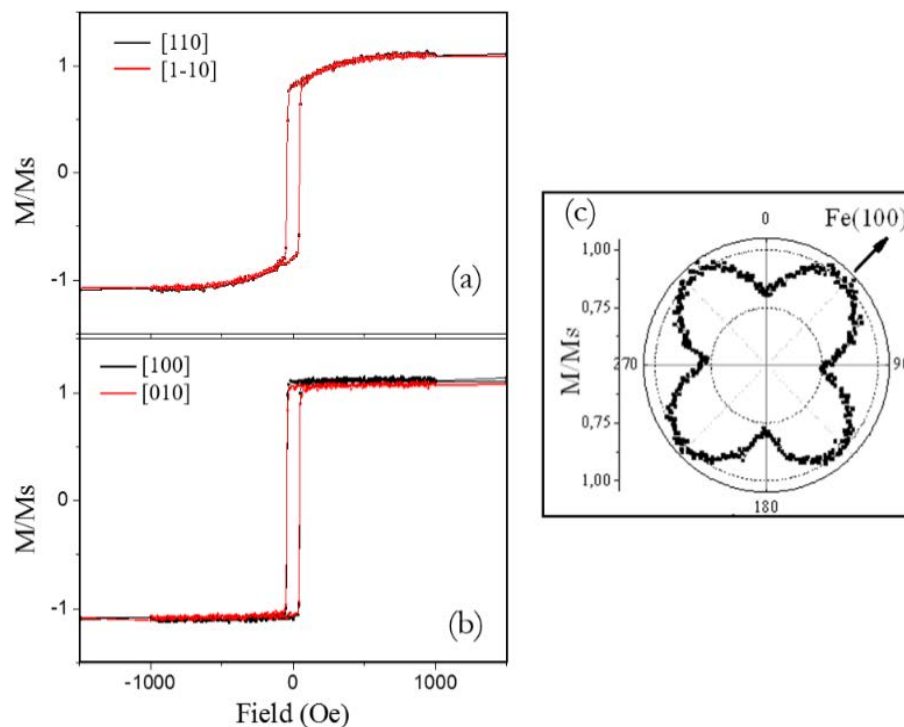


Figure 3_(a) Aimantation normalisée en fonction du champ magnétique appliqué dans le plan du film le long des directions [110] et [1-10] du fer. (b) Aimantation normalisée en fonction du champ magnétique appliqué dans le plan du film le long des directions [100] et [010] du fer. (c) Aimantation à rémanence normalisée en fonction de la direction du champ appliqué dans le plan du film de fer.

Après avoir déterminé un échantillon adéquat à la réalisation expérimentale du modèle de Potts à 4 états, les réseaux de spins artificiels ont été réalisés en utilisant la lithographie électronique. Ensuite l'observation des configurations magnétiques a été testée grâce à la microscopie à force magnétique. Les premières mesures montrent le comportement intrusif de la microscopie à force

magnétique lié au champ de fuite crée par la pointe. En effet l'utilisation d'une pointe standard ou d'une pointe bas moment perturbe les propriétés magnétiques des nano-aimants. Pour résoudre ce problème, une couche non magnétique supplémentaire a été déposée sur l'échantillon dans le but d'augmenter la distance entre la pointe (bas moment) et la couche magnétique. Premièrement, une couche de PMMA a été testée et fait apparaître un contraste de charge perturbant la détection du signal magnétique. Nous avons finalement sélectionné une couche de 20 nanomètres d'aluminium. Et nous avons démontré que cette couche permet d'observer le contraste magnétique du fer dans les nano-aimants, tout en évitant l'influence de la pointe durant les mesures.

Historiquement, les réseaux de spins artificiels ont été introduits pour réaliser expérimentalement des modèles de la physique statistique. Et l'un des principales objectifs pour ces systèmes est de déterminer le meilleur protocole pour explorer l'espace des phases, pour confronter les résultats expérimentaux avec ceux du modèle de spin. Pour cela deux protocoles majeurs sont couramment utilisés dans la communauté des réseaux artificiels. Le premier présenté par Wang et al [4] consiste à désaimanter sous champ tournant les réseaux (AC désaimantation). Le second exposé plus récemment [10] implique une désaimantation thermique, soit en recuisant l'échantillon au-dessus de sa température de Curie, soit en considérant un régime super-paramagnétique. Dans cette thèse la désaimantation sous champ tournant et la désaimantation thermique considérant un régime super-paramagnétique ont été utilisés. Le protocole consistant à chauffer au-dessus de la température de Curie a été abandonné à cause de problèmes d'interdiffusion entre les couches (V/Fe). La première étude menée sur ces désaimantations, portait sur la détermination thermique. En effet il n'est pas évident d'entrevoir s'il est possible ou non d'observer un renversement de l'aimantation dans les nano-aimants avec la température. Pour cela les réseaux ont été recuits à une température de 300°C, et il apparaît que selon la taille des nano-aimants on peut effectivement observer un renversement de l'aimantation. En effet en dessous de 500 nanomètres de côté, une température de 300°C est suffisante pour donner une énergie thermique supérieure à l'énergie de barrière intrinsèque qui sépare deux directions préférentielles pour l'aimantation. De ce fait pour l'étude portant sur les désaimantations, des carrés de 300 nm de long ont été sélectionnés. Ensuite les paramètres optimaux pour la désaimantation thermique ont été déterminés et en particulier le temps de recuit (5h), la rampe en température (montée et descente : 0.1°C/min) et la température (350°C). L'étude théorique menée sur le modèle de Potts dipolaire à 4 états montre que le fondamental de ce système est composé de trois configurations chacune correspondant à une plage d'angle particulière. De ce fait expérimentalement, trois réseaux ont été réalisés et qui sont différenciés par l'angle entre les spins et l'axe du réseau (angle α : 0°, 22.5° et 45°). Chacun de ces réseaux correspondant à une configuration particulière pour le fondamental du modèle de Potts dipolaire à 4 états. Après avoir réalisé les deux désaimantations (en champ et thermique), les configurations magnétiques ont été enregistrées suite à des mesures en microscopie à force magnétique et de ces configurations différents paramètres ont été extraits comme l'énergie dipolaire des réseaux et les corrélateurs spin-spin. De plus pour chaque angle de réseau, trois périodes ont été réalisées qui sont 500 nm, 600 nm, 700 nm. Ces trois périodes ont pour but de démontrer l'importance des interactions dipolaires lors des désaimantations. Une première conclusion importante apparaît suite aux deux désaimantations. En effet les résultats montrent une réduction de l'énergie dipolaire lorsque la période du réseau décroît, comme représenté sur la figure 4 qui montre les résultats obtenus après la désaimantation thermique.

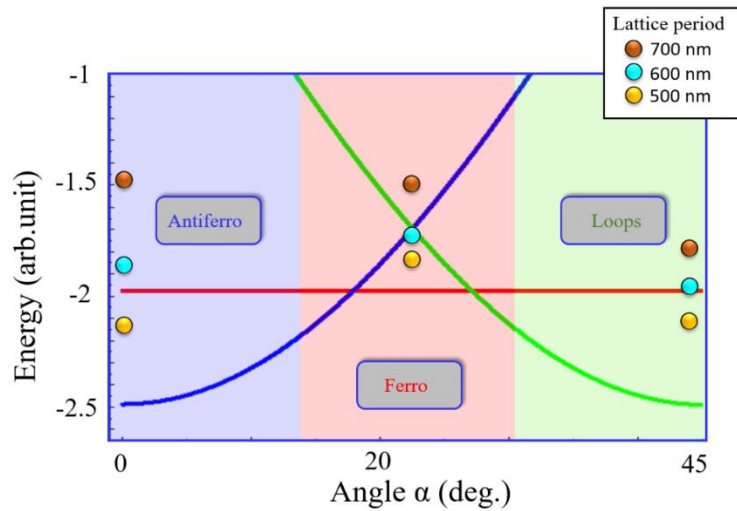


Figure 4_ Représentation des énergies dipolaires correspondantes aux configurations magnétiques expérimentales (points jaunes, points bleus et points bruns), superposées aux énergies théorique du fondamental déterminées pour le modèle de Potts dipolaire à 4 états.

La réduction des énergies dipolaires lorsque la période des réseaux décroît prouve que suite à la désaimantation (sous champ ou thermique) les interactions dipolaires conduisent le système vers un état de basse énergie. Cependant bien que les énergies dipolaires montrent l'influence du dipolaire pour les deux désaimantations, l'unique observation des configurations ne le permet pas pour la désaimantation sous champ. En effet seule la désaimantation thermique fait apparaître une nette différence entre les configurations selon la période des réseaux, ce qui tend à prouver que celle-ci est plus efficace que la désaimantation sous champ. Ce fait ce confirme en comparant les énergies dipolaires obtenues ainsi que les corrélateurs. De plus pour la période de 500 nm, les configurations obtenues après une désaimantation thermique présentent une forte signature de l'état fondamental attendu pour le modèle de Potts dipolaire à 4 états. En effet pour un angle alpha de 0° , le système expérimental présente de larges domaines anitferromagnétiques, pour 22.5° le système présente de larges domaines ferromagnétiques et pour un angle de 45° un grand nombre de boucles apparaît dans le réseau. Ces configurations sont présentées dans la figure 5.

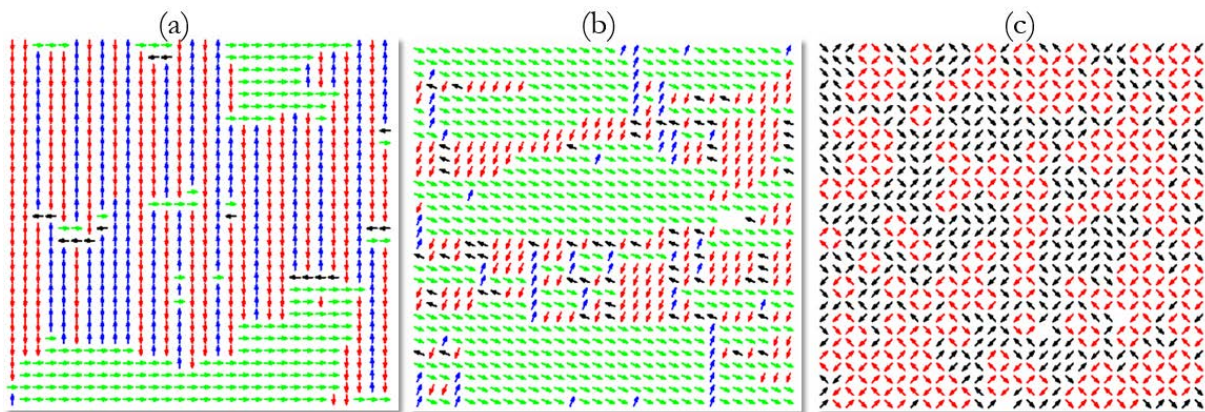


Figure 5_ Configurations magnétiques obtenues après traitement des images données par les scans MFM. (a) réseau 0° , (b) réseau 22.5° , (c) réseau 45° .

Cependant, les résultats de la désaimantation thermique font apparaître une rémanence de l'état initial, qui dans notre cas est imposé saturé dans une direction préférentielle de l'aimantation. Cette rémanence est en fait responsable en partie des faibles énergies déterminées après la désaimantation thermique. De ce fait l'origine de cette rémanence a été déterminée et après une observation

détaillée des configurations, il apparaît que cette rémanence est due à une distribution de la barrière d'énergie qui sépare deux directions préférentielles pour l'aimantation. Cette distribution donne lieu à des hard switchers thermiques qui ne se retournent pas à la même température que les autres nano-aimants, et donc restent en quelque sorte figés lors du recuit. Il s'avère donc ici que la température utilisée pour le recuit (350°C) n'est pas suffisante pour activer thermiquement tous les spins. Cependant avec notre protocole expérimental nous sommes limités à cette température et il faudrait donc trouver une alternative dans le but d'augmenter la température de recuit.

Cette thèse a permis de présenter un travail théorique et expérimental sur un nouveau système de spins artificiels: le modèle de Potts dipolaire à 4 états. L'étude théorique a démontré la richesse de ce modèle en montrant que suite à une simple rotation entre les spins et l'axe du réseau, le fondamental du système présente des propriétés drastiquement différentes (configuration ferromagnétique, configuration antiferromagnétique et configuration boucle). Après plusieurs études préalables (simulations micro-magnétiques et étude magnétométrique), le réseau expérimentale correspondant à ce modèle a pu être réalisé. Et suite à des désaimantations (en particulier thermique), il s'avère que ce système expérimental présente une forte signature du fondamental attendu pour le modèle de Potts dipolaire à 4 états. Cependant notre meilleur protocole de désaimantation ne semble pas suffisamment efficace pour activer thermiquement tous les spins du réseau. De ce fait il serait intéressant de déterminer un nouveau protocole et une idée intéressante serait d'effectuer un recuit à une température de 400°C en rotation. De cette manière si un champ magnétique se manifeste durant le recuit, la rotation permettra d'avoir un comportement du système isotrope par rapport à ce champ. Une autre façon d'améliorer la désaimantation serait d'augmenter les interactions dipolaires entre les éléments, par exemple en les rapprochant.

Bibliographie

- [1] Ising, Z.Phys. **21**, 613 (1925)
- [2] Potts, Proc. Comb. Phil. Soc. **48**, 106 (1952)
- [3] M.J.Harris et al, Phy. Rev. Lett. **79**, 2554 (1997)
- [4] R.F.Wang et al, “Artificial ‘spin ice’ in a geometrically frustrated lattice of nanoscale ferromagnetic islands,” Nature. **439**, 303–306 (2006)
- [5] A.Vansteenkiste et al, « The design and verification of Mumax3 », AIP Advances (2014)
- [6] M.Tanaka et al, J. App. Phys. **97**, 10J710 (2005)
- [7] I.A Choar et al, Phys Rev B **90**, 064411 (2014)
- [8] M.Sicot, « Des interfaces réelles métal/MgO(001) au transport dans les jonctions tunnel épitaxiées », Thèse de doctorat réalisée à l’université Henry Poincaré, Nancy, France (2006)
- [9] D.Louis et al, J.M.M.M **372**, 233-235 (2014)
- [10] S. Zhang et al, “Crystallites of magnetic charges in artificial spin ice”, Nature **500**, 553 (2013)

Table of contents

General Introduction.....	22
Geometrical frustration	22
Artificial spin ice.....	24
Motivation and Overview of the Thesis	26
1.THE DIPOLAR 4-STATE POTTS MODEL	32
1.1 The Potts model.....	32
1.2 The dipolar 4-state Potts model	34
1.3 The dipolar 4-state Potts model : Infinite 1D chain	37
1.4 The dipolar 4-state Potts model : 2D square lattice.....	42
1.4.1 Numerical issues.....	42
1.4.2 Simple and 2 spins periodic configurations.....	47
1.4.3 Monte Carlo simulations	50
1.5 Finite lattice.....	51
1.6 Summary.....	55
2.MICROMAGNETISM	58
2.1 Micromagnetism introduction: contributions of Brown free energy	59
2.2 Micromagnetism as pathway to design artificial spin	61
2.2.1 The program code.....	62
2.2.2 The stability diagram of the monodomain state	66
2.2.3 Internal magnetic configurations	68
2.3 Validity of the dipolar approximation	70
2.4 Summary and perspectives.....	72
3.EXPERIMENTAL REALIZATION OF THE DIPOLAR 4-STATE MODEL	76
3.1 Sample preparation	76
3.1.1 The buffer.....	77
3.1.2 The iron deposition.....	78
3.1.3 The capping.....	78
3.2 Magnetometric study	79
3.2.1 Fe volumic anisotropy	79
3.2.2 Thermal stability.....	81
3.2.3 Magnetization versus Fe thickness	81
3.2.4 Interfaces anisotropy	82
3.3 Samples overview	84

3.4 Lattices and alpha definition	85
3.5 Nanofabrication	86
3.5.1 Ebeam lithography	86
3.5.2 Aluminum mask	87
3.5.3 Ionic etching	87
3.5.4 Dose optimization.....	88
3.6 Magnetic characterization and tip influence.....	90
3.6.1 Standard tip.....	91
3.6.2 Low moment tip.....	92
3.6.3 Low moment tip with spacer layer at surface sample.....	94
3.6.3.1 Spacer layer of PMMA	94
3.6.3.2 Spacer layer of Aluminum	97
3.7 Lattice distortion	99
3.8 Summary	100
4.DEMAGNETIZATION OF THE 4-SATES POTTS ARTIFICIAL SPINS	104
4.1 Pathway to fundamental state: the demagnetization	104
4.1.1 AC field demagnetization.....	105
4.1.1.1 Protocol.....	105
4.1.1.2 Efficiency	106
4.1.2 Thermal demagnetization.....	108
4.1.2.1 Protocol.....	108
4.1.2.2 Thermally induced magnetization reversal as a function of square size	109
4.1.2.3 Efficiency	110
4.1.2.3.1 Heating time influence.....	111
4.1.2.3.2 Temperature influence.....	115
5.EXPERIMENTAL DEMONSTRATION OF DIPOLAR 4-STATE POTTS MODEL: COUPLED POTTS SPINS LATTICE.....	118
5.1 Coupled Potts spin lattice: qualitative study	119
5.1.1 Magnetic configurations measured after field demagnetization.....	119
5.1.2 Magnetic configurations measured after thermal demagnetization.....	121
5.1.3 Thermal demagnetization performed after field demagnetization.....	124
5.2 Discussion: spins repartition and broken symmetry	126
5.3 Dipolar coupling effects	128
5.4 Comparison between demagnetization protocols	129
5.5 Some insights in the demagnetization process	131

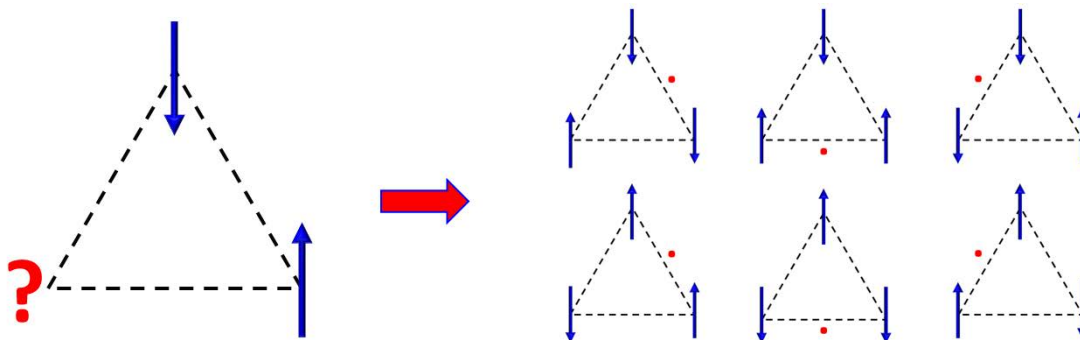
5.6 Summary of the chapters 4 and 5	136
6.CONCLUSIONS AND PERSPECTIVES	140
6.1 Conclusions	140
6.2 Perspectives	142



GENERAL INTRODUCTION

Geometrical frustration

Geometrical frustration is defined as the impossibility for a system to satisfy simultaneously all its interactions [1, 2]. In physical systems, one of the most famous example is a triangle lattice composed of Ising spins at its corners and antiferromagnetically coupled [3], as represented in the figure 1. In this system it appears that due to the antiferromagnetic coupling, it is not possible to orientate the spins in such way that the three pairwise interactions are satisfied and in the best case only two of them present antiferromagnetic configuration. This means that for this system which can take 8 configurations, 6 configurations correspond to the ground state and 2 configurations correspond to higher energy states. Through this example, it appears that geometrical frustration results from the competition between interactions and particular geometry lattice. Indeed if the triangle lattice is replaced by a square lattice, an antiferromagnetic coupling does not generate contradictory situations and so geometrical frustration does not occur. Moreover mixing triangle lattice and ferromagnetic coupling, all spins can satisfy this coupling and so once again geometrical frustration disappears.



The 6 ground states configurations

Figure 6_ Example of geometrical frustration: triangle lattice composed of Ising spins at its corners with antiferromagnetic coupling. Placing the first two spins antiparallel in order to satisfy the antiferromagnetic coupling is not a problem, but for the last spins, it is possible to satisfy only one of the two interactions. This contradiction appears as a frustration and leads to a degenerated ground state. The six ground states configurations are represented and the impossibility to satisfy all the interactions is illustrated by the red points.

An interesting property of such a frustration comes from the degenerated ground state. Indeed if for example the triangular lattice is extended in the case of larger lattice (in repeating the triangular lattice), it appears that the number of possible configurations (Ω) increases exponentially with the size lattice. It leads to a massively degenerated ground state. This degenerated ground state impacts directly the entropy of the system (S) given by the Boltzmann's relation $S=k_B \cdot \ln(\Omega)$, where k_B is the Boltzmann's constant. As the ground state is degenerated, at zero temperature, Ω takes a value much higher than 1 and this intriguing fact leads to a violation of the third principle of

thermodynamics enounced by Planck which says: “The entropy of all systems in internal equilibrium is the same at absolute zero temperature, and may be taken to be zero.” [4]. This consequence of the geometrical frustration has been firstly observed in the case of the Ising model applied for planar triangle lattices by Wannier [5], where he determined the exact value of the entropy per spin at zero temperature and demonstrated that the value is not zero but a constant which is equal to $S=0.3383R$, where R is related to the ideal gas constant. Thus in geometrical frustrated systems, the system can in theory explore all the ground state configurations and so fluctuate at low temperature. This characteristic has been a strong surge of interest in the scientific community since its discovery, not only in the case of theoretical geometrical frustrated spin models, but also experimentally in condensed matter.

Historically, the first example of geometrical frustration in condensed matter is found in the water ice whose entropy is non-null at zero temperature. This fact was revealed through the experiments made by Giauque et al. in 1933 [6] and explained by the Pauling’s description of this system in 1935 [7]. The oxygen atoms in the hexagonal phase of water ice present 4 hydrogen atoms as first neighbors, and this hexagonal phase preserves the distance between oxygen-hydrogen in the water molecule. However this distance is smaller than half the distance between oxygen-oxygen. Hence some hydrogen atoms are close to an oxygen atom and some hydrogen atoms are further away from an oxygen atom. Thus in considering the displacement vectors of 4 hydrogen atoms around an oxygen atom, we can consider a two-in/two-out configuration where the two-in vectors are related to the hydrogen atoms close to the oxygen atom and where the two-out vectors are related to the hydrogen atoms away from the oxygen atom (see figure 2 (a)). This Pauling’s description of the water ice, which given rise to the *ice rules*, explains the non-zero entropy observed at zero temperature. Indeed this particular condition on the position of 4 hydrogen atoms relative to one oxygen atom, induced a large number of possible configurations for each tetrahedral site. Similarly to the triangle lattice composed of Ising spins, this degenerated state leads to a non-zero entropy at zero temperature.

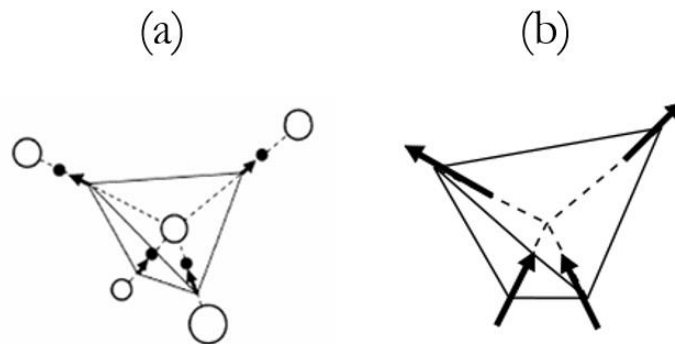


Figure 2_ (a) hexagonal phase of water ice where the hydrogen atoms are related to black points and the oxygen atoms are related to white open points. This configuration respects the two-in/two-out ice rules, as observed by the displacement vectors related to hydrogen atoms centered on an oxygen atom. (b) Spin ice example related to magnetic oxides such as the $Dy_2Ti_2O_7$ where rare earth ions match the displacement vectors of hydrogen atoms in the water ice.

This peculiar behavior of water ice can also be found in magnetic materials. Indeed if we take a tetrahedral lattice composed of spins in ferromagnetic interactions, the minimum energy of this system is obtained for a configuration where two spins point within the tetrahedron and two spins

point abroad the tetrahedron (see figure 2 (b)). Thus if we compare these spins with the displacement vectors of the hydrogen atoms in the water ice, it appears by analogy an identical behavior for these two systems which respects the two-in/two-out ice rules, hence the name spin ice system. A first equivalence between magnetic systems and water ice was identified in the pyrochlore magnetic structure of $\text{Ho}_2\text{Ti}_2\text{O}_7$, presented by Harris et al. [8]. Indeed in this material, the magnetic moments are disposed following tetrahedral meshes and these magnetic moments are ferromagnetically coupled. Thus it appears exactly the same behavior as this one describes just above, where in order to minimize the system energy, the magnetic moments in each tetrahedral meshes have to respect the two-in/two-out configuration. This analogy between water ice and pyrochlore magnetic structure of $\text{Dy}_2\text{Ti}_2\text{O}_7$ was confirmed in 1999 by Ramirez et al. [9] who made heat capacity measurements and found good agreement with water ice behavior. This first observation of the frustration in a magnetic material has attracted a large interest and has given rise to a new research field which is the pyrochlore spin ice physics where the magnetic moments present in these magnetic materials are treated as spins, hence the name “**spin ice system**”. Studies on these spin ice systems have revealed interesting results as for example (in the case of $\text{Dy}_2\text{Ti}_2\text{O}_7$) the presence of effective ferromagnetic interactions between nearest neighbors [8] induced by dipolar coupling [10] which give rise to the 2-in/2-out spins configurations. Although the pyrochlore spin ice systems present really interesting properties linked with the geometrical frustration, these magnetic properties are determined through thermodynamic quantities or via scattering techniques (in particular neutron scattering) but not by direct observations. One cannot probe the state of each spins in the direct space. Finally the spins are located on the lattices sites of the crystal structure so that the lattice is fixed and imposed by the crystallographic arrangement. Even if Nature provides a large variety of systems, being able to control the topology of the lattice and to observe in the direct space the magnetic degrees of freedom for each spins would be much simpler and efficient to study geometrical frustrations.

Artificial spin ice

Motivated by advancements in nanofabrication processes, and in particular in lithographic design, Wang et al. [11] created artificial spin systems by designing nano-islands via Ebeam lithography in magnetic thin films. It can be noticed here that, at the same time, other teams have designed independently artificial spin systems like Tanaka et al. [12]. These artificial spin systems allow to create lattices in tuning topology, size and shape, and so can be seen as a perfect playground for the frustrated systems. Moreover in playing with the size (combined with the shape) of nanomagnets and with magnetic properties of the thin magnetic layer, it is possible to design nanomagnets which can be considered classical spins and in particular Ising spins. Indeed both Ref. [11] and [12] show atomic force microscopy (AFM) and magnetic force microscopy scan (MFM) which reveal Ising spin behavior for specific size and shape of the nanomagnet. The nanomagnets present an almost uniform magnetization which can take two preferential orientations along the nanomagnet’s long axis. Uniform magnetization in ferromagnets is not obvious and domains with moments pointing in opposite directions can be stabilized due to the competition between the exchange interaction (short range interaction which tends to align the magnetic moments parallel to each other’s), and the dipolar interaction (long range interaction which can form domain walls in order to minimize the demagnetization field). Yet it appears that if the size of nanomagnet is small enough, the cost in energy for the domain walls can be higher

than that of the demagnetizing energy and thus the magnetization in nanomagnet remains uniform in its entire volume and the nanomagnet becomes a magnetic monodomain. Therefore the nanometric size of the objects secures uniform magnetization and therefore e-beam lithography is required.

“Historically”, two main lattices have been realized by e-beam lithography in order to reproduce “spin ice” lattice: the square lattice designed by Wang et al. [11] and the kagome lattice designed by Tanaka et al. [12]. Wang et al [11] contribution is considered as pioneering since they showed a protocol to explore the frustration effects and noticed the analogue behavior between artificial spin systems and the ice like physics. In the following we focus on the work of Wang et al. [11] based on a square network of permalloy nanomagnets. In figure 3 are represented both topography (AFM) and magnetic configuration (MFM) of the network. It is important to note here that MFM is a powerful technique to characterize in direct space magnetization of each elements. Nevertheless MFM can perturb the magnetic configurations of the systems due to the interaction between the leakage field of the tip and the stray field related to the magnetization of the nanomagnets. But by selecting the tip moment according to the magnetic properties of the nanomagnets it is possible to avoid this situation.

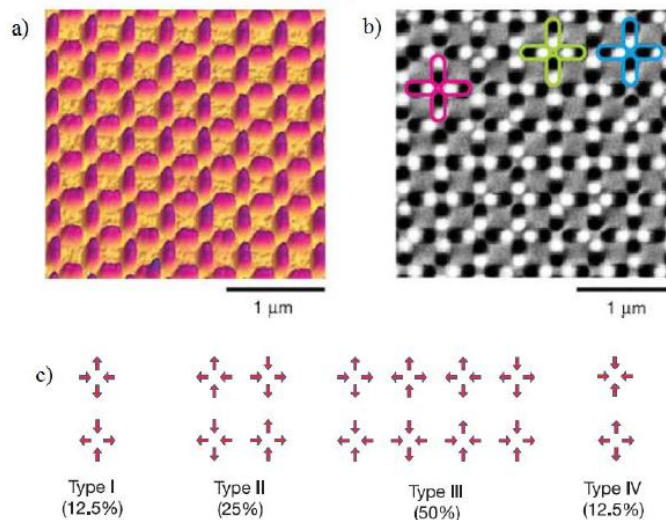


Figure 3_ (a) AFM image related to a square lattice composed of permalloy nanomagnets. The size of nanomagnets are $220\text{nm} \times 80\text{nm} \times 25\text{nm}$ ($L \times l \times b$). (b) MFM image related to the magnetic contrast of square lattice. It appears a black/white contrast for each nanomagnet, which reveals a magnetic monodomain behavior for the magnetization in these nanomagnets. (c) As these nanomagnets can behave as Ising spins, it appears 16 possible configurations for each vertex which reveal 4 degeneracy energy levels, as represented here. The Type I and Type II respect the ice rules (two-in/two-out) and appear in majority in the MFM scan (magenta and blue). This majority seems to indicate that this system presents the same behavior as the ice-like physics shown in the pyrochlore spin ices. After Wang et al [11]

As mentioned previously, the realization of these artificial spin ice systems was motivated by the possibility to probe the frustration effects. In this aim Wang et al proposed a protocol to drive its system towards the ground state: the AC field demagnetization. This demagnetization protocol is described in detail in the chapter 4, section 4.1.1. The general idea of this demagnetization is to put the sample in an oscillating external field which at the beginning is strong enough to saturate the lattice, then decreases slowly up to this field is comparable to the island switching field. Thus the nanomagnets flips are possible though being partially controlled by the interactions between

nanomagnets, and it is expected that if the demagnetization is really efficient, the system can reach its ground-state. Moreover as the magnetization in nanomagnets lays in-plane in Ref [11], the sample is rotated during this demagnetization protocol to favor in-plane isotropy.

MFM image in the figure 3 (b) shows the magnetic configuration generated by the demagnetization protocol. It appears that particular configurations are favored. Indeed for each vertex (element which is made up of 4 first neighbors spins as represented in the figure 3 (c)), the topology of the lattice combined with the spin nature (Ising spin) give naturally 16 configurations which give in fact 4 different energy levels (see figure 3 (c)). In comparing the energy levels it appears that the lowest energy states are the vertex with a configuration respecting the ice rules (two-in/two-out spins), and experimentally it is effectively the ice like configurations which seem be favored (more than 70%) after the demagnetization. Thus this particular vertex majority indicates that this system presents the same behavior as the ice-like physics shown in the pyrochlore spin ices.

Ref [11] reveals all the potential of lithography-patterns array to explore experimentally spin models, like spin ice model. Indeed in these systems it is possible to pattern practically any lattices and spins (nanomagnet with magnetic monodomain configuration) in dipolar interactions between them. Since artificial spin systems have attracted lots of curiosities, many lattices have been already designed: square lattice [11], kagome lattice [12, 13, 14, 15], lattices composed of perpendicular spins [16, 17] or more recently Shakti lattice [95].

Motivation and Overview of the Thesis

In the 1920's, lots of spin models have been described and in particular two well-known models which are the Ising model [18] and the Potts model [19]. Thereafter, "exotic" spin models have been studied as the triangle lattice composed of Ising spins antiferromagnetically coupled [3]. Thus a new concept appeared which is the geometrical frustration, characterized by a massively degenerated ground state. This concept of frustration has been a strong surge of interest, in particular (for the condensed matter field) when this frustration has been identified in magnetic systems as the pyrochlore magnetic structure of $\text{Ho}_2\text{Ti}_2\text{O}_7$ [8]. But as explained previously, these spin lattices in bulk materials present some restrictions related to the lattice topology or related to the observation techniques. In order to overpass these restrictions, new systems have been introduced (in particular by Wang et al. [11]) where it appears that thanks to nanofabrication processes, it is possible to design artificial spin systems which can be related to particular spin models as the spin ice model. Thus these artificial spin systems have been massively studied, essentially to observe and to understand the frustration effects in these systems. Up to now in all the artificial spin systems found in the literature, it emerges that all the spins designed are Ising spins where the magnetization (in-plane or out-of-plane) in nanomagnets have two preferential orientations. This particularity is one of the main motivation of this thesis, where the idea is to make use of the anisotropy (shape and crystalline) in order to design a new system where the spin is not a 2-states spin but a 4-state spin. Thus instead of playing on the topology of the lattices, like other groups did in the past in the artificial spin systems community, it is the spin himself which is used as a playground. Thus this artificial spin system is no longer linked to Ising model but to a particular case of Potts model which is the 4-state Potts model. Moreover as the coupling present in these artificial spin lattices is given by the dipolar interactions between nanomagnets, this model can be called the Dipolar 4-state Potts model. The thesis is structured into five chapters. The first

two chapters will be focused on the theoretical concepts and the essential prerequisites for the experimental realization of the dipolar 4-state Potts model. Then the remaining three chapters will be focused on the experimental results, in presenting the realization of this model then the results obtained from two main demagnetization protocols, the AC field demagnetization and the thermal demagnetization.

The first chapter focuses on the theoretical concepts related to the Potts model. First the “classical” Potts model [19] properties are exposed and a comparison with the Ising model is presented. The experimental realization proposed in this thesis, through an artificial spin system, is clearly pioneering for this spin model. Nevertheless comparison with classical Potts model is limited as, in our artificial spin systems, the number of states for the spin is fixed at a particular value which is 4 states and interaction between elements is generated by dipolar interactions. Moreover artificial spin lattices are 2D lattices and so the Potts model related to these lattices is in fact the planar Potts model. In the chapter 1, we theoretically study the behavior of two spins in dipolar interaction in the case of two Ising spins then in the case of two 4-state spins (called Potts spins). Then this study is extended for the case of an infinite 1D chain composed of Potts spins and finally extended for the case of a 2D lattice (infinite and finite) composed of Potts spins. Through these studies it is demonstrated that the 2D lattice composed of Potts spins is a very versatile system as the simple rotation between spins and the lattice axis gives rise to very different properties for the ground state.

The second chapter focuses on the prerequisites for the experimental realization. As it does not exist in the literature a realization of artificial spin system where spins are different from Ising spins, it is essential to determine the right conditions to design a 4-state spin. Up to now Ising spin have been induced using an uniaxial anisotropy shape in designing an elongated shape [11, 12, 16]. Micromagnetic simulations made with Mumax3 reveal that a shape respecting the quadratic symmetry turns out to be a good candidate to form 4-state spin. Moreover in order to enhance the nanomagnet 4-fold anisotropy, a cubic anisotropy is added through the selected material. Several shapes are studied as a function of the magnetic material thickness and low thickness square shape nanomagnet with cubic anisotropy in diagonals is found to be the best candidate. In the last part of the second chapter, we discuss the validity of the dipolar approximation, where the spins are considered as magnetic dipoles only in dipolar interactions, to represent real systems composed of nanomagnets where others energies are present, like the exchange energy.

The third chapter focuses on the experimental realization of the artificial spin system. The choice of the selected magnetic material as support for the patterning of nanomagnets is explained. A complete magnetometric study of this material is presented [20]. Then the nanofabrication process is detailed and a particular attention is given for the choice of parameters concerning the Ebeam lithography. Finally, the measurement technique used for the magnetic configurations observations and the procedure to extract information from experimental data are described. Perturbation of the magnetic configurations by the leakage field from the MFM tip [21] are especially highlighted and solutions to avoid this problem are demonstrated.

The last two chapters focus on the experimental results. As mentioned previously in the introduction, two ways lead the system towards its ground state: AC field demagnetization [11] and thermal demagnetization. For the latest demagnetization process two protocols are possible. The first protocol introduced by Zhang et al. [15] is to anneal the sample above its Curie temperature and then cooled the system. This protocol is not considered in this thesis to avoid any multilayer

sample alteration with high temperature. The second protocol is based on the tuning between magnetic material and nanomagnet anisotropy in order to obtain an adequate Néel relaxation time [22, 23, 24]. The fourth chapter reports the results obtained from two demagnetization protocols (AC field demagnetization and thermal demagnetization) in the case of decoupled Potts spins lattices. Then in the fifth chapter, the results obtained from two demagnetization protocols are presented in the case of coupled Potts spins lattices. The two demagnetizations are compared and it is demonstrated that the magnetic states obtained are different depending on the demagnetization protocol. The experimental results are compared with our theoretical calculations presented in the first chapter. The two demagnetization processes lead the system towards a low energy state which is not so far from this one expected for the dipolar 4-state Potts model, but thermal demagnetization appears to be more efficient than the AC field demagnetization.

At last, although a conclusion is given at each chapter, a general conclusion is reminded at the end of this manuscript, where it is also provided the perspectives for future works resulting of this thesis.

Bibliography

- [1] C.Lacroix, P.Mendels and F.Mila, Introduction to Frustrated Magnetism-Materials, Experiments, Theory. No. v, Springer Berlin Heidelberg (2011)
- [2] B.Canals, « Modèles de spins topologiquement frustrés : une introduction », mémoire d'habilitation à diriger les recherches, Université Joseph Fourier, Grenoble (2010)
- [3] E.Ising, "Beitrag zur Theorie des Ferromagnetismus", Z. Phys. **31**, 253-258 (1925)
- [4] S.Blundell and K.M.Blundell, Concepts in Thermal Physics. OUP Oxford (2010)
- [5] G.H.Wannier, "Antiferromagnetism. The triangular Ising net", Phys. Rev. **79**, 357-364 (1950)
- [6] W.F.Giauque and M.F.Ashley, "Molecular rotation in ice at 10°K. Free energy of formation and entropy water", Phys. Rev. **43**, 81 (1933)
- [7] L.Pauling, "The Structure and Entropy of Ice and of Other Crystals with Some Randomness of Atomic Arrangement", J. Am. Chem. Soc. **57**, 2680 (1935)
- [8] M.J.Harris et al, "Geometrical Frustration in the Ferromagnetic Pyrochlore Ho₂Ti₂O₇", Phys. Rev. Lett. **79**, 2554 (1997)
- [9] A.P.Ramirez et al, « Zero-point entropy in spin ice », Nature. **399**, 333 (1999)
- [10] B.C den Hertog and M.J.P.Gingras, "Dipolar Interactions and Origin of Spin Ice in Ising. Pyrochlore Magnets", Phys. Rev. Lett. **84**, 3430-3433 (2000)
- [11] R.F.Wang et al, "Artificial 'spin ice' in a geometrically frustrated lattice of nanoscale ferromagnetic islands," Nature. **439**, 303–306 (2006)
- [12] M.Tanaka et al, "Domain structures and magnetic ice-order in NiFe nano-network with honeycomb structure", J. Appl. Phys. **97**, 10J710 (2005)
- [13] F.Montaigne et al, "Size distribution of magnetic charge domains in thermally activated but out-of-equilibrium artificial spin ice", Scientific reports. **4**, 5702 (2014)
- [14] N.Rougemaille et al, "Artificial Kagome Arrays of Nanomagnets: A Frozen Dipolar Spin Ice", Phys. Rev. L. **106**, 057209 (2011)
- [15] S. Zhang et al, "Crystallites of magnetic charges in artificial spin ice", Nature. **500**, 553 (2013)
- [16] I.A Choar et al, « Nonuniversality of artificial frustrated spin systems », Phys. Rev. B. **90**, 064411 (2014)
- [17] S.Zhang et al, "Perpendicular Magnetization and Generic Realization of the Ising Model in Artificial Spin Ice", Phys. Rev. Lett. **109**, 087201 (2012)
- [18] E.Ising, "Beitrag zur Theorie des Ferromagnetismus", Z. Phys. **31**, 253-258 (1925)
- [19] Potts, "Some generalized order-disorder transformations", Proc. Camb. Phil. Soc. **48**, 106 (1952)

-
- [20] D.Louis et al, «Interfaces anisotropy in single crystal V/Fe/V trilayer », *J.M.M.M.* **372**, 233-235 (2014)
- [21] A.Thiaville et al, “Measurement of the stray field emanating from magnetic force microscope tips by Hall effect microsensors”, *J. Appl. Phys.* **82**, 3182 (1997)
- [22] L.Néel, “Théorie du trainage magnétique des ferromagnétiques aux grains fin avec applications aux terres cuites”, *Ann. Géophys.* **5**, 99–109 (1949)
- [23] V.Kapaklis et al, “Melting artificial spin ice”, *New J. Phys.* **14**, 035009 (2012)
- [24] A.Farhan et al, “Direct Observation of Thermal Relaxation in Artificial Spin Ice”, *Phys. Rev. Lett.* **111**, 057204 (2013)
- [95] I.Gilbert et al, “Emergent ice rule and magnetic charge screening from vertex frustration in artificial spin ice”, *Nature Physics.* **10**, 670-675 (2014)



1. THE DIPOLAR 4-STATE POTTS MODEL

1.1 The Potts model

Historically the Potts model [19] has been introduced as a generalization of the Ising model [18] to more than two values for the spin. Domb inspired by the works of Askin and Teller [25], proposed a model describing a system with q components for the spin, then Potts continued this work during his Phd [26] up to present the current Potts model. Up to now, this model has attracted large interest because it relates to many remarkable problems in lattice statistics and because it has been proved to be more general and richer than Ising model. Thus it appears in the literature a large number of publication on the subject (see Review F.Y.Wu [27]). As our work is a specific extension of Potts model, we just present below a general introduction to Potts model, in order to give only the fundamental principles of this model and to show some experimental applications.

Originally, Domb proposed a system close to the Ising spin model, taking into account interacting spins which can be parallel or antiparallel but where the spins are confined in plane and can explore specific angles given by the equation (1-1):

$$\theta_n = \frac{2\pi n}{q}, n = 0, 1, \dots, q-1 \quad (1-1)$$

Considering the nearest neighbors interactions, the most general form depends only on the angle between spins and thus the Hamiltonian of the system is given by the equation (1-2):

$$\mathcal{H} = - \sum_{\langle i, j \rangle} J(\theta_i - \theta_j) \quad (1-2)$$

Where $J(\theta)$ is a 2π periodic even function.

Thus Potts (under the supervision of Domb) used this equation (1-2) for the Hamiltonian and he defined the function $J(\theta)$ in the following way:

$$J(\theta) = -J_1 \cos \theta \quad (1-3)$$

And so the critical point (where it occurs a transition between an ordered system and a disordered system) of this model on square lattice has been determined by Potts for $q=2$ (Ising model) and for $q= 3, 4$, but he mentioned that with the equation (1-3), this model for $q>4$ has no analytical solutions for the critical points [19] and so he introduced a simpler function to replace the equation (1-3) which is: (1-4)

$$J(\theta_{ij}) = J_2 \delta_{Kr}(\theta_i, \theta_j)$$

With

J_2 : interaction energy between adjacent spins

$\delta_{Kr}(\theta_i, \theta_j)$: Kroenecher delta function which gives 1 if spins are in the same state and 0 if not.

Potts has introduced two definitions for the Hamiltonian which appear through the equations (1-3) and (1-4). In reality these two equations correspond to two different models which are called the planar Potts (or vector Potts, or clock) model for the equation (1-3) and the “standard” Potts (or Ashkin-Teller-Potts) model for the equation (1-4). These two models are identical for $q = 2$ (Ising model) and $q = 3$ (by taking respectively $J_2=2J_1$ and $J_2=3J_1/2$) but differ for larger q . In the $q = \infty$ limit, the planar Potts model becomes the XY model.

In order to describe the behavior of Potts model as a function of temperature, in statistical Physics, Potts model probability function and Potts model partition function are fundamentals and the study of these functions have stimulated a large number of works [28]. As mentioned previously, Potts model for $q=2, 3, 4$ has been resolved and its critical point (for this 3 values of q) is now well-known in the field of statistical physics. However, for $q>4$ the resolution of this model appears more complex and thus it has attracted a great interest, and especially for mathematicians which have explored properties of this model (standard Potts model) through the Potts model partition function. That is why this function has been studied in a variety of ways as:

- the evaluation of the Tutte polynomial [29]
- the approximation of this partition function using a simulation technique such as Metropolis Algorithm [30]

This calculation (in particular simulation techniques) is not exact but it is an effective way for researchers to use the Potts model in order to investigate tricky applications, as for example the foams behavior as shown in the experiment described by Sanyal et al [31]. Thus in term of applications this Potts model turns out to be useful even for the “simplest case” where $q=2$ (identical to Ising model), and in particular for magnetism. Indeed this model has in particular allowed to determine the critical temperature (called Curie temperature) at which a magnet loses its magnetism [32].

Experimental realization of the Potts model (and spin systems in general) can be made based on the principle of universality “from which one is led to seek for real systems belonging to the same universality class, having the same set of critical exponents, as the spin model in question” (extract from Review F.Y.Wu [27]). Thus in our case, one of the possible systems which can be described by the Potts model is a system governed by Landau-Ginzburg-Wilson (LGW) Hamiltonian. And an example of this case is the transition occurring in monolayers in crystal surfaces, where Domany et al [33] have shown that adsorbed systems can be described by LGW Hamiltonians of the adatoms count as a lattice gas. Thus historically the experimental realization of the Potts model has been based on this principle of universality.

More recently, with the growing interest of the frustrated systems, more experimental realizations of spin models have been explored, and in particular in an emergent sphere which is the artificial spins systems. Indeed thanks to Wang et al [11], it has been shown that it is possible to realize 2 dimensions artificial spin systems thanks to Ebeam lithography in order to study problems of lattice statistics. These artificial spins systems are used to study a particular model which is the Ice model. However up to know, these experimental systems correspond to one particular case of the Potts model which is the planar 2-states Potts model, where the lattices can take several different topologies but where the spins are always Ising spins ($q=2$). My PhD work has been especially motivated by the fact that only Ising spins have been experimentally studied so far. Here a new artificial spins system where spins can take not only two but four states is realized which allows us

to study the 4-state planar Potts model. However we must notice that our new artificial spins system is particular since it relies on dipolar coupled spins whereas most statistical physics models treat exchange like interactions.

1.2 The dipolar 4-state Potts model

The general Potts model presented in the above section describes exchange coupled spins where the interaction strength is characterized by exchange energy (J) between two adjacent spins. But in the artificial spins systems, by nature, it is the dipolar interactions which coupled the spins between each other. In the so-called dipolar Potts model, the system is composed of magnetic moments \vec{m}_i , which can be regarded as spins, and which are coupled by dipolar coupling, and where the system energy is given by the following Hamiltonian:

$$\mathcal{H} = -\frac{\mu_0}{4\pi} \frac{3(\vec{m}_i \cdot \vec{u}_{ij})(\vec{m}_j \cdot \vec{u}_{ij}) - \vec{m}_i \cdot \vec{m}_j}{a^3}, \quad (1-5)$$

Where \vec{u}_{ij} represents the unit vector between i and j magnetic moments, and a is the distance between them. Through the scalar products which appear in the equation (1-5), it appears a fundamental characteristic of the dipolar interaction which is an anisotropic behavior. Indeed due to the scalar products, it is expected different energy values according to the direction between the magnetic moments (spins). The dipolar Potts model does thus not obey equation 1-2.

As mentioned in the introduction, up to now in the artificial spins systems, the spins are always Ising spins with two states (2 equivalent directions). So it is interesting to observe firstly the dipolar energy behavior for two Ising spins and then to extend this study in the case of two Potts spins with four states (4 equivalent directions) that we can call 4-state Potts spins. Indeed this study of two spins will allow to show the interest (and also the complexity) of a system where the spins are no longer Ising spins but 4-state Potts spins.

Thus in the case of two Ising spins, the equation (1-5) gives the following relation:

$$\mathcal{H} = \pm \frac{\mu_0 \cdot m^2}{4\pi \cdot a^3} (3\cos^2\alpha - 1), \quad (1-6)$$

Where α represents the angle between spin and axis between two spins, as represented in the figure 1-1, and where “ a ” is the distance between two spins.

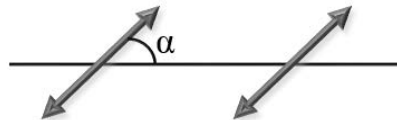


Figure 1-1_ Alpha definition in the case of two Ising spins: angle between spin and the direction between two spins

It is possible to reduce the dipolar energy writing by normalizing this equation by the coefficient $\frac{\mu_0 \cdot m^2}{4\pi \cdot a^3}$. Indeed for this part and for all the calculations presented in this work, it is considered that the distance between two first neighbor spins is the same (called a) and that the moment m is the same for all spins. Now it is possible to represent the dipolar energy given by the equation (1-6) as a function of the alpha angle.

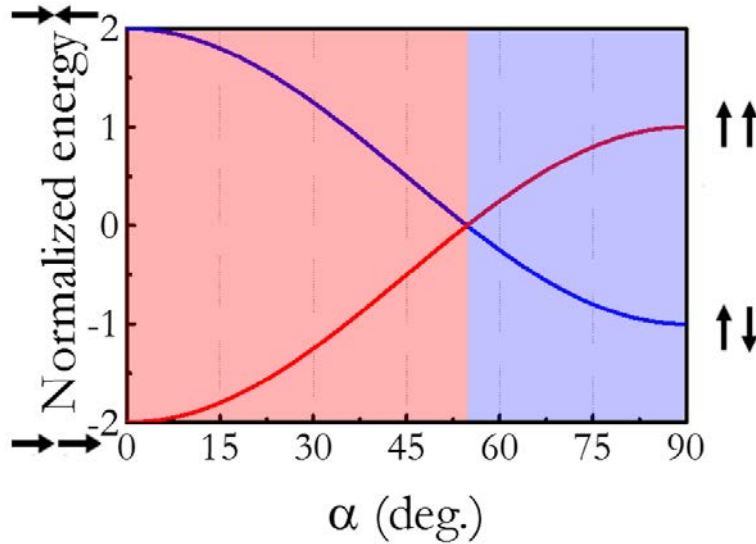


Figure 1-2_ Dipolar energy calculated for two Ising spins as function of the angle alpha. Red line corresponds to ferromagnetic configuration and blue line corresponds to antiferromagnetic configuration. The configurations for two spins related to each curve in the case of alpha equal to 0° and 90° are represented.

The figure 1-2 shows, as expected, a different behavior according to the angle range observed. For angle range from 0° to 54.7° , the system present a ferromagnetic coupling (red area) and so spins tend to form parallel configuration. For the angle range from 54.7° to 90° , the system presents an antiferromagnetic coupling, and so the spins tend to form antiparallel configuration. Moreover for an angle equal to 54.7° , it appears a singularity where the ferromagnetic and antiferromagnetic configurations are equivalent, which leads to an absence of coupling between spins. Thus in the simple case of two Ising spins in interactions via dipolar coupling, it appears two possible configurations according to the angle range which are parallel or antiparallel configurations.

Now it is interesting to extend this study in the case of two Potts 4-state spins in order to determine the difference brings by these 4 states on the dipolar energy. In this case spins can take 4 directions, orthogonal to each other, and a simple example of their configurations is represented in the figure 1-3.

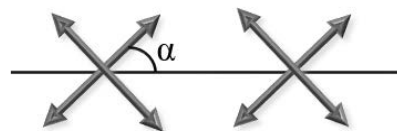


Figure 1-3_ Representation of the 4 states possible for a Potts spin and alpha definition in the case of two Potts spins

Thus in the case of two spins, 16 configurations are possible and the energies corresponding to these configurations are showed in the following equation:

$$\mathcal{H} = \begin{bmatrix} -3\cos^2\alpha + 1 & -3\sin\alpha\cos\alpha & 3\cos^2\alpha - 1 & 3\sin\alpha\cos\alpha \\ -3\sin\alpha\cos\alpha & -3\sin^2\alpha + 1 & 3\sin\alpha\cos\alpha & 3\sin^2\alpha - 1 \\ 3\cos^2\alpha - 1 & 3\sin\alpha\cos\alpha & -3\cos^2\alpha + 1 & -3\sin\alpha\cos\alpha \\ 3\sin\alpha\cos\alpha & 3\sin^2\alpha - 1 & -3\sin\alpha\cos\alpha & -3\sin^2\alpha + 1 \end{bmatrix} \quad (1-7)$$

This energy matrix sheds light on 6 different energy values which depend, as for the case of two Ising spins, on alpha angle. Thus at this step, it already appears that the fact to allow 4 states for the spin instead of 2 states brings more complicated system in term of coupling. Now it is interesting to represent these 6 energy levels as a function of the alpha angle in order to observe the coupling present in the system according to the angle range observed.

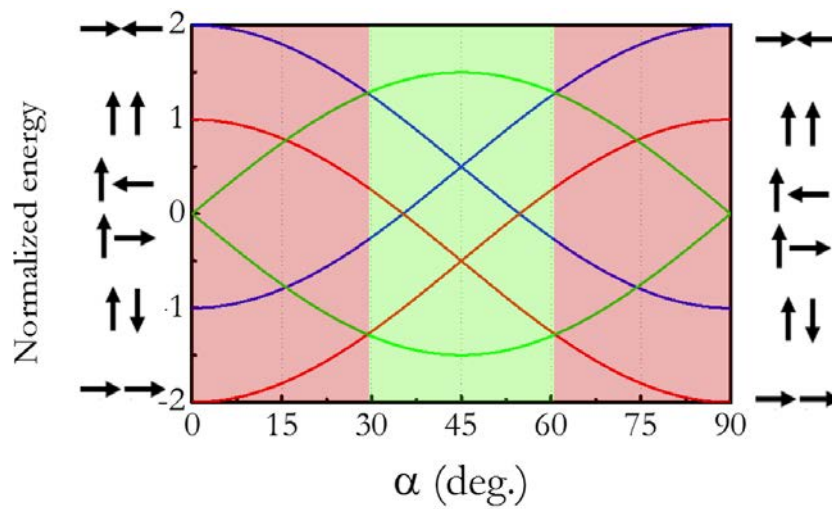


Figure 1-4_ Dipolar energies for two Potts 4-state spins as function of the angle alpha. Red lines correspond to ferromagnetic configurations, blue lines correspond to antiferromagnetic configurations and green line correspond to perpendicular configurations. The configurations for two spins related to each curve in the case of alpha equal to 0° and 90° are represented.

The figure 1-4 shows the 6 energy levels as function of the angle between spin and the axis between two spins. The red, blue and green curves correspond respectively to the energies related to ferromagnetic, antiferromagnetic and perpendicular configurations. Thus a first point to notice here is the apparition of supplementary coupling due to the possible configurations between spins, which is the perpendicular coupling. Moreover it appears that this perpendicular state, related to the perpendicular coupling, is the lowest in energy for an angle range from 29.3° to 60.7°, while for an angle range from 0° to 29.3° and from 60.7° to 90°, the system presents a ferromagnetic coupling between spins.

To conclude, the dipolar 4-state Potts model presents several specificities:

- Due to nature of the dipolar coupling, the coupling is anisotropic and depends on the direction between spins. This differs drastically from clock model or standard Potts model
- A two spin system has 6 different energy level (compared to 2 for Ising model)
- The coupling between two spins can be either ferromagnetic or perpendicular

Now it is interesting to consider the case of an infinite 1D chain composed of Potts 4-state spins.

1.3 The dipolar 4-state Potts model : Infinite 1D chain

Now that the dipolar energy behavior in the case of two spins has been determined, it is possible to extend this study in the case of an infinite 1D chain of Potts 4-state spins. Obviously an infinite 1D chain leads to an infinite of configurations. In order to do a simple analytic analysis, we will essentially restrict ourselves to configurations with a period of two spins. And so the configurations selected in this part are those directly given by the 6 configurations determined in the case of two spins. Indeed to form the infinite 1D chain, it is selected a “unit mesh” composed of two spins and this unit mesh is repeated an infinite number of times. An example of this process is exposed in the figure 1-5, which represents the 1D chain with a unit mesh composed of two perpendicular spins. Considering 6 possible configurations between two Potts 4-state spins, it will also be the case for the infinite 1D chain. Note that this study does not give the fundamental state of the chain but it provides an indication of its behavior according to the alpha angle (angle between spins and chain axis) for the 6 energy levels corresponding to configurations with a period of 2.

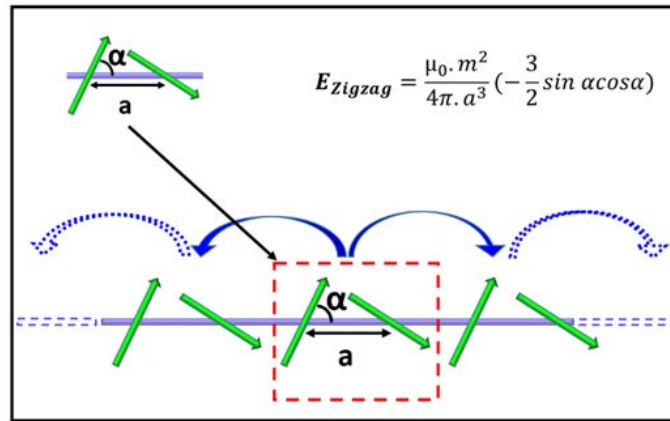


Figure 1-5_ 1D chain composed from two perpendicular spins repeated indefinitely

Thus the aim of this study is to determine the dipolar energy per spin (total energy of the chain divided by the number of spins) as function of the alpha angle and this for the 6 imposed configurations. In the following, only the calculation of the dipolar energy corresponding to the configuration represented in the figure 1-5 is detailed and results are directly given for the other configurations.

The first step to determine the dipolar energy is to identify the different coupling between two spins in function the distance between spins. This identification of the coupling according to the distance between spins is possible due to the periodicity of the chain. Thus these coupling are determined in the configuration represented in the figure 1-5 and are represented in the figure 1-6.

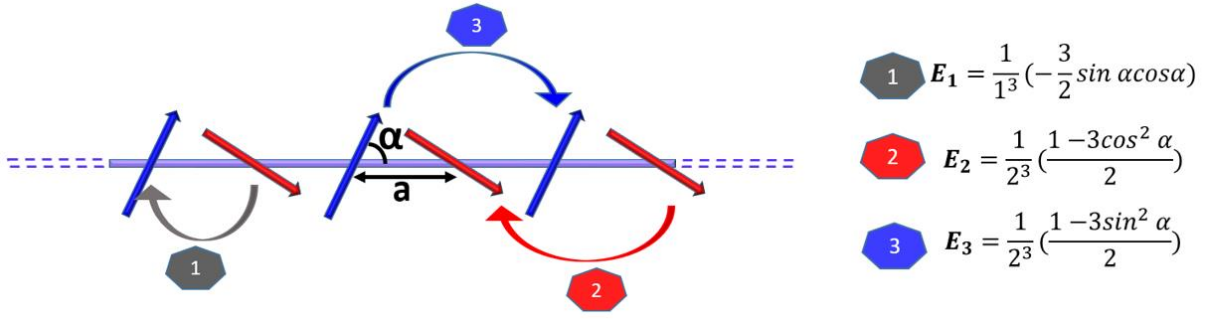


Figure 1-6_ Coupling identification between two spins according to the distance between them for the case of perpendicular chain. Pairs of blue spins or red spins represent spins in interactions via ferromagnetic coupling but with different dipolar energies. Pairs of spins composed of one blue and one red spin represent spins in interactions via perpendicular coupling. The energies given here correspond to the energies related to the possible pairs of spins.

In order to determine the total energy of this chain, it is necessary to take into account all the pairs of spins in this chain. Thus the principle is to calculate the dipolar energy for all these pairs then to sum these energies. Obviously the dipolar energy determined for pairs of spins depends on the alpha angle but also on distance between spins.

This relation for the distance between spins explains the factors present in the energies of the figure 1-6. Indeed the dipolar energy depend on the distance between spins via the following relation: $\frac{1}{a^3}$. Here a is normalized to 1 and this is why in the energies presented in the figure 1-6, it appears the factors $\frac{1}{1^3}$ for E_1 , $\frac{1}{2^3}$ for E_2 and $\frac{1}{2^3}$ for E_3 . In fact, in the figure 1-6, it is represented the dipolar energies according to the configuration given by the pair of spins, and for this particular chain it exists only three possible configurations for pairs of spins which can be related to the distance between spins. If we observe spins with an odd distance between them (1, 3, 5, ...), the relative alignment between them is perpendicular. Now for the case of spins with an even distance between them (2, 4, 6, ...), they are parallel. However it is interesting to notice here, that for this particular configuration, it exists two energy levels related to the ferromagnetic coupling and this is why it appears two energies for the same distance between spins depending on the pair of spins observed (E_2 for red or E_3 for blue).

It is now possible to calculate the total energy of the spin chain by independently calculating the three coupling energies and then summing them. Let's start by calculating the energy related to the spins with uneven distances. As the chain is infinite, each spin has the same interaction with its right neighbor and with its left neighbor, hence a factor 2 against the energy \mathcal{H}_1 presented in the figure 1-6.

$$\mathcal{H}_1 = -3 \sin(\alpha) \cos(\alpha) \left[\frac{1}{1^3} + \frac{1}{3^3} + \frac{1}{5^3} + \dots \right] = -3 \sin(\alpha) \cos(\alpha) \sum_0^{\infty} \frac{1}{(2n+1)^3} \quad (1-8)$$

Then we calculate the energy related to pairs of red spins. As for the previous case, due to the infinite chain a factor 2 against the energy \mathcal{H}_2 is present in the following energy. Moreover in this case and for the case of pairs of blue spins, it is important to notice that for this chain only the half of spins are concerned, hence another factor which appears and which is $\frac{1}{2}$.

Thus the dipolar energy related to pairs of red spins is given by the following equation:

$$\mathcal{H}_2 = \frac{1}{2}(1 - 3\cos^2\alpha) \left[\frac{1}{2^3} + \frac{1}{4^3} + \frac{1}{6^3} + \dots \right] = \frac{1}{2}(1 - 3\cos^2\alpha) \sum_1^{\infty} \frac{1}{(2n)^3} \quad (1-9)$$

And finally we calculate the energy related to pairs of blue spins:

$$\mathcal{H}_3 = \frac{1}{2}(1 - 3\sin^2\alpha) \left[\frac{1}{2^3} + \frac{1}{4^3} + \frac{1}{6^3} + \dots \right] = \frac{1}{2}(1 - 3\sin^2\alpha) \sum_1^{\infty} \frac{1}{(2n)^3} \quad (1-10)$$

Now in order to determine the total energy of the chain per spin, the energies given by (1-8), (1-9), (1-10) are summed, hence the following relation for the total energy:

$$\mathcal{H} = -\frac{1}{2} \sum_1^{\infty} \frac{1}{(2n)^3} - 3 \sin(\alpha) \cos(\alpha) \sum_0^{\infty} \frac{1}{(2n+1)^3} \quad (1-11)$$

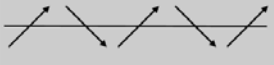
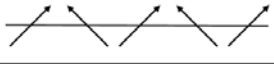
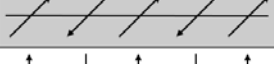
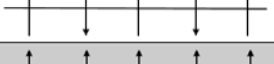

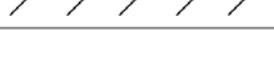
These two sums converge and can be expressed conveniently with the Riemann zeta function as:

$$\sum_0^{\infty} \frac{1}{(2n+1)^3} = \frac{7\zeta(3)}{8} \quad (1-12) \quad \text{and} \quad \sum_1^{\infty} \frac{1}{(2n)^3} = \frac{\zeta(3)}{8} \quad (1-13) \quad \text{with} \quad \zeta(3) \approx 1.202$$

Thus the total energy corresponding to this chain is given by the following equation (1-14):

$$\mathcal{H} = -\frac{\zeta(3)}{16} (42 \sin(\alpha) \cos(\alpha) + 1) \quad (1-14)$$

By the same way, it is possible to determine the dipolar energies corresponding to the 6 configurations studied in this part, and it turns out that these 6 energies converge. These energies are represented in the following table:

Infinite chain configuration	Energy
	$E = [(-3 \sin(\alpha) \cos(\alpha)) \frac{7\zeta(3)}{8} - \frac{1}{2} \frac{\zeta(3)}{8}]$
	$E = [(3 \sin(\alpha) \cos(\alpha)) \frac{7\zeta(3)}{8} - \frac{1}{2} \frac{\zeta(3)}{8}]$
	$E = (1 - 3\cos^2\alpha) \frac{-3\zeta(3)}{4}$
	$E = (1 - 3\sin^2\alpha) \frac{-3\zeta(3)}{4}$
	$E = (1 - 3\sin^2\alpha)\zeta(3)$
	$E = (1 - 3\cos^2\alpha)\zeta(3)$

Now it is interesting to run the same study as this one done in the case of two spins, which means to represent these 6 energies as function of the alpha angle, as showed in the figure 1-7.

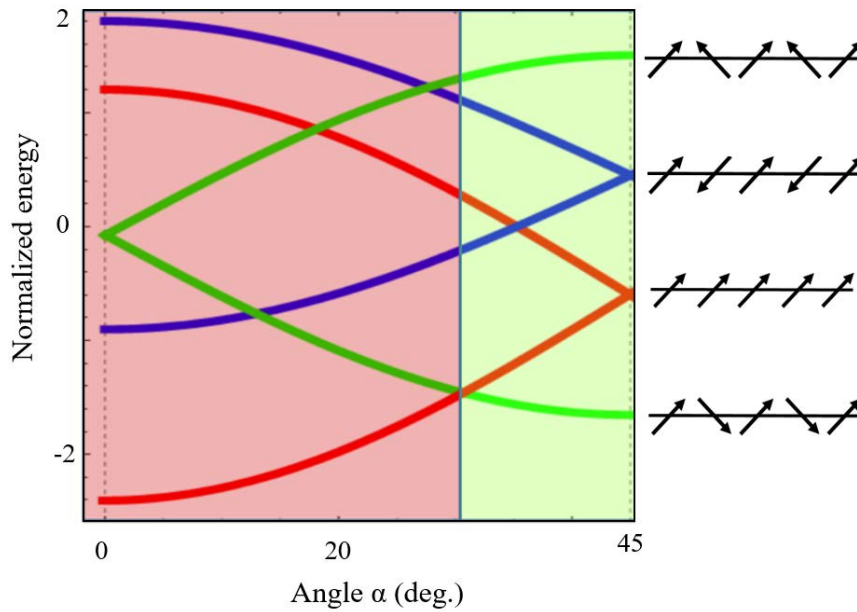


Figure 1-7_ Dipolar energies corresponding to 6 configurations (based on 6 possible configurations for two spins) as function of the alpha angle. Red curves correspond to parallel configurations (ferromagnetic configuration in the unit mesh), blue curves correspond to antiparallel configurations (antiferromagnetic configuration in the unit mesh) and green curves correspond to perpendicular configurations (perpendicular configuration in the unit mesh). The configuration related to each curve in the case of alpha equal to 45° is represented.

In the figure 1-7, the green, red and blue curves correspond respectively to unit meshes where the configuration between the two spins is perpendicular, ferromagnetic and antiferromagnetic. Thus it appears that the results for the infinite 1D chain are really similar to those observed for the case of two spins, as the order of the energy levels remains the same. Indeed between these 6 configurations, the ferromagnetic configuration for the spins composing the unit mesh is the lowest in energy for an angle range from 0° to 30.7°. And for an angle range from 30.7° to 45°, it is the perpendicular configuration for the spins composing the unit mesh which is the lowest in energy. Thus it appears a similar behavior between the energy levels related to two spins and the energy levels related to the infinite 1D chain composed of infinite repetitions of two spins (unit mesh).

But the simple configurations, with a period of two spins, envisaged here are not necessarily the lowest energy one. We thus have tested numerically all the possible configurations having a periodicity of 2, 3, 4, 5, 6, 8 and 10 spins. The figure 1-8 (a) represents (in black) the smallest energy among the configuration related to the different periodicities layered on the smallest energies represented in the figure 1-7. In a small angular range (from 29.3 to 33.2), the smallest energy is neither the ferromagnetic nor the perpendicular configuration. Some of these lower energy configurations are represented in figure 1-8 (b).

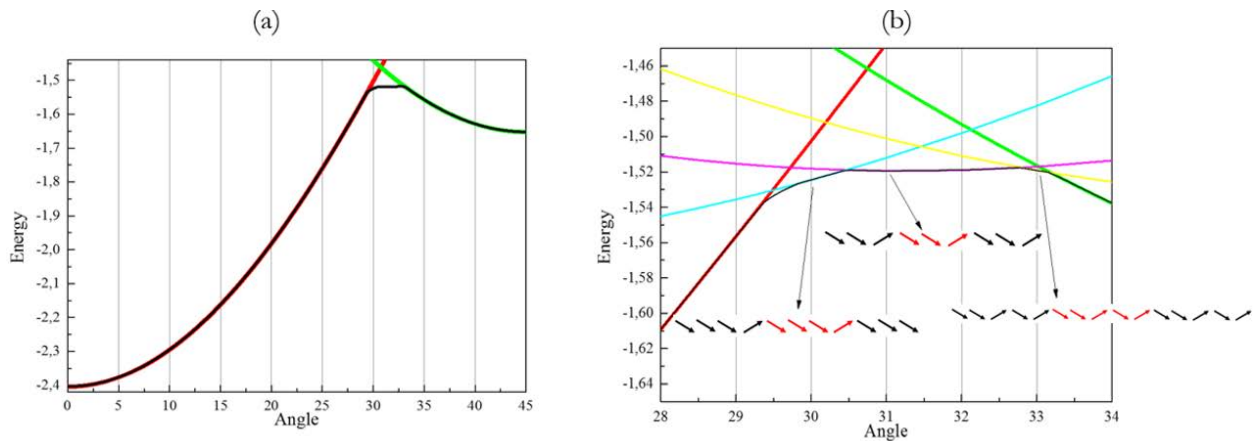
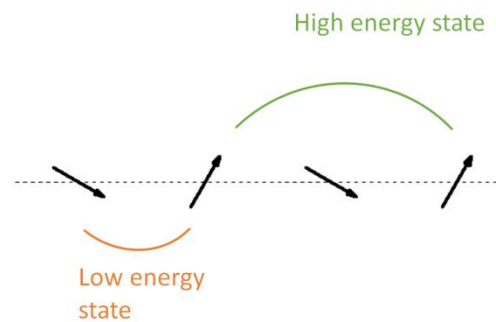


Figure 1-8_ (a) Dipolar energy related to the infinite 1D chain as function of the alpha angle: the black curve corresponds to the smallest energy among the configuration related to different periodicities (2, 3, 4, 5, 6, 8, 10). The red curve and green curve are the smallest energies determined for a 1D chain with a periodicity of two spins (see figure 1-7). (b) Some of lower energy configurations for an infinite 1D chain with different periodicities (2, 3, 4, 5, 6, 8, 10).

These identified configurations are not necessarily the ground state as the ground state might have a periodicity longer than 10 (or no periodicity!). Nevertheless, it is possible to explain qualitatively this zone of "complex" ground state. If we consider only the coupling between the closest neighbors, a transition from the ferromagnetic to the perpendicular state should occur at an angle of 29.3 (just as for two spins). However, taking into account the coupling between the next neighbors (see sketch), it appears two type of ferromagnetic coupling and one of them has a high energy. It is only above 33.2 degrees that the gain provided by the perpendicular configuration between first neighbors compensates this higher energy and that the ground state is the perpendicular state. In the intermediate angular range, a frustration arises between 1st and 2nd neighbor coupling and results in more complex patterns.



Through the dipolar energy between two spins and the dipolar energy for a particular infinite 1D chain, the behavior of these systems reveals a strong correlation between the properties shown and the angle between spin and the axis between spins. Now it is interesting to observe 2D lattices composed of 4-state Potts spins and to try to characterize its ground state thanks to the dipolar energy behavior.

1.4 The dipolar 4-state Potts model : 2D square lattice

As represented in figure 1-8, the (infinite) square lattice of 4-state Potts model is defined by a lattice constant, a , which is just a scaling factor and the alpha angle between spins and lattice which is very important as, as we have seen before, it drastically changes the interactions between spins.

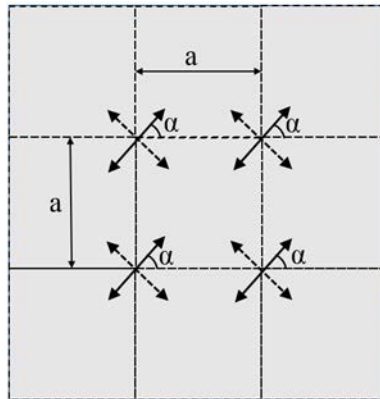


Figure 1-9_ Convention used for the lattice parameters, where the angle between the spin and the lattice direction is called alpha, and the period, which is the distance between two spins, is called a.

Calculating the energy of such a lattice requires summing an infinite number of configurations and issues related to the convergence of the sum can occur in the case of a long range interaction. This numerical aspect will be preliminary checked with two simple configurations before studying the nature of the ground state as a function of alpha.

1.4.1 Numerical issues

For evaluating the convergence issues, we will focus on two different configurations: the ferromagnetic and antiferromagnetic states.

The ferromagnetic and antiferromagnetic configurations, are represented in the figure 1-10.

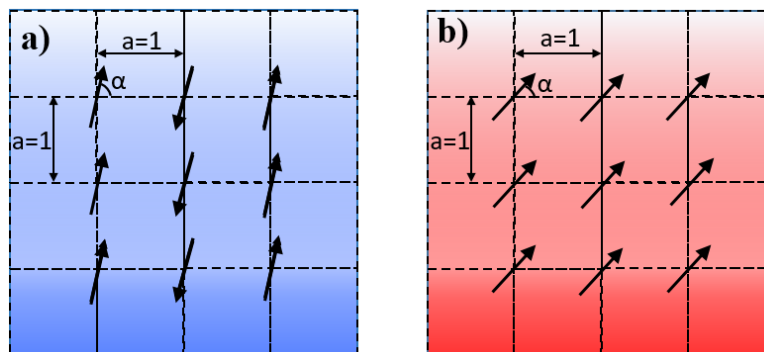


Figure 1-10_ (a) Representation of an antiferromagnetic state ; (b) Representation of a ferromagnetic state

The method of calculation to determine the dipolar energies related to the ferromagnetic and antiferromagnetic state is similar to the one used for the 1D chain. Indeed the first step is to select a spin and to determine all the possible couplings with others spins, and so all the possible configurations for pairs of spins formed with the selected spins. In order to detail the calculation we take the ferromagnetic state as example.

First an orthogonal base is defined where the base vectors represent the distances between two first neighbor spins (distance which is normalized to 1) and whose origin is a particular spin that we call (\mathbf{m}_{00}). Thus in the particular case of the ferromagnetic state all the spins are given, in Cartesian coordinates, by this equation:

$$\overrightarrow{m}_{ij} = \begin{pmatrix} \cos \alpha \\ \sin \alpha \end{pmatrix} \cdot m \quad (1-15)$$

Where i and j represent the coordinates respectively along x and y axes and $i, j \neq 0,0$, and m the magnetization related to spins which is common for all spins.

Now the dipolar energy between \mathbf{m}_{00} and the others spins is calculated from the following equation:

$$\mathcal{H}_{m_{00} \leftrightarrow m_{ij}} = -\frac{\mu_0}{4\pi \cdot a^3} \frac{3 \left(\overrightarrow{m}_{00} \cdot \overrightarrow{u}_{m_{00} \rightarrow m_{ij}} \right) \left(\overrightarrow{m}_{ij} \cdot \overrightarrow{u}_{m_{00} \rightarrow m_{ij}} \right) - \overrightarrow{m}_{00} \cdot \overrightarrow{m}_{ij}}{r_{m_{00} \rightarrow m_{ij}}^3} \cdot \frac{1}{2} \quad (1-16)$$

$$\text{with } \overrightarrow{u}_{m_{00} \rightarrow m_{ij}} = \begin{pmatrix} i \\ j \end{pmatrix} \frac{1}{\sqrt{i^2 + j^2}} \quad (1-17) \quad \text{and} \quad r_{m_{00} \rightarrow m_{ij}}^3 = \frac{1}{\sqrt{i^2 + j^2}^3} \quad (1-18)$$

Thus it is possible to separate the terms appearing in the equation (1-16) and we obtain:

$$\overrightarrow{m}_{00} \cdot \overrightarrow{u}_{m_{00} \rightarrow m_{ij}} = \overrightarrow{m}_{ij} \cdot \overrightarrow{u}_{m_{00} \rightarrow m_{ij}} = \frac{i \cos \alpha + j \sin \alpha}{\sqrt{i^2 + j^2}} \cdot m \quad (1-19)$$

$$\overrightarrow{m}_{00} \cdot \overrightarrow{m}_{ij} = 1 \cdot m^2 \quad (1-20)$$

hence

$$\mathcal{H}_{m_{00} \rightarrow m_{ij}} = -\frac{\mu_0 m^2}{4\pi \cdot a^3} \sum_{i=-M}^M \sum_{j=-M}^M \frac{3}{i^2 + j^2} \frac{(i \cos \alpha + j \sin \alpha)^2 - 1}{\sqrt{i^2 + j^2}^3} \cdot \frac{1}{2} \quad (1-21)$$

Where, in the case of infinite lattice, M tends towards infinity.

And after the same normalization as used for the previous parts, the dipolar energy related to infinite lattice with ferromagnetic state is given by the equation (1-22):

$$\mathcal{H}_{Ferro} = -\frac{1}{2} \sum_{i=-M}^M \sum_{j=-M}^M \frac{3(i \cos \alpha + j \sin \alpha)^2}{\sqrt{i^2 + j^2}^5} - \frac{1}{\sqrt{i^2 + j^2}^3} \quad (1-22)$$

It emerges that the equation (1-22) is independent of the alpha angle and we can observe this fact in modifying this equation by the following way:

Since i and j take all the possible values (infinite lattice), it is possible to replace i by j and j by $-i$:

$$\mathcal{H}_{Ferro} = -\frac{1}{2} \sum_{i=-M}^M \sum_{j=-M}^M \frac{3(j \cos \alpha - i \sin \alpha)^2}{\sqrt{i^2 + j^2}^5} - \frac{1}{\sqrt{i^2 + j^2}^3} \quad (1-23)$$

Thus the sum of the equation (1-22) and (1-23) divided by 2 give the following equation:

$$\begin{aligned} \mathcal{H} = & -\frac{1}{4} \sum_{i=-M}^M \sum_{j=-M}^M 3 \frac{(i \cos \alpha + j \sin \alpha)^2 + (j \cos \alpha - i \sin \alpha)^2}{\sqrt{i^2 + j^2}^5} \\ & + \frac{1}{2} \sum_{i=-M}^M \sum_{j=-M}^M \frac{1}{\sqrt{i^2 + j^2}^3} \end{aligned} \quad (1-24)$$

Then developing the equation (1-24), it is obtained the equation (1-25):

$$(i \cos \alpha + j \sin \alpha)^2 + (j \cos \alpha - i \sin \alpha)^2 = i^2 + j^2 \quad (1-25)$$

And so the final expression for the dipolar energy related to the infinite lattice with ferromagnetic state is given by the equation (1-26):

$$\mathcal{H}_{Ferro} = -\frac{1}{4} \sum_{i=-M}^M \sum_{j=-M}^M \frac{1}{\sqrt{i^2 + j^2}^3} \quad (1-26)$$

Equation (1-26) shows that the dipolar energy for the ferromagnetic state for 2D lattice is independent of the alpha angle.

After a similar calculation, the dipolar energy related to antiferromagnetic state for an infinite lattice is given by the equation (1-27):

$$\mathcal{H}_{Antiferro} = -\frac{1}{2} \sum_{i=-M}^M \sum_{j=-M}^M (-1)^i \cdot \frac{3}{i^2 + j^2} \frac{(i \cos \alpha + j \sin \alpha)^2 - 1}{\sqrt{i^2 + j^2}^3} \quad (1-27)$$

Contrary to the dipolar energy determined for ferromagnetic state, the equation (1-27) can't be simplified in order to remove the angular dependence. And so we can observe two dipolar energy behaviors really different according to the concerned configuration.

The sums involved in equations (1-26) and (1-27) must be convergent. Roughly speaking, with the increasing distance r from the origin, the number of spin varies as r with an interaction decreasing as $1/r^3$ so in the worst case (ferromagnetic configuration) the energy should converge as $1/r$ (this is drastically different from the 3D case with a number of spin varying as r^2 which leads to no convergence). However, to compute numerically the sum, it is necessary to introduce a cut-off (in the framework of this PhD, we have not studied more efficient method like Ewald summation). In

the following, we will address the effect of this cut-off values, in order to determine a reasonable compromise between speed and precision.

In order to simplify the discussion, the results for only one alpha angle is presented here which is 0° , but this study has been realized for one other angle (45°) and present the same results. We have also compared the evaluation of energy in an infinite lattice (with a cut-off) with the “exact calculation” of energy in a finite lattice. The advantage of this calculation is the accuracy of the energy determined, but obviously the disadvantage is the limitation of the lattice size (in our case 450×450 spins). In comparing these two ways to determine the energies, it is expected that for a large number of spins the results are similar, but a difference should appear for small number of spins (we recall here that we are interested here in the energy per spin and not the total energy of the lattice).

The two methods are compared (for our two reference configurations) in figure 1-11. In this figure the energy is plotted as a function of the finite lattice length, L . To be comparable, the cut-off value is expressed also in term of lattice length with the relation $L = 2M + 1$.

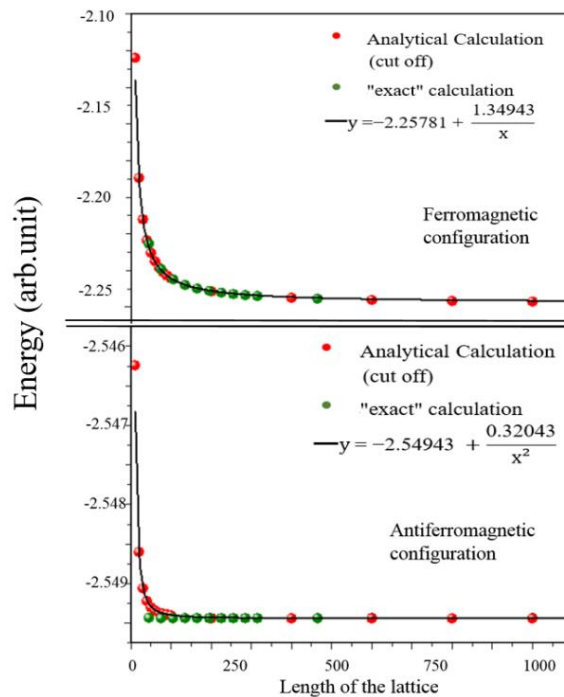


Figure 1-11_ Energies of ferromagnetic and antiferromagnetic state as function of lattice length. Green points: “exact” calculation and red points: analytical calculation.

Firstly it is interesting to compare the two calculation ways in order to observe the edges influence on the energies. Indeed for the case where the length size is defined by the cut off (energies for infinite lattice) we consider that all spins have the same energies, but in the “exact” calculation we consider the energies of each spin and this one can be different due to the lattice edges. Thus the figure 1-11 shows that in the case of ferromagnetic state, the infinite lattice approach gives similar results as those observed for the “exact” calculation. This fact can be explained by the common configurations of all spins. Indeed as the spins are all in the same direction, the coupling between spins are identical. However in the case of antiferromagnetic states, the figure 1-11 shows that for small lattices (from 30×30 spins to 150×150 spins), a difference between the energies given by the two calculation ways occurs. And from size lattice of 150×150 spins the results between these two

calculation ways are similar. This difference present for the small lattices can be understand due to the edges lattices. Indeed for antiferromagnetic state, two coupling between spins are present (ferro and antiferro) and the presence of edges can favor one of these coupling, and so bring a difference in energy according to the spins observed. However even if it is possible to notice a difference between the energies, it remains that this difference is really weak and does not change drastically the energy behavior as function of the lattice length.

Now we can study the main purpose of this section which is the dipolar energy convergence for ferromagnetic and antiferromagnetic state as function of the lattice length. In this aim the curves presented in the figure 1-11 are fitted, and we can observe a difference in the convergence according to the selected configuration. Indeed it appears thanks to the fits that the dipolar energy related to ferromagnetic state (given by the equation (1-26)) converges as $\frac{1}{L}$ whereas the dipolar energy related to antiferromagnetic state (given by the equation (1-27)) converges as $\frac{1}{L^2}$. The faster convergence of the antiferromagnetic is simply explained by alternating signs in the term of the sum or equivalently by the global zero magnetization of this configuration. The fits also give a very good estimation of the converged values which are:

-dipolar energy for an infinite lattice with ferromagnetic state: -2.258

-dipolar energy for an infinite lattice with antiferromagnetic state: -2.549

In order to compare directly the convergence of the energies for the two configurations, we normalize these energies against the respective values determined for the infinite lattice. And so the energies represented in the figure 1-11 are divided by the energy values for infinite lattices and then represented in the same graphic, as showed in the figure 1-12.

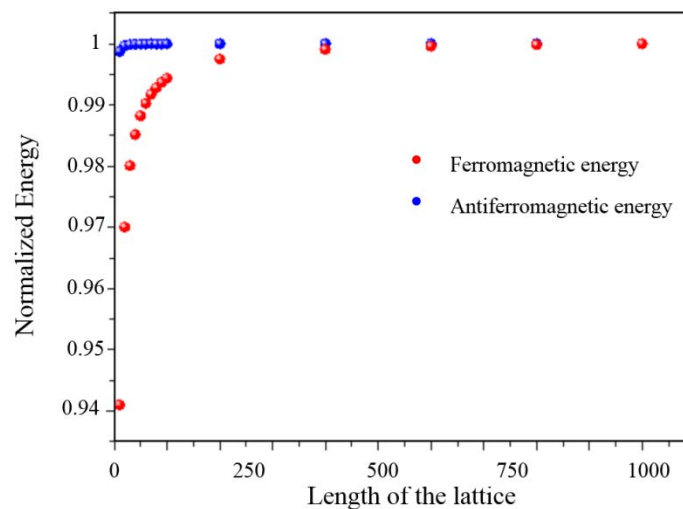


Figure 1-12_ Normalized energies as function of the lattice length for ferromagnetic and antiferromagnetic states.

After the normalization, the figure 1-12 shows clearly the difference in the convergence of the dipolar energies according to the selected configurations. Moreover with this figure it appears that for these equations, a cut off equal to 250 (which corresponds to 500x500 spins lattice) seems an adequate agreement between time calculation and “quality” calculation. Indeed for this value the two energies are really close to those determined for infinite lattices (error less than 0.01%) and the time calculation remains reasonable.

Moreover these energies are also calculated for finite lattices by calculating the energies of each spin composing the lattices and the comparison between the two calculation ways allows to confirm the exactitude of our calculations. Indeed the “exact” calculation for the finite lattices is determined thanks to python program, but it is difficult to verify the validity of this program for big lattices. And thanks to the equations determined for these simple configurations, this python program is validated, and thus it will be possible to determine easily the dipolar energies related to various configurations for finite lattices.

Thanks to this study carried out two simple configurations, the calculation methodology and the requirement to represent the dipolar energy according to the alpha angle are established. But it exists others interesting configurations which can be explored by the same method as this one showed for the ferromagnetic and antiferromagnetic state. Indeed as the lattice is infinite, it is complicated to determine the ground state of this one but it is possible to observe simple configurations which could be not so far away from this ground state. And so it is interesting to study these simple configurations in order to have an indication of the ground state behavior according to the alpha angle.

1.4.2 Simple and 2 spins periodic configurations

The main purpose of this section is to determine the behavior of the ground state for an infinite lattice according to the alpha angle. As it is not possible to determine directly this ground state, a way is to observe firstly the behavior of simple configurations. Towards this goal, a possibility to realize these simple configurations is to define (as for the infinite chain) a unit mesh composed by 2x2 spins and then to repeat this one an infinite number of times. Obviously “manually” it is not possible, for a reasonable time, to calculate all the energies related to the 256 possible configurations for the unit mesh. Thus 4 simple configurations are selected and these configurations are chosen due to the type of coupling present in the unit mesh. Indeed thanks to the two spins study it appears that according to the alpha angle, some configurations that we know (see section 1.2) are lowest in energy. And so in observing the possible configurations for 2x2 spins, 4 configurations seem to be advantageous in term of energy, and these 4 configurations are represented in the figure 1-13.

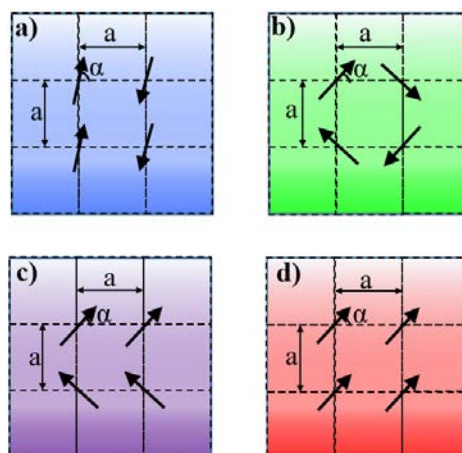


Figure 1-13_ Unit meshes with the lowest energies for a lattice composed by 4 Potts 4-state spins. (a) antiferromagnetic state ; (b) loop state ; (c) wave state ; (d) ferromagnetic state.

Thus as expected the two configurations presented previously (ferro and antiferro) are part of the possible unit meshes. In using the same calculation as for the ferromagnetic and antiferromagnetic state, it is possible to determine the energies of these 4 infinite lattices. Then we suppose that the behavior of these 4 energies according to the cut off is similar to this one determined for the ferromagnetic and antiferromagnetic states, and so that taking a cut off equal to 250 we can consider that the energies are really close to their value for the infinite lattice. And so the energies as function of the alpha angle are represented in the figure 1-14.

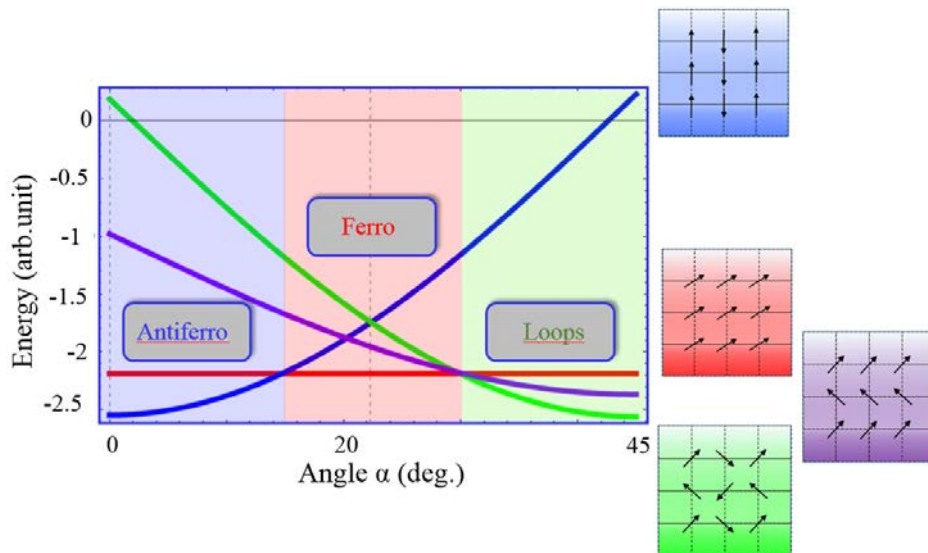


Figure 1-14_Dipolar energies related to 4 simple configurations as function of the alpha angle (cut off equal to 250 which means equivalent to 500x500 spins lattice). Simple configurations are defined from unit meshes which are ferromagnetic state (red), antiferromagnetic state (blue), loop state (green) and wave state (purple).

Thus the figure 1-14 shows, through the energies of 4 simple configurations, that the ground state of infinite lattice should reveal different properties according to the alpha angle. Indeed in observing the figure 1-14, it appears that the dipolar 4-state square lattice is complex system as a simple rotation between spin and lattices directions give rise to very different properties. Thus with these 4 configurations we can observe that for spin directions close to the lattice direction, the ferromagnetic coupling between two adjacent spins tends to form lines of parallel spins and so to form a lowest energy state which is an antiferromagnetic state (blue curves). For spin directions close to 45 degrees from the lattices directions, the perpendicular coupling between two adjacent spins tends to form a “loop crystal” assuring a local flux closure. And for intermediate spin directions with the lattices directions, it is the ferromagnetic state which is the lowest energy state. An interesting point to notice here, is that the loop crystal phase can be consider as a generalization of the square ice proposed by Wang et al. [11], following a 2 in-2 out ice rule, but with a number of different configurations which is much higher. Moreover it seems that for a specific angle range (typically from 15° to 30°), with only dipolar interactions, the ferromagnetic state is the lowest in energy (for these 4 configurations). This observation is really interesting because “classically” in magnetism the dipolar interactions tend to form configurations which assure a flux closure, yet with this dipolar Potts model, it seems that ferromagnetic state can be one of the lowest energy states.

Thus the observation of the infinite square lattice composed of Potts 4-state spins reveals (through 4 simple configurations) a really interesting behavior with just a rotation between spin and lattices directions. In this section, only 4 simple configurations are studied because the analytical calculation becomes really complex for more complicated configurations, but with just these 4 simple configurations, it is difficult to conclude on the ground state of infinite lattice, apart from the fact that this ground state should present an angular dependence. Thus a way to observe if it exists configurations which are lowest in energy as these 4 simple configurations, is to determine the energies related to all the possible configurations for lattices composed from a 2x2 spins unit mesh.

In order to calculate the 256 energies, an alternative to the analytical calculation has to be found. And the way selected here is the use of the python program mentioned previously with some modifications. Indeed to realize the lattices, a unit mesh composed of 2x2 spins is defined and repeated a sufficient number of times to consider that the energies are these related to the infinite lattices. In this aim it is used the same calculation way as previously (“exact” calculation) with a cut off which corresponds to a 500x500 spins lattice. Thus the 256 possible configurations are generated by the program and the related energies are calculated. These energies as function of the alpha angle are represented in the figure 1-15.

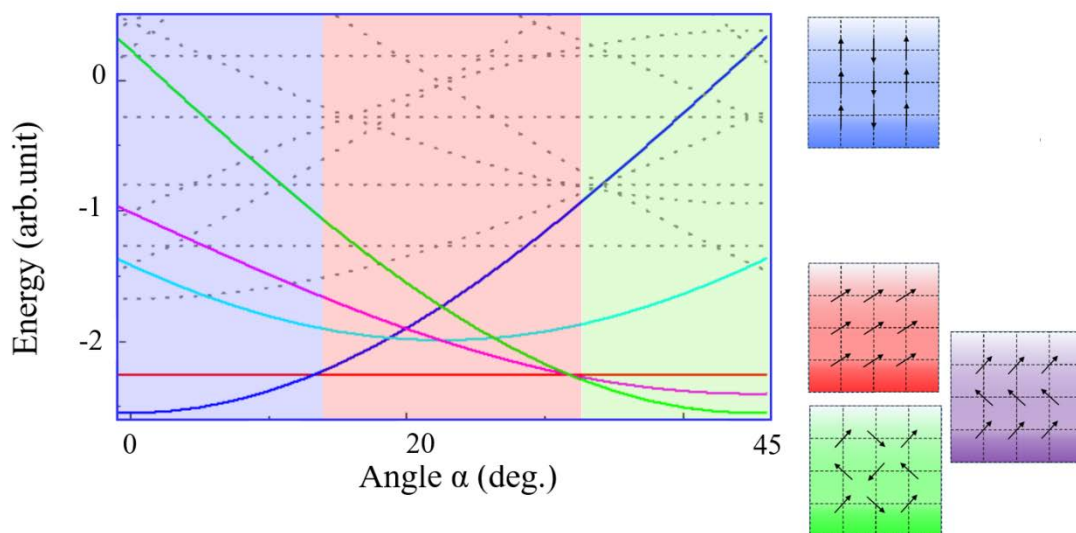


Figure 1-15_ Dipolar energies related to 256 configurations as function of the alpha angle (cut off equal to 250 which means equivalent to 500x500 spins lattice). The configurations are defined from unit meshes composed of 2x2 spins the lowest energy states as function of alpha are ferromagnetic state (red), antiferromagnetic state (blue), loop state (green).

The figure 1-15 shows that in the particular case where the infinite square lattice is given by the repetition of unit mesh composed of 2x2 spins, the simplest configurations determined in the previous section are the lowest in energy. Indeed the 256 energies represented according to the alpha angle reveal that the antiferromagnetic state (blue curve), the ferromagnetic state (red curve) and the loop state (green curve) are the lowest energy states.

This study seems to confirm that these 3 simplest configurations are good candidates to reveal the behavior of the ground state for the infinite square lattice. However with this study it is not possible to identify this ground state due to the particular way to generate the infinite lattice. Indeed the fact to impose a unit mesh composed of 2x2 spins limits the number of possible configurations for the lattice. A solution could be to increase the unit mesh size and to generate all the possible configurations, but for obvious reasons (time calculation) it is not possible to apply this solution.

Another way is actually to increase the unit mesh, but instead of generate all the possible configurations, it is used Monte Carlo simulations in order to reach a state close (or in the best case corresponding) to the ground state of the system.

1.4.3 Monte Carlo simulations

The previous considerations focus essentially on the low energy states of the system. In order to capture the thermodynamic of the system, it is necessary to take into account all the states and the partition function of the system. Even for system of few hundreds elements, it is not possible to consider all the states (especially for Potts spins with even more possible configurations than Ising spins). The Monte Carlo method is a widely used algorithm to solve this problem. An extensive and rigorous Monte Carlo study of the dipolar 4 Potts model is beyond the scope of this PhD work, however we present below some preliminary results.

The infinite lattice is implanted here as a 30 x 30 lattice and taking into account periodical dipolar interactions up to 5 times the size of the lattice. At each Monte-Carlo step, 900 spins are consecutively chosen randomly. For each of these spins, the 4 energies corresponding to its 4 different states are computed and one of them is selected according to a Boltzmann probability law (a spin can therefore rotate by 180 degree). For each temperature, after 100 Monte Carlo step thermalization, the energy is averaged over 100 supplementary Monte Carlo steps. Note that all these values have been chosen in order to achieve a reasonable computation time and that the results are therefore only indicative and should be confirm by "longer" simulations. Figure 1-16 represents the results of this calculation for three different angles (4 different simulations for 22.5 degree).

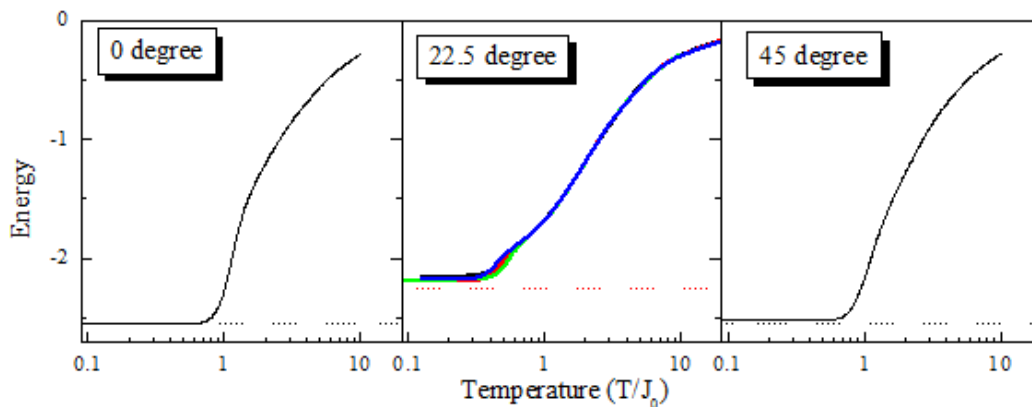


Figure 1-16_Energy as a function of the temperature given by Monte Carlo simulations for three infinite lattices: 0° lattice, 22.5° lattice and 45° lattice. Dashed lines represent the expected energies related to the ground state.

As expected, the energy decreases with temperature, from 0 at high temperatures toward the ground state. For the 0 degree lattice, the antiferromagnetic ground state is perfectly achieved. For 45 degree, the ground state is nearly achieved and the difference with the ground state is higher for the 22.5 degree angle. These differences originate from the presence of two or three domains of the ground state which cannot be removed at low temperature with the single spin flip algorithm that we have implemented. Nevertheless, the Monte-Carlo simulations perfectly reproduce the nature of the ground states that we have determined in the previous sections.

Considering the evolution toward the ground state, it appears as very regular for the 0 and 45 degree with a maximum of specific heat around a reduced temperature around 1. For the 22.5 degree geometry, some irregularities can be identified at reduced temperature about 0.5. This might be an indication of a two phase ordering of the system. These aspects have to be studied in more detail before any definitive conclusion.

Thus this theoretical observation is really motivating for the realization of an experimental system which can match this dipolar Potts model. But experimentally, it is obvious that an infinite lattice is not practicable. And so a study of finite squares lattices is necessary, in order to observe the edges influence of these finite lattices on the energies represented in the figure 1-14. Experimentally finite lattices composed of 30x30 4-state Potts spins are designed (see section 3.3) and so this lattice size is used in the next section.

1.5 Finite lattice

Previous considerations deal with infinite lattices without border. However finite size effects are very important considering dipolar interactions and are responsible for effects like demagnetizing field, shape anisotropy, flux closure domains... In the following, finite lattice is studied and the study is concentrated on the size of the lattice which will be studied experimentally: 30 x 30 spins.

First one address the case of $\alpha=22.5$ degrees which corresponds to a ferromagnetic ground state for the infinite lattice. Different Monte-Carlo simulations have been made in order to determine if it is indeed the case in a finite lattice. Figure 1-17 compares two configurations: the uniform ferromagnetic state and a low temperature configuration from Monte-Carlo simulations (selected among the smallest energy). The color code indicates the individual contribution of the spin to the total energy (blue for the lowest energies, red for the highest). The energy of the non-uniform state is significantly reduced compared to the saturated state, which is consequently not the ground state for a finite lattice.

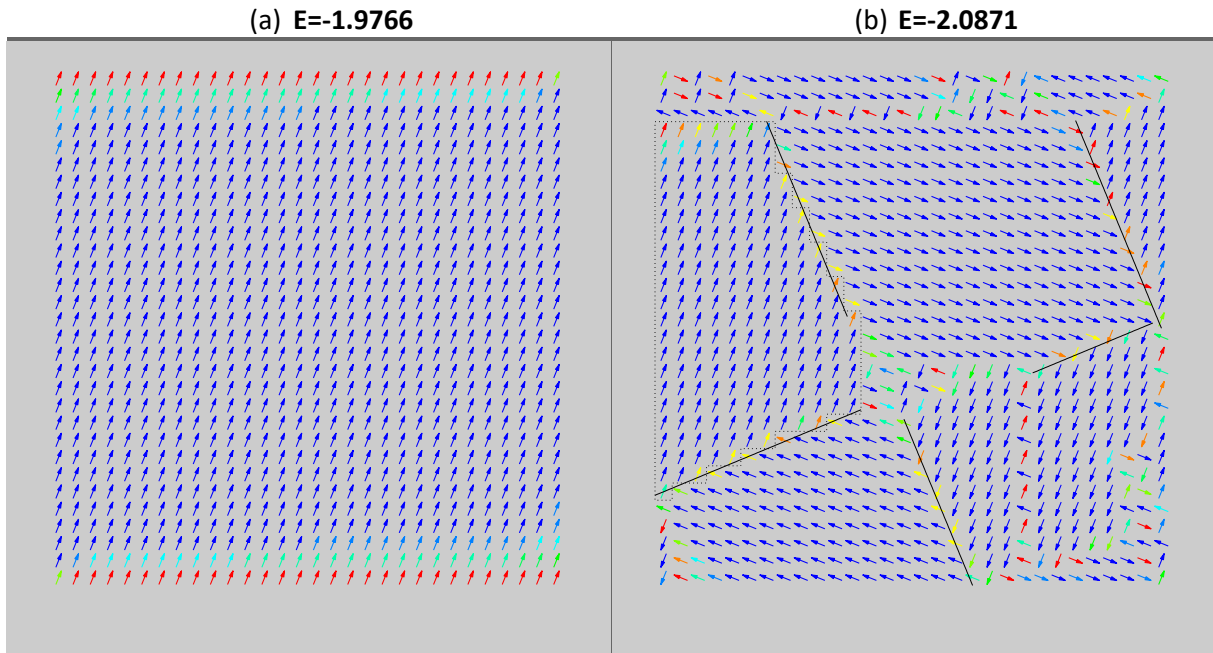


Figure 1-17_ These two dipolar energies and these two configurations are determined for the case of alpha equal to 22.5°. (a) Dipolar energy and configuration related to a uniform ferromagnetic state. (b) Dipolar energy and configuration related to a low temperature configuration from Monte-Carlo simulations.

The qualitative observation shows that:

- The local spins arrangement is ferromagnetic. As exemplified in the figure 1-17 (b), this configuration is a multi-domain state with ferromagnetic domains separated by domain walls.
- On the lattice borders, spins tend to be "parallel" to the borders. This is the cause of the energy reduction compared to the uniform state in which "perpendicular" spins increase significantly the total energy. This is analog to the reduction of surface magnetic charges ($\sigma = \vec{M} \cdot \vec{n}$) which occurs for continuous ferromagnets.
- The most common domain walls are 90 degree domain walls. There is a clear tendency for these walls to lie at 22.5 degree of the lattice (in figure 1-17 (b)). This is analog to the orientation of a 90 degree domain wall in continuous ferromagnets for reduction of bulk magnetic charges ($\rho = \vec{\Delta} \times \vec{M}$). We can also note that some domain walls sit along the lattice directions.

The single spin-flip Monte-Carlo method is not necessarily efficient to determine the ground state of a system with many local minima and long range interactions. Therefore, we tried to determine the ground state by applying different energy reduction schemes to different "classical" configurations. One of them is the border domains configuration, its optimal configuration is represented in figure 1-18 (a). It is interesting to note that contrary to the usual situation, a S configuration (two border domains with same orientation) is less energetic than a C configuration (opposite orientation minimizing the long range dipolar interaction). The energy of this configuration is not reduced compared to the previous multi-domain state obtained by Monte-Carlo simulation.

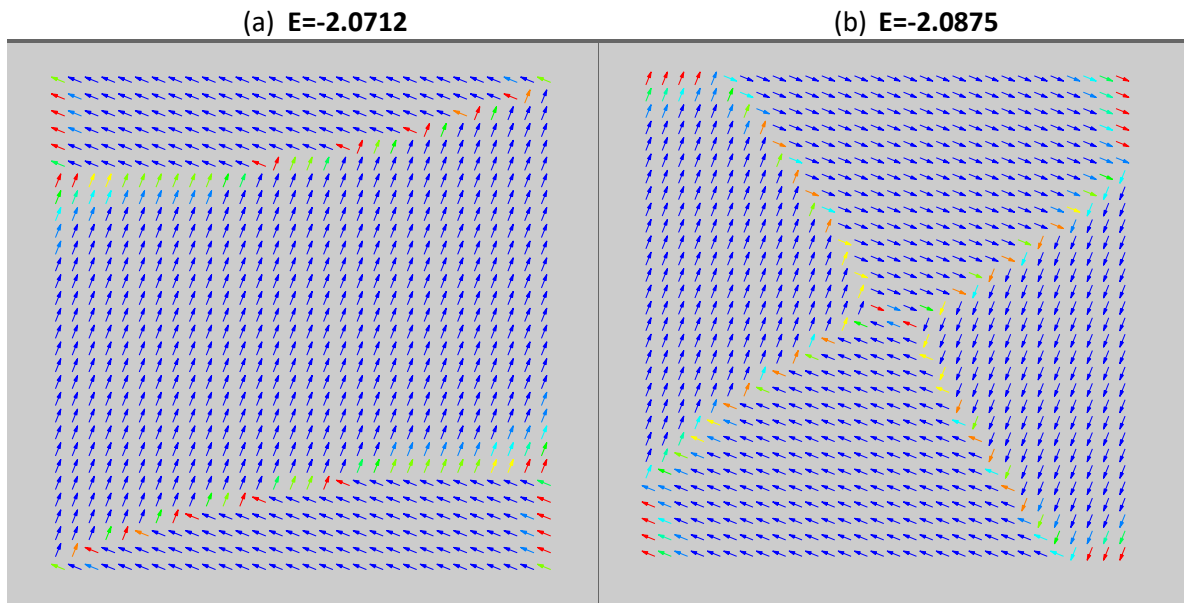


Figure 1-18_ These two dipolar energies and these two configurations are determined for the case of α equal to 22.5° . (a) Dipolar energy and configuration related to the optimal border domains configuration determined thanks to Monte Carlo simulation. It is interesting to note that contrary to the usual situation, a *S* configuration (two border domains with same orientation) is less energetic than a *C* configuration (opposite orientation minimizing the long range dipolar interaction). (b) Dipolar energy and configuration related to the lowest energy realization of a vortex.

Another "classical" configuration often encountered in finite size magnet is the vortex. Its lowest energy realization is represented in figure 1-18 (b). This configuration achieves a lower energy than our reference multi-domain configuration. This energy reduction is due to a compromise between the orientation of the four domain walls and the number of spins "perpendicular" to the borders. Actually another configuration, similar to the vortex, further minimizes the energy: the Landau state with an energy of -2.105. This configuration, represented in figure 1-19 (a), is actually the better one we have determined. It is however not possible to state definitively that is the ground state of the system. Nevertheless, we believe that this is a quite good overestimation of ground state energy for spins at 22.5 degrees from the lattice and if it exist other configuration with lower energy the gain would be marginal.

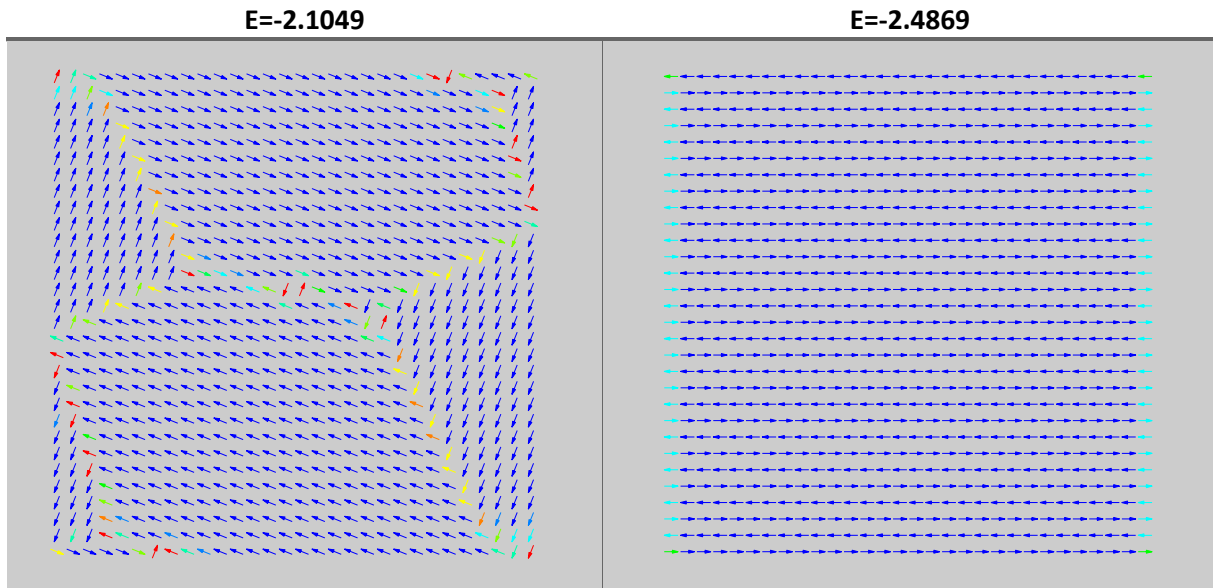


Figure 1-19_ (a) Dipolar energy and configuration related to a similar vortex configuration: the Landau state. The dipolar energy and the configuration are determined for an alpha angle equal to 22.5° (b) Dipolar energy and configuration related to the lowest energy state for an alpha angle equal to 0° .

We can now consider the case of others angles between directions of spins and lattice. A priori, the finite size effects should be negligible for low magnetization configurations like antiferromagnet and loop crystal. As exemplified in figure 1-19 (b) for the antiferromagnetic configuration (0 degree angle), if there is an energy increase due to spins normal to the lattice border, this energy increase is lower than the cost of a domain wall between two antiferromagnetic domains. We have verified with Monte-Carlo simulations and energy minimization from typical configurations that the antiferromagnet ($\alpha < 15$ deg.) and loop crystal ($\alpha > 29$ deg.) are actually the ground state of the system. The figure 1-20 represents the energy of the ground state as a function of alpha, this energy is compared to the one of the simple configuration (antiferromagnet, ferromagnet, loop crystal).

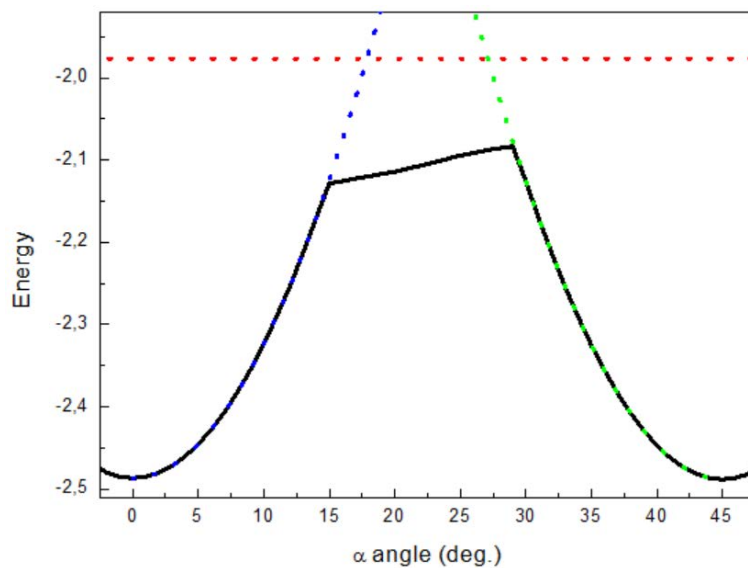


Figure 1-20_ The black curve represents the energy of the ground state as a function of alpha determined thanks to Monte Carlo simulations, and this energy is compared to the one of the simple configurations (antiferromagnetic state in blue dashed line, ferromagnetic state in red dashed line, loop crystal state in green dashed line).

It emerges in observing the figure 1-20, that for an alpha angle between 0° and 15° and for an alpha angle between 29° and 45° , the ground state present the same properties for the finite lattice as for the infinite lattice (respectively antiferromagnetic state and loop state). However for an alpha angle between 15° and 29° it exists, in the case of the finite lattice, lower energy state than the uniform ferromagnetic state observed for the infinite lattice. But it remains that the ground state is a multi-domain ferromagnetic state.

1.6 Summary

Historically, in the 1920's, lots of spin models have been described and in particular two well-known models which are the Ising model [18] and the Potts model [19]. However up to know in the artificial spin systems, all the nanomagnets designed in the arrays present themselves as classical Ising spins where the magnetization (in-plane or out-of-plane) in nanomagnets have two preferential orientations. Thus motivated by this observation, the idea was to design in playing with the anisotropy (shape and crystalline), a new system where the spin is not a 2-states spin but a 4-state spin.

In this context, this chapter has described briefly the "classical" Potts model with the general definition of the Hamiltonian related to this model, then a particular case was detailed which was the dipolar 4-state Potts model. Indeed in the artificial spin systems the number of states for the spin is fixed at a particular value (in this thesis 4 states) and the interaction between elements is generated by dipolar interactions, hence the spin model described. Moreover in the case of artificial spin systems the lattices are in two dimensions and so a supplementary condition on the spin model was introduced. Considering these properties linked to the nature of the artificial spin systems, the particular case of the Potts model described in this thesis was the dipolar planar 4-state Potts model. In this model it is considered spins with 4 states confined in a plane which interact between each-other via dipolar interactions.

Thus it was firstly described the behavior of two spins in dipolar interaction in the case of two Ising spins then in the case of two 4-state spins (called Potts spins). This study shows that the introduction of 2 supplementary states for the spins, induced a more complex behavior for the system. Indeed in comparing the case of two Ising spins with the case of two Potts spins, it appears that the Potts spin model presents six energies levels (against two for the Ising spin model) which correspond to three coupling (against two for the Ising spin model) which are ferromagnetic coupling, antiferromagnetic coupling and perpendicular coupling. Moreover for the two spin models, it is revealed that the behavior of energy levels is related to the angle between the spin and the axis between the two spins (called alpha angle), and so that according to this angle, the coupling present in the system is different.

As this last observation was interesting, the study was extended in the case of an infinite 1D chain composed of Potts spins. And through the study of dipolar energy for an infinite 1D chain, the behavior of this system reveals a strong correlation between the properties shown and the angle between spin and the axis between spins (alpha angle). Indeed as for the case of two spins, it appears a different behavior for the system according to the alpha angle. However for this study only simple configurations was observed, like ferromagnetic state, antiferromagnetic state and

perpendicular state, but with these simple configurations it is demonstrated that according to the alpha angle, the configuration with the lowest energy is different.

Then this study was extended to the case of 2D lattices composed of 4-state spins. For this study, the aim was to determine if it exists an angular dependence (linked to alpha angle) of the properties related to the ground state of this system, and if it exists this dependence, which configurations are favored according to this angle. As part of these questions, an infinite lattice was firstly studied. For that, the first idea was to simplify the problem in observing only two simple configurations which was ferromagnetic state and antiferromagnetic state. Thus the calculation of the dipolar energies related to these two configurations reveals an angular dependence clearly different. Indeed the ferromagnetic state shows a dipolar energy which is constant according to the angle between spins and the axis lattice (alpha angle), while the antiferromagnetic state shows a dipolar energy different according to the alpha angle. Thus the study was extended to the case of four simple configurations, which were ferromagnetic state, antiferromagnetic state, loop (or spin ice) state and wave state. And it appears that if it is considered only these four states, according to the alpha angle, the ground state present the properties of the antiferromagnetic state (spin directions close to the lattices directions), of the spin ice state (spin directions close to 45 degrees from the lattices directions) and of the ferromagnetic state (intermediate spin directions). Thus through the study of these four simple configurations, the behavior of the ground state was approached, but it was not enough to determine the ground state of a 2D infinite lattice. Thus another extension of this study was done in considering a unit mesh composed of 4 spins (2x2 spins) repeated an infinite times to obtain the infinite lattice. Creating the infinite lattice from this unit mesh, it was possible to determine all the possible configurations (256 configurations) and to determine the angular dependence of the dipolar energies related to these 256 configurations. And it appears that the three simple configurations studied previously (ferro, antiferro and spin ice states) remain the lowest energy states according to the alpha angle. Thus it seemed that these three configurations could be good candidates in order to describe the ground state of the infinite lattice. And in order to confirm this hypothesis, Monte Carlo simulations were performed and it appears effectively that according to the alpha angle, the ground state shows the same properties as the antiferromagnetic state (spin directions close to the lattices directions), the spin ice state (spin directions close to 45 degrees from the lattices directions) and the ferromagnetic state (intermediate spin directions). This observation reveals that the 2D lattice composed of Potts spins is a very versatile system as the simple rotation between spins and the lattice axis gives rise to very different properties for the ground state. This interesting properties has motivated the experimental realization of this spin model. But experimentally it was not possible to design an infinite lattice and so this "limitation" has motivated the study of a finite lattice, especially to determine the influence of the edges on the properties of the ground state. The choice of the number of spins composing the lattice was motivated by the experimental measurements, where it appears that a good compromise between time measurements and accuracy measurements is for a 30x30 lattice. And under this condition, a finite lattice composed of 30x30 spins was studied. This study reveals that for an alpha angle equal to 0° and 45° the ground state for the finite lattice presents the same properties as these for the infinite lattice. However for the part where the ferromagnetic state was the ground state for the infinite lattice, this study shows a lower energy state which is a Landau state composed of domains which follow the edges. But in term of dipolar energy, the difference between the ferromagnetic state and the Landau state can be considered as "reasonable". Thus it was decided that, unless a perfect demagnetization, the ferromagnetic state can be a good indicator to determine the efficiency of the demagnetization performed on the experimental systems.

Bibliography

- [17] S.Zhang et al, “Perpendicular Magnetization and Generic Realization of the Ising Model in Artificial Spin Ice”, *Phys. Rev. Lett.* **109**, 087201 (2012)
- [18] E.Ising, “Beitrag zur Theorie des Ferromagnetismus”, *Z. Phys.* **31**, 253-258 (1925)
- [19] Potts, “Some generalized order-disorder transformations”, *Proc. Camb. Phil. Soc.* **48**, 106 (1952)
- [25] Ashkin and Teller, “Statistics of Two-Dimensional Lattices with Four Components”, *Phys. Rev.* **64**, 178 (1943)
- [26] Potts, Phd thesis, “The mathematical investigation of some cooperative phenomena”, University of Oxford (1951)
- [27] Wu, “The Potts model”, *Review of Modern Physics.* **54**, 1 (1982)
- [28] Chang et al, “Exact partition function for the Potts model with next-nearest neighbor couplings on arbitrary-length ladders”, *International Journal of Modern Physics B.* **15**, No 5, 443-478 (2001)
- [29] Welsh et al, “The Potts model and the Tutte polynomial”, *J. Math. Phys.* **41**, No 3, 1127-1152
- [30] Jorgensen et al, “Perspective on “Equation of state calculations by fast computing machines””, *Theoretical Chemistry Accounts.* **103**, 225-227 (1999)
- [31] Sanya et al, *Journal of Statistical Mechanics* (2006)
- [32] Cibra et al, “Statistical Physicists Phase Out a Dream”, *Science.* **288**, No 5471, 1561 (2000)
- [33] Domany et al, “Classification of Order-Disorder Transitions in Common Adsorbed Systems: Realization of the Four-State Potts Model”, *Phys. Rev. Lett.* **38**, 1148 (1977)

2. MICROMAGNETISM

In order to realize experimentally the dipolar 4-state Potts model, a preliminary micromagnetic study is required in order to know if it is possible to design artificial spin with properties as close as possible to the "ideal" dipolar 4-state Potts model. Up to now in order to obtain a nanomagnet which can be analogue to an Ising spin, an uniaxial shape anisotropy was mainly imposed [11, 12] by designing an elongated shape. Perpendicular anisotropy (associated to the material) is another option which has been used for perpendicular Ising spins [16]. The uniaxial anisotropy combined with adapted magnetic material induces two nearly uniform magnetic states in nanomagnet which can be mapped onto an Ising spin. To realize the artificial Potts model, we envisage taking profit from the 4-fold anisotropy present in iron epitaxial thin films. But the proper anisotropy is only a necessary but not sufficient condition, and it is the micromagnetic study which will guide us to design an artificial Potts spin.

The main issue is the achievement of four nearly uniform states. As a matter of fact, these states are required for mapping onto the spin model but also for generating a sufficient stray field to induce the dipolar coupling between the nanomagnets. This point is not trivial as nanomagnets tend to form multidomain or non-uniform magnetization patterns like vortex in order to decrease magnetostatic energy, even in the presence of cubic anisotropy [34, 35]. In this chapter, we will study the stability and relative energies of uniform and non-uniform states as function of the geometry of the nanomagnet.

Another point is discussed in this chapter, which is the validity of dipolar approximation. Indeed the aim is to observe an experimental system composed of nanomagnets in order to design a spin model. Thus it is necessary to check if the spin model presented in the first chapter, where the spins are considered as magnetic dipoles only in dipolar interactions, is compatible with a real system composed of nanomagnets with spatial extension.

2.1 Micromagnetism introduction: contribution of Brown free energy

As mentioned previously the support of this chapter is the micromagnetism. Indeed micromagnetic simulations are based on a theory developed in the 1940's by W.F.Brown: the micromagnetism. This theory describes the properties of ferromagnetic environment [36] in taking the magnetization and also the different internal fields as continuous thermodynamic variables. In order to understand the different processes taking part in ferromagnetic environments as well as the difficulty to obtain a nanomagnet which can be considered as a macrospin (uniform magnetization in all the volume), it is essential to describe the different energies involved in the magnetization behavior for magnetic materials.

This section is based on [37, 38, 39].

The magnetization behavior in magnetic material is fixed by the Brown free-energy minimization E_{Tot} . This energy is given in the following equation:

$$E_{Tot} = E_{Exchange} + E_{Zeeman} + E_{Dipolar} + E_{Anisotropy} \quad (2-1)$$

Where it appears 4 energies which are exchange energy, Zeeman energy, dipolar energy and anisotropy energy.

Thus in this section, the different energies reported in the equation (2-1) are described and we discuss the required compromises between these energies in order to minimize the Brown free-energy.

Exchange energy

The exchange interaction, introduced by Heisenberg [40] as part of quantum mechanics, is an electrostatic interaction. It is induced by the overlapping of electronic waves functions related to atoms combined to the Pauli Exclusion Principle. This interaction, which is order of magnitude stronger than the others energies, is a short range interaction. This energy is given by the following equation:

$$E_{Exchange} = \int_V A_E \left(\Delta \frac{M}{M_S} \right)^2 dV \quad (2-2)$$

Where A_E is the exchange stiffness and can take, regarding the nature of the material, a positive or negative value. This interaction is the source of the magnetic moments alignment.

Furthermore, these magnetic orders exist up to a particular temperature. Indeed this interaction is in competition with the thermal agitation, which means that if the temperature increases, it will occur a reduction of the magnetization [41] up to “lose” the magnetization for a particular temperature which is the Curie temperature.

Thus as part of the dipolar 4-state Potts model, a ferromagnetic material with a high exchange stiffness seems the most appropriate choice. Indeed this one via exchange interaction, will favor the apparition of domains within the magnetic moments are parallel between each other and therefore an uniform state.

Zeeman energy

This energy appears when an external field (\vec{H}_{app}) is applied on the magnetic material, and it is the result of the interaction between this magnetic field and the magnetization \vec{M} related to the material. Its expression is given by the following equation:

$$E_{Zeeman} = -\mu_0 \iiint \vec{M}(\vec{r}) \cdot \vec{H}_{app} dV = -\mu_0 M_s \iiint \vec{m}(\vec{r}) \cdot \vec{H}_{app} dV \quad (2-3)$$

Where M_s is the spontaneous magnetization and where the integral takes into account all the volume related to the magnetic material. This energy tends to align the magnetic moments with the applied magnetic field.

In this thesis, this energy is important only for the demagnetization protocol. Indeed as mentioned in the general introduction, one way to lead the artificial spin system towards its ground state, is the AC field demagnetization. And so in the following simulations reported in this chapter, which are focused on the determination of monodomain stability in nanomagnets, this energy will not be taking account.

Dipolar energy

The dipolar energy is the result of the interaction between magnetic dipoles, and this short range energy is order of magnitude smaller than the exchange energy. This one depends directly of a magnetic field (\vec{H}_d), which is created by a magnetization distribution inside magnetic materials. The magnitude of this field is proportional to the magnetization inside material and its orientation is opposed at this one of the magnetization in order to close the magnetic flux.

$$E_{Dipolar} = -\frac{\mu_0}{2} \iiint \vec{M}(\vec{r}) \cdot \vec{H}_d dV = -\frac{\mu_0 M_s}{2} \iiint \vec{m}(\vec{r}) \cdot \vec{H}_d dV \quad (2-4)$$

For the artificial spin, it will be favorable to minimize this energy (for example in playing with the shape of nanomagnet: in our case shape with cubic symmetry) in the aim to avoid the formation of domains in the nanostructure. But on the other hand, this energy is also the cause of the coupling between the nanomagnets and has to be high enough.

Anisotropy Energy

The anisotropy energy have different sources. In what follows, only one source is explained considering its importance in our study.

-The magneto-crystalline anisotropy, which result of interactions between electronics orbitals of an atom and charge distribution of their environment. This energy depends directly on the material structure and on its symmetries. Its expression, for a cubic material, is given by this equation:

$$E_{Anisotropy} = \int (K_1(\cos^2\alpha_1\cos^2\alpha_2 + \cos^2\alpha_2\cos^2\alpha_3 + \cos^2\alpha_1\cos^2\alpha_3) + K_2\cos^2\alpha_1\cos^2\alpha_2\cos^2\alpha_3 + \dots) dV \quad (2-5)$$

Where K_i are anisotropy constants and α_i the angle between magnetization and crystallographic axes.

The magneto-crystalline anisotropy shows that there are spatial directions where it is easier to magnetize a material and these directions are the easy magnetization axes.

Although anisotropy energy is weaker than exchange energy, this one can be determinant for the magnetization direction. In our case, it is expected that the magnetization in nanostructure can take four directions. Thus, for the magneto-crystalline anisotropy, it will be wise to choose a material with a cubic anisotropy like iron, in order to stabilize four directions for the magnetization.

With this preliminary study, it is possible to give some restrictions on the material and the shape of nanostructures which will describe experimentally the dipolar Potts model. Indeed with the minimization of those energies, it appears that a good candidate for the material should be a ferromagnetic material with cubic anisotropy and for the shape of nanostructures, squares or circles which have cubic symmetry should constituted favorable starting points for this experimental study.

Now, to determine under which conditions on the material and on the shape, it is possible to design an artificial spin which respects all the properties expected by the spin model, a way is to use micromagnetic simulations.

2.2 Micromagnetism as pathway to design artificial spin

In order to carry out micromagnetic simulations, the processing of the different equations governing the dynamic of the magnetization, impose to split the magnetic nanostructures in cells which can take several shapes (tetrahedral, orthorhombic, cubic...). In each cell, the parameters like magnetization, energy or effective field are fixed. According to the cells uniformity, two main micromagnetic models allow to describe the magnetization inside nanomagnets. The first is based on the finite elements method [42, 43, 44] and the second is based on the finite differences method [45, 46, 47, 48].

As part of this thesis, the software used is an open-source-GPU accelerated micromagnetic simulation program: Mumax3 [49]. This program is based on a finite elements space discretization, as it is the case for a lot of micromagnetic simulation programs like “The object Oriented MicroMagnetic Framework” (OOMF). The main advantage related to Mumax3 is the use of GPU in order to make the calculations, which allows a time calculation shorter than the others softwares. In the aim to use the finite differences method, the space is discretized in a structured grid (2D or 3D) composed of orthorhombic cells. Thus the volume quantities, like magnetization or effective field, are defined in the center of each cell while the coupling, like exchange, are defined at the interfaces between two cells. Moreover at each cells is associated a region with a value ranging from 0 to 256. These regions are independent and for each number related to one region, it can correspond a different material (with different parameters). This software allows also to define a lot of shapes for the nanomagnets. In this aim the geometry is defined as a function $f(x, y, z)$, which gives true if (x, y, z) are inside geometric shape and false in the contrary case. In order to determine the magnetization dynamic, Mumax3 calculates the evolution of the reduced magnetization $\vec{m}(\vec{r}, t)$, where this reduced magnetization can presented a time and space dependence but where the amplitude is kept constant. Thus to determine the time and space dependence of the reduced

magnetization, the program calculates the time derivative of the reduced magnetization which represents the torque $\vec{\tau} = \frac{\partial \vec{m}}{\partial t}$, where $\vec{\tau}$ possesses three contributions which are: the Landau-Lifshitz torque, the spin transfer torque of Zhang-Li and the spin transfer torque of Slonczewski. As part of this thesis, only the Landau-Lifshitz torque is relevant, the two other being related to electron transport phenomena.

To make micromagnetic simulations, the first point is to fix the different parameters use for the magnetic material, like exchange stiffness, anisotropy constant, saturation magnetization and Landau-Lifshitz damping constant. In this aim all the simulations presented in this study have been realized with iron parameters with the values shown in the following table.

Parameters	Values
Saturation magnetization	$1700 \cdot 10^3$ (A/m)
Exchange Stiffness	$21 \cdot 10^{-12}$ (J/m)
Landau-Lifshitz damping constant	0.2
Anisotropy constant	$48 \cdot 10^3$ (J/m ³)

Indeed, as mentioned previously, the selected material has to be ferromagnetic with cubic anisotropy and iron is a perfect material to respect those properties. The damping constant is nonrealistic but it is fixed at this value in order to increase the speed of convergence for our simulations. In the following section, the program code used in mumax3 is described.

2.2.1 The program code

In this section, the program code is briefly described in order to understand how are obtained the results shown in the next section. In this aim a standard simulation used for this thesis is used as example and the program is constructed step by step in detailing each step.

1. **Grid and cell:** The grid defines the size of the box around the magnetic nanostructure and this size is defined by the number of cells that we choose. Then it's necessary to select the cell's size in meters. Grid and cell size must be set at the beginning of the script.

An example for the script:
 Square grid with a length of 300 nm and a thickness of 2 nm:

```

Nx := 150
Ny := 150
Nz := 1
sizeX := 2e-9
sizeY := 2e-9
sizeZ := 2e-9
SetGridSize(Nx, Ny, Nz)
SetCellSize(sizeX/Nx, sizeY/Ny, sizeZ/Nz)

```

$N_{x,y,z}$: cells number in x, y, z direction for the grid
 $Size_{X,Y,Z}$: cells size in x, y, z direction
Sets the number of cells for X, Y, Z
Sets the X, Y, Z cell size in meters

2. Material parameters: the material parameters define the parameters in the nanostructure use for describe the magnetization in the nanostructure. For mumax3 the vector's origin is given by the grid center.

An example for the script:

Iron parameter with two anisotropy axis directions along the diagonals of the grid:

```

Msat = 1700e3
Aex = 21e-12
alpha = 0.2
AnisC1 = vector (0.5, 0.5, 0)
AnisC1 = vector (-0.5, 0.5, 0)
Kc1 = 48e3

```

Set the two anisotropy axes directions

3. Setting geometry: A magnet shape can be specified, other than the grid. If it's the case, the magnetic material with the previous parameters is only in the shape and for the rest of the grid all the parameters (Msat, Aex...) take the value 0. In mumax3, without precision on the shape position, the shape is placed at the grid center.

An example for the script:

Square shape which has the same size as the grid size. In this position, the anisotropy axes defined previously are in the diagonals of the square.

```

a:=Rect (Nx*sizeX, Ny*sizeY)
setgeom (a)

```

Sets a shape
Sets the geometry to the given shape

4. Initial magnetization: At the simulation beginning, it is possible to set an initial magnetic configuration in the shape by assigning for example uniform, vortex or random magnetization.

An example for the script:

Uniform magnetization along a shape diagonal as initial state.

```

m = Uniform(1, 1, 0)

```

-
5. Output quantities: Lots of quantities as magnetization, exchange energy, anisotropy energy, etc. can be output at the end of the simulation. Moreover those quantities can also be saved every period times during the simulation if we want a time dependence for those quantities.

An example for the script:

```
Save (m)
tableadd (E_total)
tableadd (E_anis)
tablesave ()
autosave (m, 10e-12)
tableautosave (1e-9)
run (20e-9)
```

Now that the program code for mumax3 is described, it is essential to determine if mumax3 gives proper consideration to the cubic anisotropy. Thus, to check the cubic anisotropy, two simulations are realized:

- (a) Square with a length of 300 nm and only uniaxial anisotropy along a diagonal.
- (b) Square with a length of 300 nm and only cubic anisotropy along diagonals.

For these two simulations, the magnetization is imposed uniform in one direction and the program reports the anisotropy energy related to this particular configuration. Then the magnetization rotates by one degree and the anisotropy energy is saved and this procedure is repeated for every angles (from 0° to 360°). For these simulations the magnetization is always imposed in-plane.

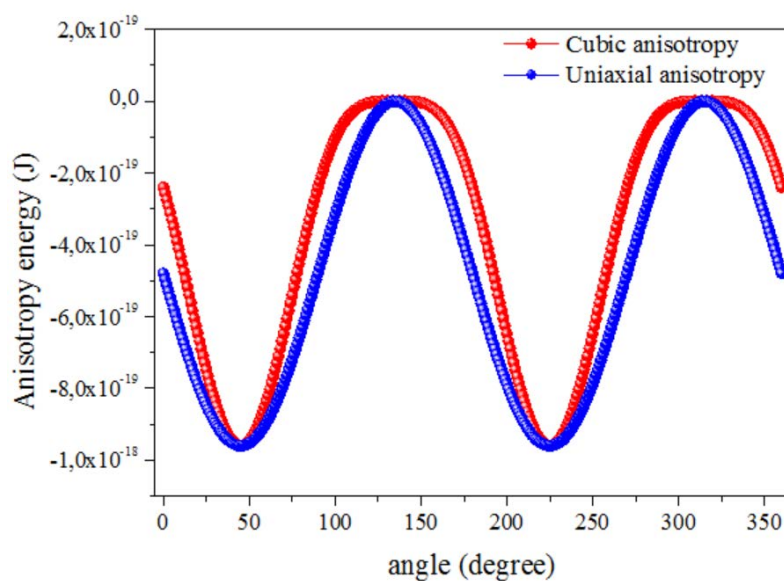


Figure 7-1_ Anisotropy energies as function of the magnetization direction. The red points are the results related to a square with a cubic anisotropy defined in mumax3. The blue points are the results related to a square with a uniaxial anisotropy.

The figure 2-1 shows the anisotropy energy as a function of the uniform magnetization angle in the case where the square has cubic anisotropy (red curve) and uniaxial anisotropy (blue curve). And it appears a similar behavior for the energies, regardless the nature of the anisotropy related to the square. Indeed on this graphic, the two energy curves are minimum for two angles (45° and 225°) which correspond at the angles where the magnetization is aligned with an easy magnetization axis (uniaxial axe in the diagonal square). Thus this figure reveals the presence of only one easy axis for the magnetization, regardless the nature of the anisotropy related to the square, while it is expected two easy axes in the case of the cubic anisotropy. With this study it appears that mumax3 had a problem with the cubic anisotropy definition. This problem has been reported to MuMax authors and has been corrected in version 3.3.

The easy way, to determine how mumax3 takes into account the cubic anisotropy, is to observe the magnetic configuration in a disc with cubic anisotropy when the initial magnetization is vortex. Indeed with cubic anisotropy, it should appear four domains in the disc and only two with uniaxial anisotropy.

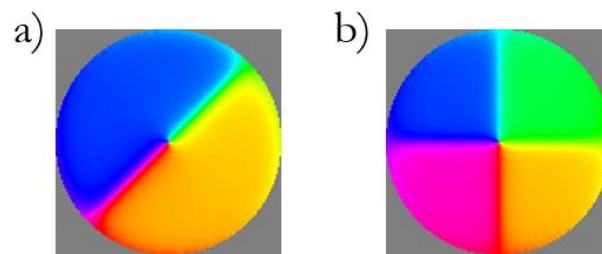


Figure 2-2_ Magnetic configuration obtained after relaxation from a disc with cubic anisotropy where the initial magnetization is vortex. These two figures are related to two versions of Mumax3: a) version 3.2 ; b) version 3.3.

The figure 9 (a) shows the disc's magnetic configuration after relaxation for the first version of mumax3, and this configuration shows two domains (represented in blue and yellow). However it was expected four domains for the equilibrium configuration, so we can conclude that for this version of mumax3, it exists a problem with the cubic anisotropy definition. We can observe in the configuration obtained with the latest version of mumax3 that this problem is solved (fig 9 (b)). Indeed with this latest version, the equilibrium state in the disc shows four domains, as expected for a disc with cubic anisotropy.

After the description of mumax3 function and the verification of stability with cubic anisotropy definition, the next step is to realize “real” simulations in order to find under which conditions it's possible to realize experimentally a spin with all the expected properties in order to match the dipolar 4-state Potts model.

2.2.2 The stability diagram of the monodomain state

As exposed in the beginning of this part, the selected material for the micromagnetic simulations presented in this section is iron with cubic anisotropy. Generally in the nanostructures, the equilibrium state is not necessarily monodomain but can be more complex (Landau structures, vortices...). Up to now in the artificial spin systems, the spin model is related to Ising spins and in order to design this spin, one find in the literature that a magnet with typical size around a hundred nanometers combined with an uniaxial shape anisotropy (elongated shape) is a good candidate [11, 12, 16]. In our case, where the aim is to design a spin with an uniform magnetization presenting 4 preferential directions, this elongated shape is not adapted, however one can assume that the nanometric scale for the magnet remains an appropriate choice. Moreover as it is required 4 preferential orientations for the magnetization in the nanostructure, the elongated shape seen in the literature is replaced by a shape presenting a cubic symmetry. Thus the cubic symmetry of the shape combined with the cubic anisotropy of Fe should allow the realization of an artificial spin which matches the spin used in the dipolar 4-state Potts model. Consequently, three shapes are selected for the simulations: a disc and two squares named square 0° and square 45° after the relative orientations of their borders with respect to the magnetic anisotropy axes (see figure 2-3).

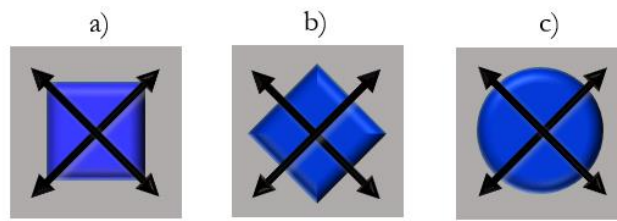


Figure 2-3_ Three possible candidates in order to design artificial spin which can match the properties expected to describe the dipolar 4-state Potts model. These three shapes are related to the position of the anisotropy axes of Fe. (a) Square 45° : square with anisotropy axes in the diagonals. (b) Square 0° : square with anisotropy axes aligned with the edges of the square. (c) Disc: for this shape the position of the anisotropy axes are not important.

As exposed in the literature [50], it exists several magnetic configurations for magnet. Depending of the size and thickness of nanomagnet, different magnetic configurations arise like single domain uniform, several uniform domains separate by domain walls [51] or vortex structure where the magnetization continuously curls around the center with the magnetization in-plane and in the center of the core the magnetization is perpendicular to the plane [52]. Micromagnetic simulations have been used in order to determine the stable configuration of thin nanomagnet as a function of different parameters (thickness, size or magneto crystalline anisotropy). An example is shown in the figure 2-4 (extracted of the Ref [53]) where it is studied the single domain to flux closure (vortex) transitions in thin ferromagnetic disks of Co, according to a variable uniaxial magneto crystalline anisotropy.

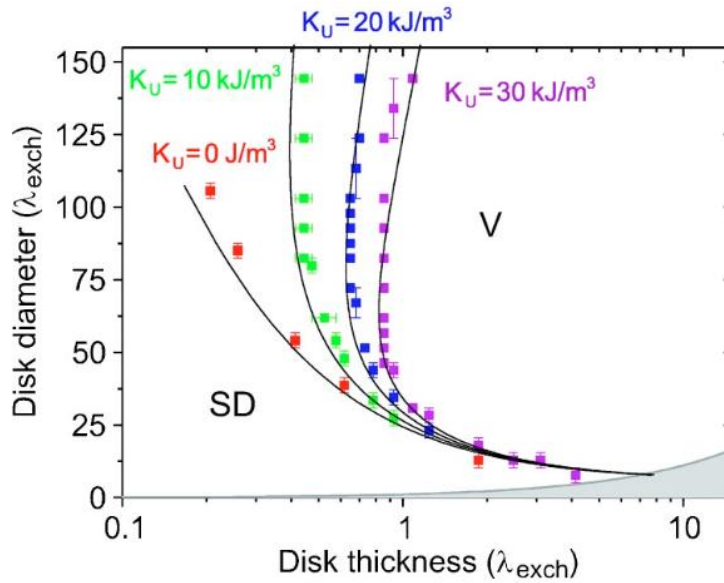


Figure 2-4 SD-V boundary for disks of diameter S and thickness t with varying uniaxial anisotropy ($K_u=0 \text{ kJ/m}^3$, $K_u=10 \text{ kJ/m}^3$, $K_u=20 \text{ kJ/m}^3$, and $K_u=30 \text{ kJ/m}^3$). Lines correspond to the analytical model, dots to micromagnetic simulations. The error bars estimate the inaccuracy of the simulation results introduced by the fact that the simulations were done on a finite grid in the (S, t) parameter space. The gray area shows the region in which the out-of-plane SD state prevails over the in-plane SD state. Figure and legend extracted from Ref [53]

This figure 2-4 compares the stability of the single domain with the stability of the vortex state (as a function of the disk diameter and disk thickness). The results show that without uniaxial anisotropy the single uniform domain is stabilized for small thickness and small size of disks. Regarding the uniaxial anisotropy, the single uniform domain is stabilized by the anisotropy. The transition between single domain and vortex state results from the competition between the exchange energy in the vortex state and the dipolar energy of the single domain. Although the anisotropy studied is uniaxial (and not cubic as in our case), this approach is a good starting point for our study.

Thus we have done a similar study where it is probed the influence of the size of the nanostructure combined with the thickness of the Fe layer on the stability of the uniform single domain. In our case the magneto crystalline anisotropy is cubic and its value is fixed at this one recorded in the literature for the iron and the three cases presented in the figure 2-3 are studied.

For the three shapes, the magnetic state is firstly imposed like monodomain along the direction [110] which is related to an anisotropy axis direction, and we look at the equilibrium state's total energy for the different shapes after relaxation (~ 20 nanoseconds with a "numerical" damping of 0.2). And this for different thicknesses combined with different size of nanomagnets (widths). Then the same protocol is applied but with an initial magnetization which is imposed like vortex. Finally the energies related to uniform state and vortex state are compared at equilibrium.

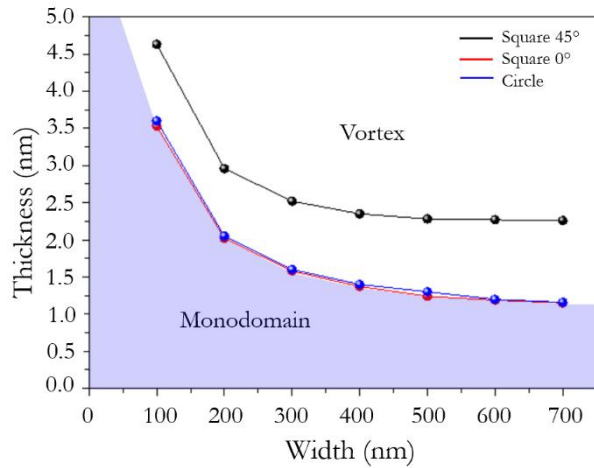


Figure 2-5_ Stability diagram in energy for two magnetic configurations (monodomain and vortex state). It is represented the comparison between the energies related to monodomain state and vortex state according to the Fe thickness combined with the shape width. Thus it is reported the region where either configuration is the lowest in energy and this for the three shapes. The lines (black, red and blue) represent the region where the two configurations possess the same energy (respectively for square 45°, square 0°, and circle).

In figure 2-5, the (black, red, blue) lines represent the borders where the two configurations possess the same energy (respectively for square 45°, square 0° and circle) according to the iron thickness and of the shape width. Below the curves the monodomain state is the lowest in energy and above the curves, it's the vortex state which is the lowest in energy. It appears with this stability diagram, that if the aim is to stabilize the monodomain state, it is necessary to work with a thin film. Moreover, according to the shape, the required thickness is not the same. Indeed for the square 0° and the disc, the monodomain is stabilized against the vortex state for a Fe thickness around 1 nm (for a shape width up to 700 nm). However for the same shape width range, the square 45° shows monodomain state stabilized for a thickness around 2 nanometers. So it seems that experimentally, the square 45° is the easiest way to obtain a monodomain state. But it is important to notice here, that it is assumed that these two configurations are the most probable possibilities for the magnetic configurations, but it is possible that others configurations are stable or metastable.

2.2.3 Internal magnetic configurations

Thanks to the stability diagram presented in the previous section, it appears a possibility for disc, square 0° and 45° to possess monodomain state as the lowest energy state when the iron thickness is around 1 or 2 nanometers. Now it is possible to observe the micromagnetic configurations at equilibrium for those monodomains, and see if either appears more stable according to the shape. Thus, the micromagnetic configurations obtained with the previous simulations (with initial magnetization like monodomain) for an iron thickness of 1 nanometers and a length shape of 300 nanometers which are detailed.

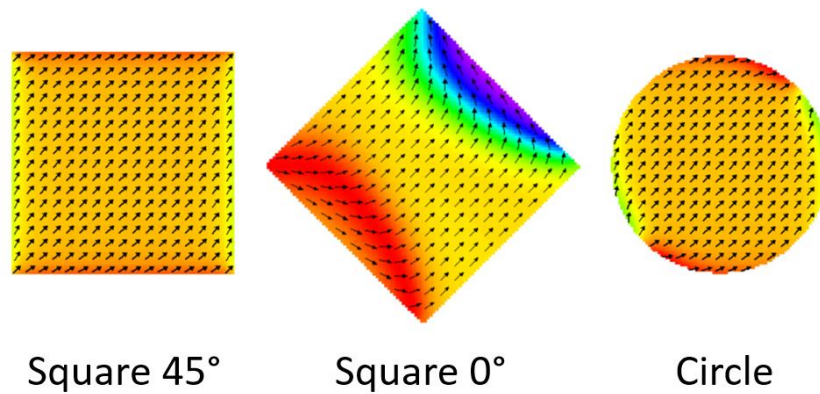


Figure 2-6_ Micromagnetic configuration related to three cases. The figure at left represents the micromagnetic configuration corresponding to square where the anisotropy axes of Fe are aligned along the diagonals square. The center figure represents the micromagnetic configuration corresponding to square where the anisotropy axes of Fe are aligned with the edges square. The figure at right represents the micromagnetic configuration corresponding to disc. These micromagnetic configurations correspond to the configurations obtained from the previous simulations after relaxation for an Fe thickness of 1 nm and a shape width equal to 300 nanometers (length for square and diameter for disc).

The figure 2-6 shows three different equilibrium configurations for the three shapes.

1. For the square 45°, the equilibrium state stays monodomain (remanent magnetization equal to 0.99) in the same direction as the initial magnetization which is along a diagonal square. Moreover in this equilibrium state, the moments are all symmetric against the diagonal square and thus it exists only one way to obtain this equilibrium state.
2. For the square 0°, the equilibrium state is mostly monodomain but this time the magnetization direction slightly rotates from the easy axis direction and two side domains are observed. Both aspects originate from the interplay between magnetocrystalline anisotropy and shape anisotropy which favors a magnetization along the square diagonals. Moreover micromagnetic simulations shows that the equilibrium state can take slightly different configurations with different orientations of the side domains. Thus the monodomain can be composed by C state formed of border domains antiparallel between each other or S state formed of border domains parallel between each other.
3. For the disc, the equilibrium state is monodomain along the anisotropy axis as the initial magnetization but as for the Square 0° case, this monodomain can be composed by C state or S state.

The occurrence of different configurations for the same global orientation of magnetization leads to internal degrees of freedom in the context of artificial spins. These internal degrees of freedom can enrich the physics of the system [54, 55]. However for the first studies on this new spin systems, it is preferable to avoid any supplementary degree of freedom (especially as these border domains can significantly affect the coupling between elements).

Consequently the square 45° appears to be the best choice of shape, as it combines a better stability in the phase diagram (easiest to stabilize monodomain state) to a high remanence (absence of internal degree of freedom).

2.3 Validity of the dipolar approximation

Now that the best condition to realize experimentally the spin is determined, it is useful to study the coupling between these two spins. Indeed in the first part of this work, the theoretical study concerned dipolar interactions between spins (magnetic dipole) possessing 4 states. But experimentally even if the magnetization in nanostructure is monodomain, the magnetic configuration is not really a magnetic dipole but it has a spatial extension and some deviation from the strictly uniform state. So in this section, it is shown how the micromagnetism changes the interaction behavior between two spins possessing 4 states. In this aim, it's interesting to study the energy levels given by the micromagnetic simulations and to compare with the energy levels expected in the case of two magnetic dipoles.

For these simulations, the energy of a system composed by two squares with a length of 300 nanometers is determined. The magnetic material is a 2 nanometers layer of iron with cubic anisotropy (to stabilize monodomain state) and these anisotropy axes are aligned with diagonals squares. The initial magnetization is always uniform along a diagonal square and the magnetic configurations in a square can take 4 preferential directions which are the four directions along diagonals square. For these simulations the system probes the 16 possible configurations between the magnetic configurations squares and give the total energy for each equilibrium state. Moreover with the theoretical study, it is determined that the energy levels of a system composed by two spins with four states depend on the angle between the two spins. So in these simulations two angle are studied: 0 and 45 degrees. As squares stay in the same position against the anisotropy axes, to define the angle, it's the position between two squares which is modified. Indeed the angle alpha defined in the chapter 1 is represented in these simulations as the angle between mondomain direction in a square and the axis between two centers squares. On the figure 2-7, it is represented the configurations for an angle of 0 degree and 45 degrees.

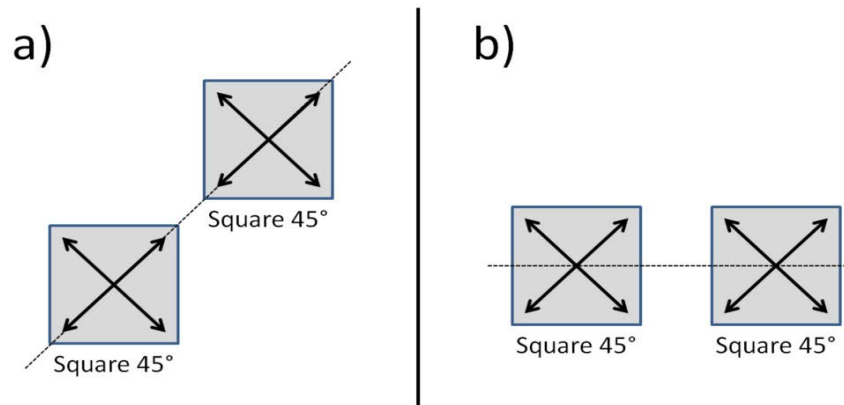


Figure 2-7_ Configurations imposed for the micromagnetic simulations, where the distance center to center is the same for the two configurations. (a) Configuration related to an alpha angle equal to 0°, (b) Configuration related to an alpha angle equal to 45°.

An automatic procedure probes the 16 magnetic configurations of these two configurations and gives the energy related to each configuration. Then these energies are normalized in order to be compared with the energies determined in the section 1.2 which were normalized by the coefficient $\frac{\mu_0 \cdot m^2}{4\pi \cdot a^3}$, where « a » represents the distance between two spins. So for the simulations, the energies

given by mumax3 are divided by this term $\frac{\mu_0 \cdot m^2}{4\pi \cdot a^3}$ where “m” is equal to $V * M_s$. After this renormalization, we can represent the energies given for two nanostructures and for two dipoles in the same graphic as showed in the figure 2-8.

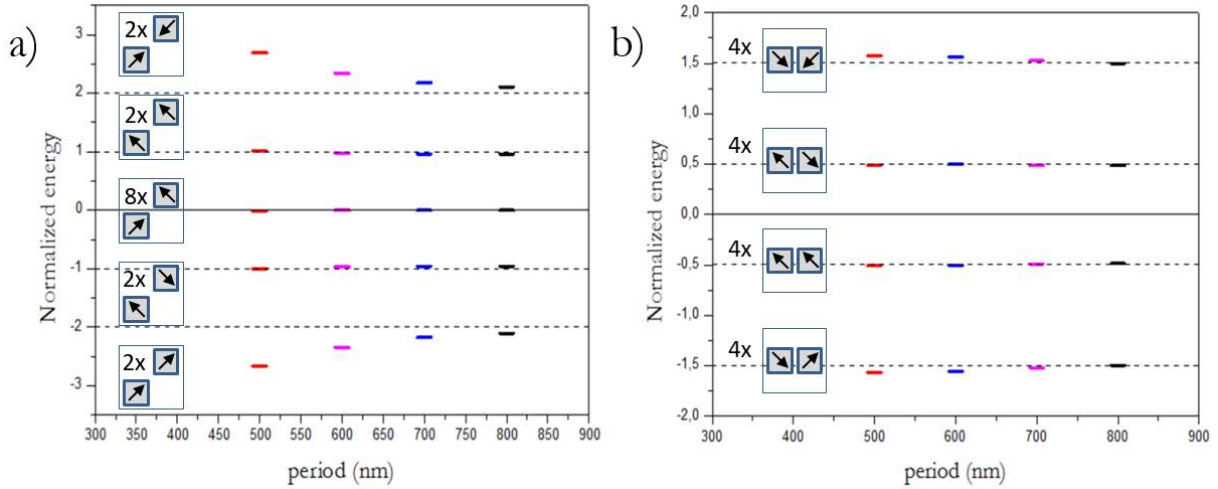


Figure 2-8_ Normalized energies as a function of period (given by micromagnetic simulations) for all the possible magnetic configurations between two nanostructures in the case of an alpha angle equal to 0° (a) and equal to 45° (b). The dashed lines represent the energies determined for a system composed by 4-state Potts spins (section 1.2).

Results from micromagnetic simulations are compared to the punctual dipoles energies (dashed lines) and we observe the same number of energy levels as in dipolar approximation framework and the energy hierarchy is conserved. Thus the micromagnetism, regardless the distance, does not show others properties than a system composed of two punctual dipoles, and so it seems reasonable to assume that the fundamental state for the experimental system should behave as expected in the first chapter.

Quantitatively, the coupling between elements should converge towards the dipolar approximation in the limit of large distances. It is indeed the case and for distance above 800 nm there are virtually no differences as the dipolar interactions decrease in $1/r^3$. For smaller distances, a difference exists and increases as the distance is reduced. This effect is very low for alpha of 45° but is significant for alpha of 0° with a coupling increased by 50% for a distance of 500 nm. This difference is simply explained by geometrical considerations as the distance between "closest moments" (the gap between elements) is smaller in the 0° geometry (77 nm at 0° versus 100 nm at 45° for 300 nm elements with a period of 500 nm).

To conclude, taking into account the spatial extension and a realistic magnetization distribution does not change drastically the interaction between artificial spins compared to the dipolar model. The nature of the coupling is exactly the same (same number of energy levels with identical sequence). It is only for the smallest distances and for alpha equal to 0° that a significant quantitative difference appears. This difference is limited to the energy of the low energy configuration (parallel spins) so the structure of the coupling is slightly different. Experimentally we will have to keep in mind that the coupling can be more efficient (and the system more prone to evolve towards its ground state) for alpha equal to 0° . Note that these differences are limited to the nearest neighbor coupling as it is negligible for large distances.

2.4 Summary and perspectives

Motivated by the properties shown by the dipolar 4-state Potts model in the case of systems composed by pure spins, the possibility to design experimentally this model was studied. In this aim, micromagnetic simulations have been selected as support in order to identify the conditions for the realization of this model. Up to now in the artificial spin systems, the nanomagnets designed could be count as Ising spins, thanks to an uniaxial shape anisotropy which imposes two preferential directions for the magnetization in nanomagnets [11, 12, 16]. Yet in this thesis, this solution could not be selected, due to the expected nature of the spin for the Potts model. In this aim several shapes were selected with one common property which is the respect of the cubic symmetry in order to stabilize the uniform monodomain in four preferential directions. Moreover due to a competition between exchange energy, dipolar energy and anisotropy energy, the mostly uniform monodomain configuration for the magnetization required for the realization of a Potts spin can be difficult to obtain experimentally. Thus added to the shape anisotropy (cubic symmetry), a particular crystalline anisotropy was selected which is the cubic anisotropy. In order to make the micromagnetic simulations, the material selected to respect the expected anisotropy was an iron layer. Two shapes were selected: a square and a disc, and for one of these shapes (square) the influence of the anisotropy axes was discussed. As one of the main purpose of this micromagnetic study was to determine under which conditions it is possible to obtain a nanomagnet with a uniform magnetization in its volume which can take 4 preferential directions, the stability of the monodomain state was studied. This study demonstrates that it is possible to obtain a uniform magnetization which can take 4 preferential directions in imposing as condition on the Fe layer a thickness around 2 nanometers.

Then as the two shapes could reveal the expected properties for the experimental state, a detailed observation of the magnetic configurations inside the nanostructures was realized. And it appears that a square with anisotropy axes aligned with its diagonals present the most adequate configuration for the realization of the spin model. Indeed this shape combined with this position of the anisotropy axes shows only four freedom degrees for the magnetization contrarily to the disc or to a square with anisotropy axes parallel to its edges.

Finally a last point remained to check: the validity of the dipolar approximation. And effectively the micromagnetic simulations reveal in the case of two nanomagnets that the coupling present the same behavior as this one revealed by the spin model.

In all the simulations presented here, no effects of temperature are considered. Nevertheless these effects are very important as we envisage to drive the system towards its ground state thanks to thermal fluctuations. It would be highly desirable to estimate the energy barrier between the four equilibrium states in order to optimize it. This barrier should be high enough to assure the stability at room temperature during the observation but low enough to achieve thermal reversal at reasonable temperature. Unfortunately it is not easy to estimate the barrier height from standard micromagnetic simulations. It would require to introduce a fluctuating field and follow the time evolution of the system during periods of the order of the second while keeping a temporal precision below the nanosecond. This is currently numerically impossible even for small systems. An alternative is to apprehend precisely the energy landscape between stable minima to compute directly the smallest barrier height between them. To do so, a collaboration has been establish with V. Lomakin (University of California San Diego) to use its FastMag code which include a Nudged Elastic Band method to determine the saddle point between two configurations. Preliminary results

show that the magnetization reverses in our system by nucleation in a corner and propagation of a 90 degree domain wall (figure 2-9). The barrier height associated to a 90 degree rotation is much smaller than the one associated to a complete reversal (which actually would take place by two 90 degree rotation). A barrier height of $60kT$ (at room temperature) has been estimated but these values rely on low temperature magnetic parameters (which are not relevant in our case). First quantitative evaluation of the barrier height leads to values not compatibles with experiment. Further investigations are necessary, particularly it is important to determine the magnetic parameters at the temperature of the thermal treatment.

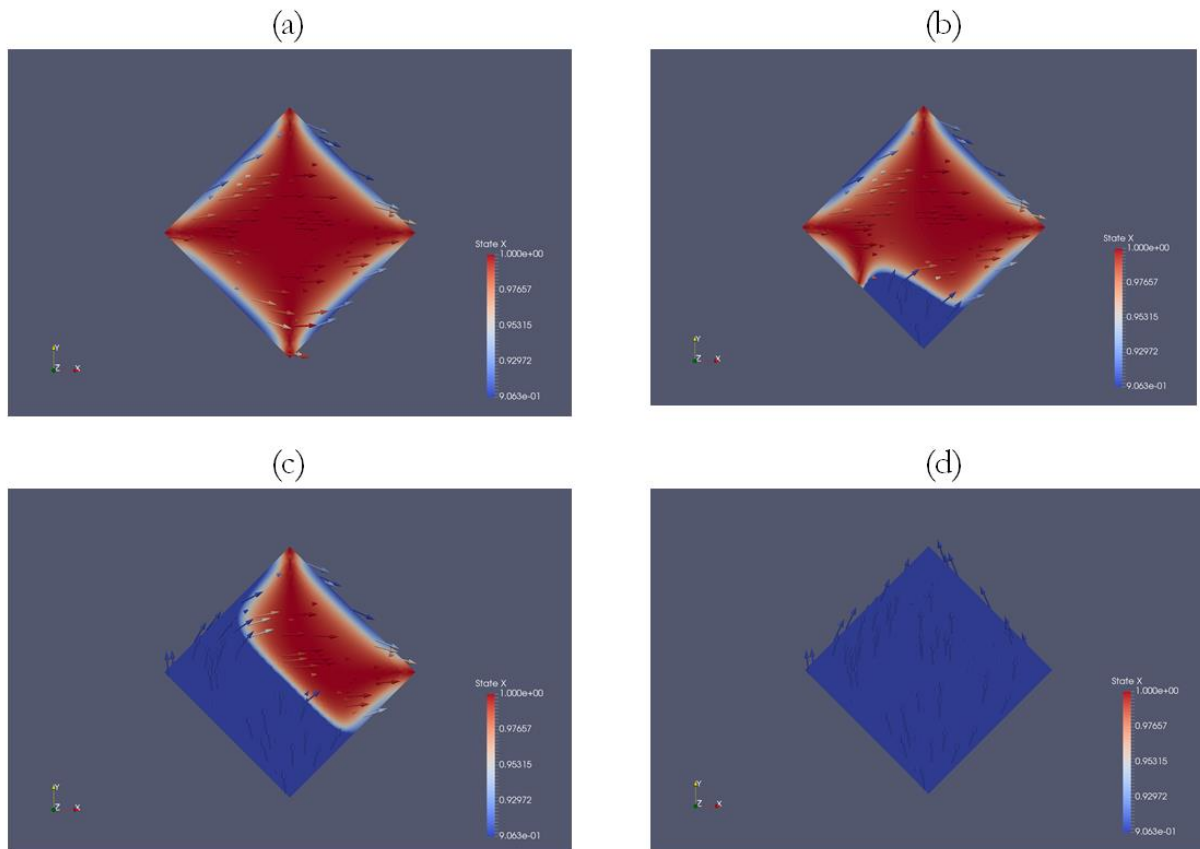


Figure 2-9_ 90° reversal process determined by FastMag for a square with a length of 300 nanometers patterned in a Fe layer with a thickness of 1.7 nanometers. The cubic anisotropy axes of the Fe are along the corner of the square. The four images represent different steps of the reversal process: (a) initial state where the magnetization is imposed along the x direction, (b) beginning of the nucleation in a corner, (c) propagation of the 90 degree domain wall, (d) final state where the magnetization is along the y direction (90° against the initial state). The red color corresponds to the spins along the x axis and the blue color corresponds to the spins along the y axis.

Bibliography

- [11] R.F.Wang et al, “Artificial ‘spin ice’ in a geometrically frustrated lattice of nanoscale ferromagnetic islands,” *Nature*. **439**, 303–306 (2006)
- [12] M.Tanaka et al, “Domain structures and magnetic ice-order in NiFe nano-network with honeycomb structure”, *J. App. Phys.* **97**, 10J710 (2005)
- [16] I.A Choar et al, « Nonuniversality of artificial frustated spin systems », *Phys. Rev. B.* **90**, 064411 (2014)
- [34] K.Mitsuzuka et al, « Magnetic vortices in single Fe-V disk with four folds magnetic anisotropy » *Appl. Phys. Lett.* **100**, 192406 (2012)
- [35] C.A.F.Vag et al, “Direct observation of remanent magnetic states in epitaxial FCC Co small disks”, *Phys. Rev. B.* **67**, 140405 (2003)
- [36] W. F. Brown, Jr. : *Micromagnetics*, Interscience Publishers, J. Wiley and Sons, New York (1963)
- [37] Kittel, « Introduction à la physique de l’état solide », Dunod, Paris, (1972).
- [38] N. W. Ashcroft et N. D. Mermin : *Physique des solides*. EDP Sciences, Les Ulis, (2002).
- [39] E. du Trémolet de Lacheisserie *Magnétisme*. Editions EDP Sciences (2000)
- [40] C. Kittel, “Physical theory of Ferromagnetic Domains”, *Rev. Mod. Phys.* **21**, 541 (1949)
- [41] D. J. Dunlop et al, *Rock Magnetism*, Cambridge studies in magnetism, Cambridge, p. 52 (1997)
- [42] D. R. Fredkin et al, “Numerical Micromagnetics by the Finite Element Method,” *IEEE Transactions on Magnetics MAG-23*, 3385 (1987)
- [43] A. Bagnérés-viallix et al, “2D and 3D calculations of micromagnetic wall structures using finite elements”, *IEEE Trans. on Magn.* **27**, 5 (1991)
- [44] T. Schrefl et al, “Modelling of exchange-spring permanent magnets,” *J. MAGN. MAGN. MATER.*, vol. **177–181** (1999)
- [45] M. E. Schabes et al, “Magnetization processes in ferromagnetic cubes”, *J. Appl. Phys.* **1**, 1347–1357 (1988)
- [46] R. Nakatani et al, “Changes in soft magnetic properties of Fe multilayered films due to lattice mismatches between Fe and intermediate layers”, *J. Appl. Phys.* **66**, 4338 (1989)
- [47] Scheinfein MR et al, “Micromagnetics of domain walls at surfaces”, *Phys. Rev. B.* (1991)
- [48] D. V. Berkov et al, “Solving micromagnetic problems - towards on optimal numerical”, *Phys. Stat. Sol.* **137**, 297 (1993).
- [49] A.Vansteenkiste et al, « The design and verification of Mumax3 », *AIP Advances* (2014)
- [50] Kittel, “Theory of the Structure of Ferromagnetic Domains in Films and Small Particles”, *Phys. Rev.* **70**, 965 (1946)
- [51] Prejbeanu et al, *IEEE Trans Mag* **37**, 20108 (2001)

-
- [52] A. Wachowiak et al, «Direct observation of internal spin structure of magnetic vortex cores », *Science* **298**, 577(2002)
- [53] P.O.Jubert et al, “Analytical approach to the single-domain-to-vortex transition in small magnetic disks”, *Phys. Rev. B.* **70**, 144402 (2004)
- [54] N.Rougemaille et al, “Chiral nature of magnetic monopoles in artificial spin ice”, *N. J. Phys.* **15**, 035026 (2013)
- [55] L.Heyderman et al, “Broken vertex symmetry and finite zero-point entropy in the artificial square ice ground state”, *Phys. Rev. B.* **92**, 060413 (2015)

3. EXPERIMENTAL REALIZATION OF THE DIPOLAR 4-STATE MODEL

3.1 Sample preparation

In the first section, the interest of the dipolar Potts model has been shown and in particular the modification of the ground state properties when rotating the angle between the spins and the lattice axis. In the second section, micromagnetic simulation demonstrated that nanomagnets under specific conditions can effectively reproduce the properties expected for the Potts spins. Our micromagnetic study shows that one of the most important parameters to design an “ideal” Potts spin (monodomain state in 4 possible direction) are a nanomagnet thickness below 2.5 nanometers, the presence of a cubic anisotropy and an in-plane magnetization. Based on micromagnetic simulation, patterned 2 nm-thick thin film of iron has been proposed as a good candidate for our study.

In order to get the best quality film (with high precision on the thickness and controlled crystalline structure), we used a molecular beam epitaxy method under ultra-high-vacuum. The set up I used is a Riber UHV-MBE with 2 electron-guns (for MgO and V deposition), 5 Knudsen cells (with Fe, Co, Ni, Au, and Cr). A reflection high-energy electron diffraction (RHEED) is used to control the crystal quality during deposition. The films were grown with the help of S. Andrieu and L. Pasquier. Further description of the techniques and the tools can be found in [56, 57]

The growth of epitaxial thin film of iron requires to choose a proper buffer layer. Not only the crystalline structure of the buffer matters but also the electronic properties at the buffer/iron interface (and in fact at iron/capping layer interface too). Indeed as showed for example in [58] for the case of Fe/MgO, an hybridization of the Fe layer due to a chemical contamination with the O present in MgO modifies the anisotropy of the Fe layer, and so in our case a chemical contamination of the Fe layer could modify the properties expected which would be problematic for the realization of Potts spins. And even without chemical contamination, the magnetic properties of the deposited thin film can be disturbed due to another effect which is a magneto-elastic effect linked with the strain during the deposition. Indeed as showed in the literature [59], and in particular for the Co/Au multilayers, this effect can lead to pseudomorphic growth of the thin film on the surface of the bottom layer, and thus given an anisotropy different as this one expected for the bulk. A large number of studies on ferromagnetic/non-magnetic interface have demonstrated the impact of the interface on the magnetic properties of the ferromagnetic layer and even demonstrate that the interface can be used in order to tune the properties in the magnetic layer [60, 61, 62]. For our experimental study of the dipolar spin Potts model, it is important to obtain a magnetic layer with only in-plane magnetization and cubic anisotropy in order to stabilize four monodomain states in the final nanomagnets. Thus an ideal choice for the sample composition would be a stack which allows very similar features as bulk iron for a 2 nm thick film.

3.1.1 The buffer

In order to determine the material composition, the first choice to do is to select a suitable buffer for this study with a negligible interface magnetic anisotropy. Based on previous works done in the laboratory, and in particular the thesis of Muriel Sicot, it appears that a Vanadium layer of 20 nm grown on single-crystalline MgO (100) substrate is a perfect candidate to obtain a good iron growth. This choice is motivated by the presence of a limited parametric misfit which is for the V/Fe around 5.6% [63], and also by the fact that their surface energies are really close, which suggest a 2D growth type [56]. Moreover it has been shown in previous study [64] that the critical thickness for plastic relaxation during Fe growth on V at room temperature in the same MBE as this one used for this work, is lower than 1 monolayer. Yet the targeted Fe thickness for this work is around 2 nanometers (15 monolayers) which is significantly larger than this 1 monolayer. And the last point which is also in favor of the V use, is the fact that the interface anisotropy observed in the literature [65-67] is always reported around few mJ/cm^2 . Thus this V buffer seems to match our criteria for buffer layer.

Thus the Vanadium deposited on the single-crystalline MgO (100) grows with the following epitaxial relation: V (001) [110]//MgO (001) [100], which means a growth at 45° angle between the V and MgO meshes. In our case the sample is grown on single-crystalline MgO (100) substrate using MBE with a base-pressure lower than 10^{-10} Torr and the bcc V (20nm) buffer layer is deposited at room temperature and annealed at 600°C . The annealing step is important in order to obtain the smoothest V surface possible, which is determinant in order to obtain a good epitaxial thin film of Iron. Usually the higher the annealing temperature is, the smoother the surface is. Nevertheless the V annealing temperature has been limited at 600°C because a surface reconstruction appears above 750°C due to a chemical contamination by oxygen absorption [68]. During the deposition, the growth and the crystalline quality is controlled by RHEED oscillations in-situ and the RHEED pattern for annealed V (at 600°C) along the (001) direction (figure 3-1) confirms a good crystalline quality of the V film.

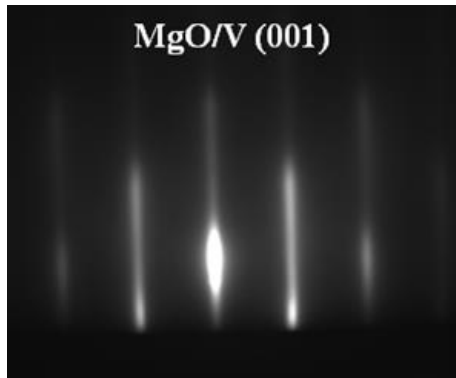


Figure 3-1_ RHEED patterns along the (001) bcc axis for annealed V (20nm) buffer layers deposited on MgO.

3.1.2 The iron deposition

After the V buffer deposition and annealing, 2 nm of bcc Fe is deposited in the same MBE chamber. During the deposition the bcc Fe grows in such a way that the direction [100] of Fe is finally aligned with the direction [110] of the MgO substrate. This Fe layer is grown at room temperature, then annealed at 350°C. For the same reasons as for the V layer, this annealing is essential in order to have the best crystalline quality and thus to have a Fe layer presenting the expected anisotropy. Annealing temperature of the Fe layer is kept much below 600°C at which V and Fe interdiffuses. The deposited thickness and crystalline quality of Fe has been controlled in-situ during the annealing thanks to RHEED oscillations and RHEED patterns (figure 3-2). From the RHEED pattern, one can note that the expected crystalline structure is obtained although the quality is not optimum due to the limited annealing temperature. Especially atomic roughness exist at the Fe surface and generate some dotted spot on the RHEED pattern.

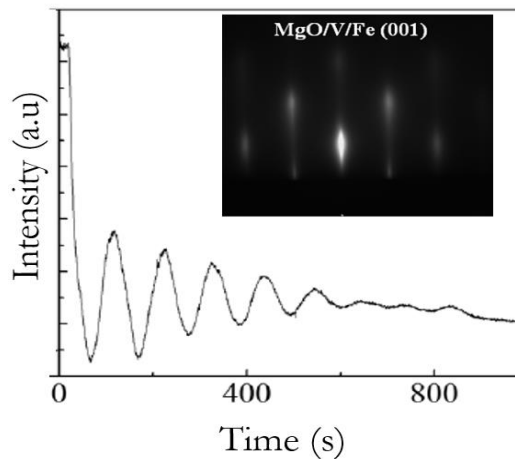


Figure 3-2_ RHEED intensity oscillations recorded during the growth of Fe on V (001). In inset, RHEED patterns along the (001) BCC axis for (a) annealed Fe (20nm) buffer layers deposited on MgO.

3.1.3 The capping

After the deposition of the Fe layer, it is important to cover it in order to avoid oxygen contamination. But, as for the buffer layer, the interfaces between the Fe layer and this capping layer can significantly affect the magnetic properties of the iron layer. In the literature, most of the time, the capping layers used are noble metals (weak porosity for the O) like Au layer, Pt layer or Pd layer. In our case and for the convenience (availability of the material) it has been decided to use Au layer. But this layer must not be deposited directly on the Fe layer. Indeed it appears that the interface Fe/Au present a perpendicular magnetic anisotropy [59]. Yet this perpendicular anisotropy could modify the stability diagram shown in the figure 2-4 in favor of the vortex state which in our case would be a problem. Thus in order to avoid perturbations on the targeted magnetization behavior, we tested 2 layers that could be inserted between Fe and Au, namely MgO and V. As discussed previously, Fe/MgO possesses also strong perpendicular magnetic anisotropy [63], so we have selected the V layer for the intermediary layer between the Fe layer and the Au layer. The final stack of the sample stack is MgO/V/Fe/V/Au.

3.2 Magnetometric study

Our sample composition includes two interfaces V/Fe. Yet, contrary to the interfaces MgO/Fe and Au/Fe, we should not find a significant value of the interface anisotropy for V/Fe interface. Although this interface has been widely studied [29, 69-71], we could not find any study providing a clear thickness dependence allowing to precisely determine this interface anisotropy value. Besides it is crucial to determine if with this composition, the sample obtained present effectively a cubic anisotropy and if it does not appear a supplementary anisotropy in the material due for example to a problem during the growth (crystallographic arrangement) or due to the interface anisotropies. This is why a detailed analysis of the magnetic properties is needed, and for this study the magnetization curves are measured using rotating sample vibrating sample magnetometer (VSM) and SQUID-VSM.

In order to obtain the interface anisotropies and all the magnetic properties of the sample, we have realized a magnetometry study on epitaxial V/Fe (t)/V trilayer, for different Fe thicknesses. And so the Fe layers of thickness t ranging from 0.7 nm (5 atomic layers) to 5 nm (35 atomic layers) were grown on V (20 nm) buffer and capped with V (5 nm)/Au (5 nm).

3.2.1 Fe volumic anisotropy

First, the volume (“bulk”) magnetization of a V/Fe (2 nm)/V film has been probed under both for in-plane and out-of-plane magnetic field in order to determine the magnetic easy and hard axes directions. The two hysteresis loops are presented in the figure 3-3.

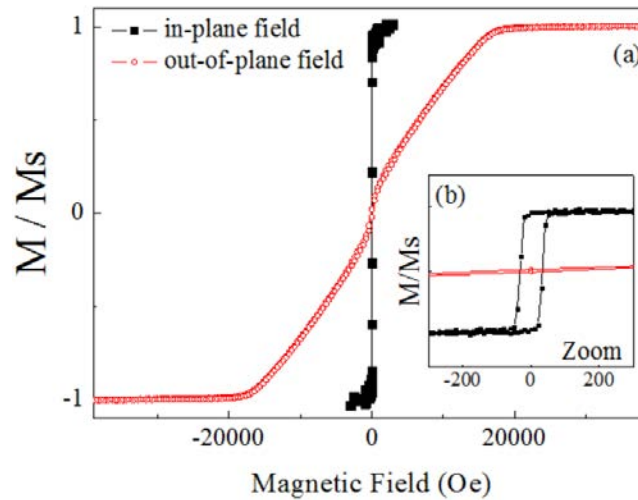


Figure 3-3_ (a) Normalized magnetization versus field loop for in-plane along (100) Fe direction (black solid squares) and out-of-plane (open red circles) field respectively for a V/Fe (2 nm)/V stack. (b) Zoom of the main figure around zero field show square hysteresis cycle.

The figure 3-3 shows normalized magnetization versus field loops for in-plane (black squares) magnetic field applied along Fe (100) direction and for out-of-plane (red circles) magnetic field. Thus it appears that the out-of-plane direction corresponds to a hard axis direction for the magnetization in the Fe layer. Moreover the figure 3-3 (b) shows clearly that the Fe (100) direction correspond to an easy axis direction. Indeed the black curve represent a square loop with full magnetization at remanence which is characteristic of magnetic easy axis. Thus thanks to the figure 3-3 it can be conclude that, as expected for the Fe bulk, the magnetization in the Fe layer lies

preferentially in the film plane. Now let's confirm the quadratic anisotropy of the Fe layer. In this aim the normalized remanent magnetization extracted from hysteresis loops obtained for in-plane applied field, where the field is applied in all sample directions from 0 to 360 degrees with a step of 1 degree, is plotted in the figure 3-4 (c).

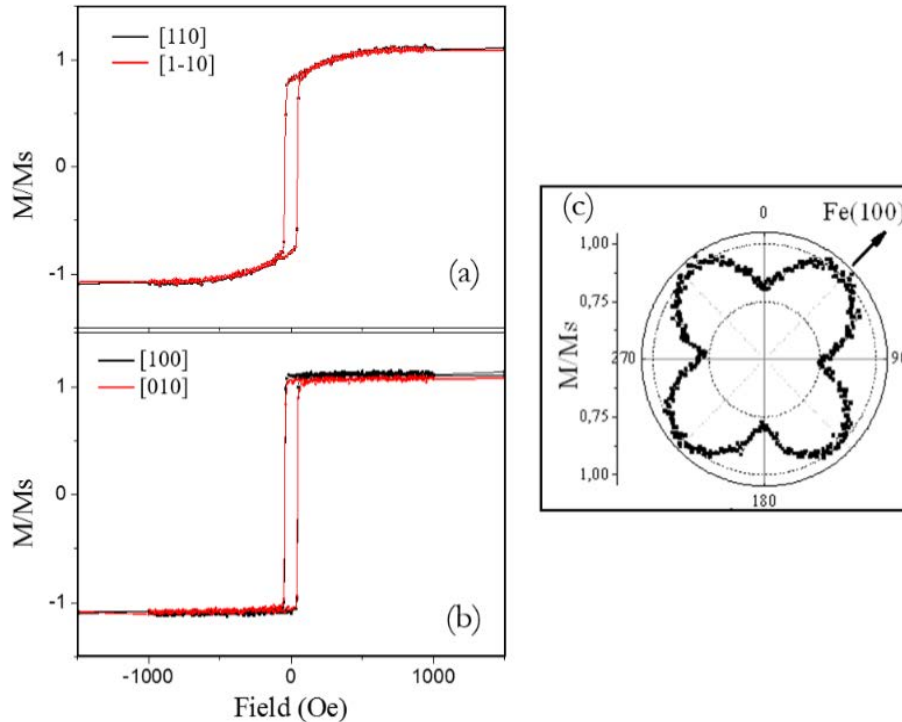


Figure 3-4_ (a) Normalized magnetization as a function of magnetic field applied in film plane along [110] and [1-10] directions. (b) Normalized magnetization as a function of magnetic field applied in film plane along [100] and [010] directions. (c) Normalized remanent magnetization as a function of field angle when applied in film plane demonstrates bulk cubic anisotropy.

The figure 3-4 (c) reveals four lobes with full remanence in Fe (100) directions and a remanent magnetization close to 71% in Fe (110) directions. This behavior of the normalized remanent magnetization is characteristic of cubic anisotropy as expected for cubic Fe bulk magnetic anisotropy. Thus with this figure, it appears that our sample possesses effectively a cubic anisotropy where the easy axes for the magnetization are in the Fe (100) directions. No distortion of these four lobes (four-fold symmetry) is observed so we can attest that no supplementary anisotropy like a uniaxial anisotropy exist in our Fe (2 nm) film. Indeed magnetization loops obtained for [110] and [1-10] are identical (figure 3-4 (a)) and [100] and [010] are also identical (figure 3-4 (b)). One can concludes from these measurements that there is no other in-plane anisotropies in addition to the “bulk-like” cubic anisotropy in the Fe layer.

3.2.2 Thermal stability

The thermal stability of the Fe film magnetic properties at high temperature is to be checked since annealing will be later used to reach ground states of the final Fe-based artificial spins system, as explained in details in the section 4.1.2. And so it is necessary that after an annealing, the sample keeps the magnetic properties shown here. In order to determine the thermal stability of this sample, it is annealed up to 400°C, cooled, and then the same magnetic measurements as those described in the previous section are realized. It appears that up to 400°C the material presents the same magnetic properties before and after annealing.

Thus thanks to these measurements, it seems that this MgO/V/Fe/V/Au respects the properties expected to design an artificial spins system which can correspond to the dipolar Potts model. But in order to be sure, it is necessary to determine precisely the interface anisotropies V/Fe and Fe/V presents in the sample, hoping that these interface anisotropies can be considered negligible. And for that a first step is to characterize the Fe magnetization according to the Fe thickness.

3.2.3 Magnetization versus Fe thickness

A way to determine the magnetization in the Fe layer is to represent the product of the magnetization at saturation by the Fe thickness (t), which is the areal magnetization, as a function of the deposited Fe thickness (t). Indeed this representation is supposed to give a straight line going through zero with a slope equal to the bulk Fe magnetization if there are not dead layers in the system. The term dead layer appoints an interfacial layer where the magnetization of the Fe is reduced when compared with the bulk magnetization. Thus the magnetization at saturation has been determined thanks to the magnetization versus field curves for the different Fe thicknesses, and represented in the figure 3-5. In this figure the magnetization at saturation values are obtained by dividing the measured moment values by the Fe volume corresponding.

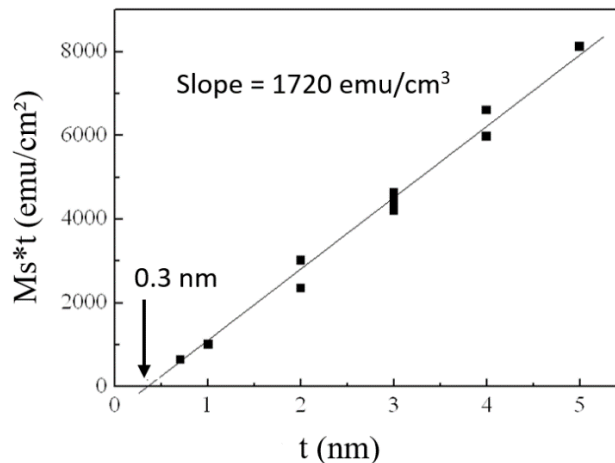


Figure 3-5_ Areal magnetization (M_s*t) versus Fe thickness (t), and the linear fit corresponding with a slope of 1720 emu/cm^3

The linear fit corresponding to the areal magnetization as a function of the Fe thickness presents a slope equal to 1720 emu/cm^3 , which is the value expected for bulk Fe. However this line does not cross zero for 0 nanometers but for 0.3 nanometer. This result shows a reduced Fe magnetization which occurs in average 2 atomic layers corresponding to the dead layers thickness. This result is

in concordance with a reduction of Fe magnetization at the V/Fe interface as reported in the literature. Indeed the literature explains this reduced Fe magnetization at this interface by roughness, intermixing and anti-parallel polarization, charge transfer of the V [69, 29, 72]. Moreover a study about V/Fe/MgO [64] where the Fe is grown on V with same conditions (same setup), has determined the same dead layer thickness while no dead layers were observed at Fe/MgO interface in Ref [73]. Therefore we can conclude that the reduction of the Fe magnetization in our V/Fe/V stack is mainly due to the bottom V/Fe interface. A possibility to explain this, is to compare the deposition processes for the two V layers. Indeed for the buffer layer (bottom interface), and contrary to the top layer (top interface), the V layer is annealed. Yet this annealing can be source of Oxygen contamination [70], which could explain why it is only at the bottom interface that the reduction of the Fe magnetization occurred.

The representation of the areal magnetization as a function of the Fe thickness showed that in the following part, we may need to consider an effective thickness for the Fe ($t-t_{dl}$) instead of the nominal deposited thickness (t).

After the determination of the effective Fe thickness ($t-t_{dl}$), it is possible to investigate in detail the role of the V/Fe and Fe/V interfaces on the Fe anisotropy, especially if they stabilize or destabilize in-plane Fe magnetization.

3.2.4 Interfaces anisotropy

The effective anisotropy constant is calculated from the anisotropy field H_{keff} . This anisotropy field is extracted from the out-of-plane field hard axis loops and the effective anisotropy constant is given by:

$$K_{eff} = \frac{1}{2} M_S \cdot H_{Keff} \quad (3-1)$$

This effective anisotropy possesses various origins which are: the magnetic volume anisotropy (K_v) in the Fe layer, the interfaces anisotropy (k_i), and the shape anisotropy for a thin film. Thus it is possible to write the effective anisotropy in CGS as follows [59]:

$$K_{eff} \cdot (t - t_{dl}) = (K_v - 2\pi M_S^2) \cdot (t - t_{dl}) + K_i \quad (3-2)$$

In the equation (3-2) a negative sign reflects the fact that the effective anisotropy tends to stabilize the in-plane Fe magnetization. Now it is interesting to plot the effective anisotropy times ($t-t_{dl}$) as a function of ($t-t_{dl}$), in order to quantify the different terms present in the equation (3-2) and thus determine the interfaces anisotropy.

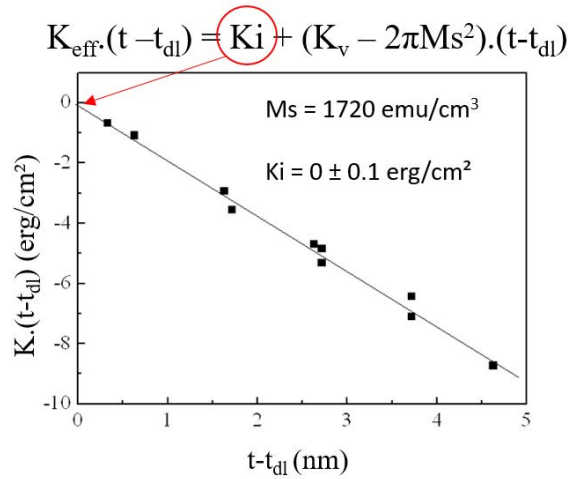


Figure 3-6_ Effective anisotropy constant K_{eff} times the corrected thickness $t - t_{\text{dl}}$ as a function of $t - t_{\text{dl}}$ at 300K for both V/Fe/V. The line is a fit using Eq. (3-2) where the negative slope corresponds to a magnetization 1720 emu/cm³ and the intercept corresponds to a value of $K_i = 0 \pm 0.1$ erg/cm²

In the figure 3-6, it appears that all the values are negative which confirms that the effective anisotropy favors in-plane Fe magnetization. The fit presented in the figure 3-6 uses the equation (3-2) with $K_v - 2\pi Ms^2$ negative and an intercept equal to 0. Moreover if it is taken the value of this slope and that it is considered only the $-2\pi Ms^2$ term, it can be extracted a value for M_s which is 1720 emu/cm³, and this value is in great agreement to the value measured in the figure 3-5. This observation confirms that K_v is small compared with the shape anisotropy [74, 75]. The intercept of this fit at zero thickness provide a direct determination of the value for the interfaces anisotropy. A value close to zero is extracted from figure 3-6. More precisely, taking into account the accuracy of our measurements and fit, we estimate the interface anisotropy as 0 ± 0.1 erg/cm². This value relates to both V/Fe (bottom) and Fe/V (top) interfaces. Since the atomic arrangement at V/Fe and Fe/V are different, it is not sure that the both interfaces lead to zero anisotropy. Nevertheless for our purpose, the most important information is that no additional interface anisotropy exist in addition to the bulk Fe anisotropy.

The above magnetic characterization confirms that MgO/V/Fe (2 nm)/V/Au stack is adequate to design an “ideal” Potts spin. It has an in-plane magnetization favorable for monodomain stabilization. Interface anisotropy is negligible so that it will not strongly affect the barrier height against spin reversal. Besides bulk-like cubic anisotropy is found which will help stabilizing the four possible monodomain states of the final nanomagnets. Finally thermal stability of the magnetic parameters have been demonstrated up to 400°C annealing. This fact is primordial because one of the main objective, as explained in the section 4.1.2, is to perform thermal demagnetizations to lead the system towards its ground state, and so it is essential that the system keeps the same properties after several annealing.

3.3 Samples overview

Thanks to the magnetometry study, it is confirmed that a sample with the following composition, MgO/V/Fe/V/Au, is a good candidate in order to design artificial spins systems which could represent experimentally the Dipolar Potts model. Then it remains to select the Fe thickness in this material. By observing the results of micromagnetic simulations (stability diagram), it appears that a Fe thickness below 2.5 nanometers is required. Thus in order to favor the stabilization of monodomain state in nanomagnets while maintaining enough magnetic signal to be detected during MFM measurements, we select a nominal Fe thickness of 2 nanometers for all the samples realized for this work. Considering the magnetic dead layers presence, the effective Fe thickness is in fact 1.7 nanometers.



Figure 3-7_ Sample composition (applicable to all the samples used for the realization of artificial spins systems in this work). The mentioned thicknesses are the nominal thicknesses, and so the effective thickness of Iron is 1.7 nm.

The experimental results shown in the chapter 4 are related to three different samples which have been realized in the same conditions (same setup) but at different dates. The common stack is detailed in figure 3-7. The first sample (sample #1) has been realized in November 2014, the second sample (sample #2) has been realized in January 2015 and the third sample has been realized in June 2015. It is assumed that these samples present the same properties but it is possible that it exists some minor differences between them. Note that for the preliminary tests described at the end of this chapter, previous samples made with the same setup and presenting the same properties have been used. Now that the adapted material to design an artificial Potts 4-state spins system is selected, it is possible to design the lattices. But before this realization, it is necessary to define the experimental parameters related to the theoretical parameters used to describe the dipolar Potts model.

3.4 Lattices and alpha definition

For the experimental realization of arrays of “Potts spins”, with four preferential directions, it’s necessary to describe the different lattices which are studied as well as the alpha angle mentioned in the section 1.2. Indeed in the previous chapters, it is shown that the behavior of the fundamental state changes drastically as a function of the angle alpha between the spin direction and the axis connecting two spins as shown in the figure 3-8.

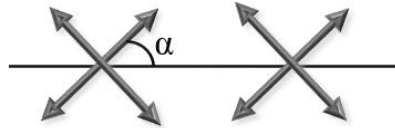


Figure 3-8_ Representation of the alpha angle in the case of two Potts spins

Experimentally, in lattices, this angle is defined as the angle between the magnetization direction inside nanostructures and lattice axis. As shown in micromagnetic simulations, an easy way to stabilize monodomain configuration in nanostructures is to use thin Fe squares where the easy magnetization axes of Fe are placed along the squares diagonals. Thus in a lattice, the alpha angle represents the angle between the easy magnetization axes which is the magnetization direction and the lattice axis.

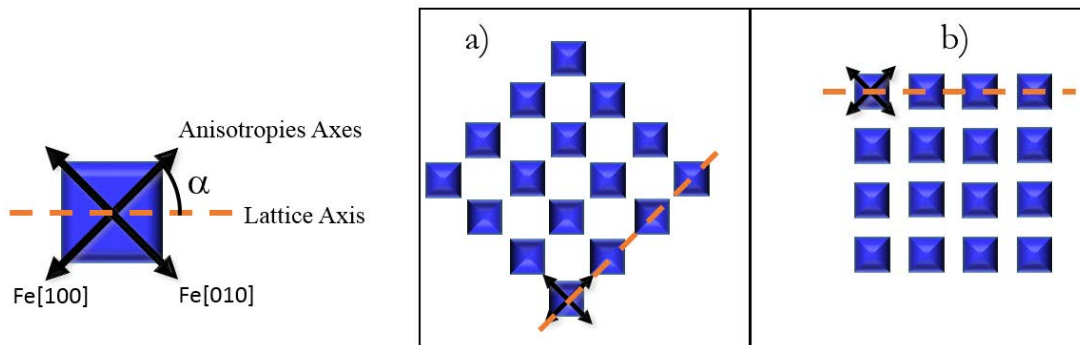


Figure 3-9_ Experimental definition of the alpha angle, which is defined as the angle between the [100] Fe direction and the lattice axis. (a) Representation of a 0° lattice, where the [100] Fe direction is aligned with the lattice axis. (b) Representation of a 45° lattice, where the [100] Fe direction generates an angle equal to 45° with lattice axis.

It would be great to compare experimental fundamental states of a lattice for an infinity of angles to compare the results with these predict by the dipolar 4-state Potts model. But experimentally the system can’t be studied for an angle continuum and for an infinite lattice. Thus for the experimental study the choice is done to study three angles which are 0, 22.5 and 45 degrees, and to take squares lattices including 30x30 nanomagnets (squares). The choice of these angles is relevant in the way it’s expected different fundamental states for the three angles. The lattice size is selected for the convenience during the imagery. Indeed for time issues, it’s preferable to limit the necessary number of scans to observe an entire lattice. However, as observed in the stability diagram, the squares size composing the lattices should range between 100 nanometers and 1 micrometers, in order to stabilize monodomains states in nanostructures. Experimentally (after several tests presented further in the manuscript) the ideal frame size to maximize magnetic contrast for the maximal number of squares in the field of view is 20 micrometers. Thus with a size of 30x30 squares, depending of the period lattice, the entire lattice can be observed with reasonable number of scans, typically four scans.

For the lattices realization, the choice is done to produce different square sizes in order to find which size shows the best agreement between MFM measurement and demagnetization efficiency. Indeed the larger is the square size, the larger the magnetic contrast is. Nevertheless as a function of the square size, the demagnetization parameters may be modified, for both field demagnetization and thermal demagnetization. Therefore testing several nanomagnet sizes is interesting in order to check which size is the most adapted ones.

The last important parameter is the distance between nanostructures inside the lattice since neighboring nanomagnets interact through long range dipolar interactions. For the purpose of having the strongest coupling between nanomagnets, the lattice period which is defined as the distance center at center between two squares, must be the smallest possible. In order to observe the dipolar coupling influence in experimental results, different periods are realized and these lattice periods depend on the squares size. Finally, the different sizes of the nanostructures and the different periods of lattices are identical for the three studied angles.

3.5 Nanofabrication

3.5.1 Ebeam lithography

To realize an artificial spin lattice, the use of Ebeam lithography is the best candidate, as this experimental technique allows to produce patterns with a nanometric resolution on micrometric scale [76]. The Ebeam lithography principle is the following: an electron beam controlled by a software (in our case RAITH 150) allows to draw patterns in an electron-sensitive resist. In our case the different patterns (lattices composed of squares) for the Ebeam lithography have been defined with the software Mathematica then imported in the lithography software.

The use of an e-beam gives a really high resolution for the patterns, better than in photolithography where it's use a photon beam which limits the resolution due to the wavelength. But this high resolution has a price which is the time. Indeed for the Ebeam lithography, the e-beam does not draw all the patterns at the same time but draw progressively the patterns one by one. As mentioned previously, in Ebeam lithography the use of photosensitive resist is necessary. This resist has the property to change its solubility or its speed chemical attack after an insolation by the e-beam, and this property allows to obtain the patterns by solubility difference. Indeed after insolation, according to the resist nature (positive or negative) the exposed resist is more (for negative resist) or less (for positive resist) soluble in the developer than the unexposed resist and so after a development of the resist, only the exposed areas stay (for positive resist and the other way for negative resist).

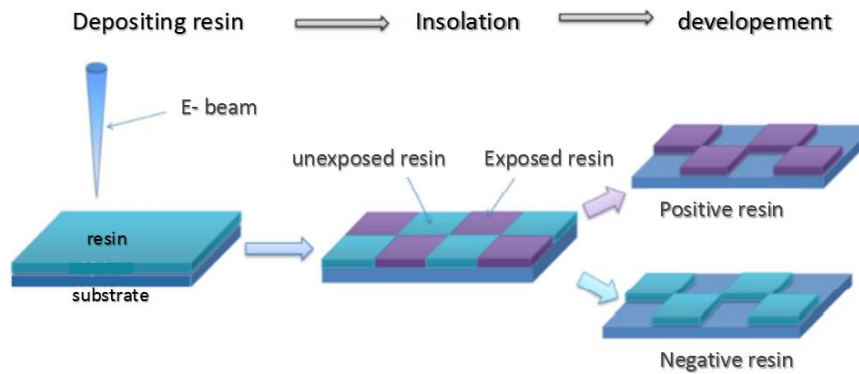


Figure 3-10_ Ebeam lithography process

For the realization of our patterns, the resist used is a two-layer positive resist composed of PMMA/MMA, whose the superior layer is harder than the underlying layer. The use of this two-layer resist present the advantage to create a “cap” profile which will favor a discontinuity in the aluminum layer deposited in the next step. Indeed when the patterns is drawn in the resist by Ebeam lithography, an aluminum layer is deposited and this layer is used as mask for the ionic etching.

3.5.2 Aluminum mask deposition

For the aluminum deposition, the experimental technique used is the thermal evaporation technique which is based on ebeam evaporation. Indeed the Aluminum is heated up to evaporation by ebeam evaporation in order to deposit some aluminum atoms on our sample. In our case an aluminum layer with a thickness of 60 nanometers is deposited on the surface of our sample. Then the resist is removed with acetone (lift-off) and thus at the end it appears on the surface of our sample, areas in aluminum which represent the desired patterns.

3.5.3 Ionic etching

After the aluminum deposition and the lift-off, the last step is to etch the sample. In order to etch the sample, the technique used is the ion beam etching (IBE). The principle of this technique is to send a directional beam composed of rare gas ions on the sample. During the etching, the whole sample surface is exposed, i.e. the magnetic layer as well as the area protected by the aluminum. In our case, the thickness of 60 nanometers for the aluminum layer has been chosen in order to insure that at the end of the etching, it remains aluminum in the protected areas while for the unprotected areas, the magnetic layer has been totally removed. So at the end of the etching, we can observe on the sample the nanostructures in the magnetic layer covered of aluminum and the material which separates these nanostructures will be only the substrate. Thus the last step should be the removing of the aluminum present on the top of the patterns. Unfortunately the usual aluminum removers (Remover PG...) are not adapted for our sample as they also attack vanadium (see figure 3-11).



Figure 3-11_ MEB image after chemical etching of the aluminum layer. The surface appears dirty due to the attack of the remover on the Vanadium layer.

This “problem” is not studied in detail because the aluminum remaining at the end of the process does not prevent to observe, with magnetic force microscope (MFM), the magnetic contrast in the nanostructures.

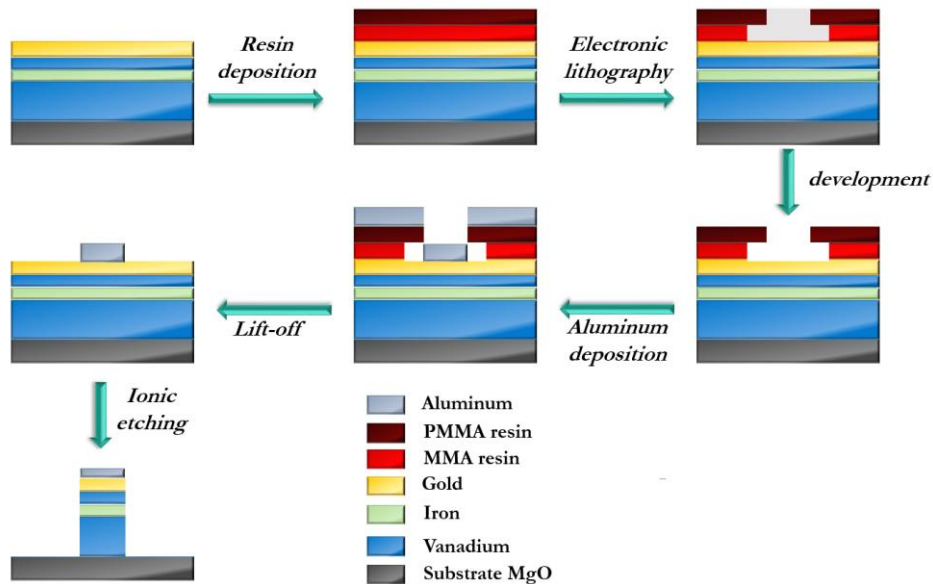


Figure 3-12_ Nano-structuration process used for the experimental realization of the artificial spin system

3.5.4 Dose optimization

The quality of lattices depends strongly on the exposure dose used during the lithography process. The dose represents the quantity of charges by unit area. This factor is determined at the beginning of the lithography and depends on the resist, the size and the environment of the patterns. Thus in our case this factor will depend on the squares size composing the lattices, and also the period of the lattice, which can be incorporated in one parameter, the filling rate. The easy way to determine which dose is the most adapted for the different lattices, is to use a dose test. For that, the different lattices are realized with different doses on the same sample and then the lattices are observed with the scanning electron microscope (SEM) in order to determine which doses give the lattices expected (squares size and periods respected). The doses used for the realization of the lattices are calculated from a nominal dose, which is $120 \mu\text{C}/\text{cm}^2$, at which it's multiplied a dose factor.

For all the lattices, the nominal dose chosen is $120 \mu\text{C}/\text{cm}^2$ and the dose factor varies from 0.8 to 2.2 with 0.2 increments, and it's observed for all the dose factors which dose is adapted. In the following images, we can observe an example corresponding to the lattice with a square size of 1000 nm and a period of 2000 nm for three doses.

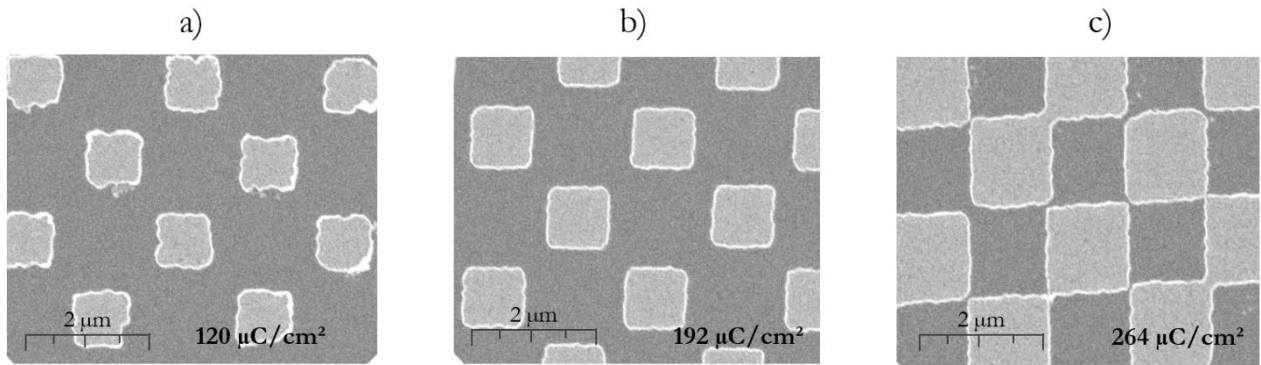


Figure 3-13_ Comparison for a lattice obtained with different doses: (a) underexposed; (b) well exposed; (c) overexposed

When the dose is too low, the square size is smaller than expected and the squares are not completely formed (figure 3-13 (a)), while when the dose is too strong, the square size is bigger than expected, decreasing in this way the period (figure 3-13 (c)). By doing the test dose for the different lattices and so the different filling rates, we can observe the minimal dose for which lattices are well defined (as expected) as a function of the filling rate. But before that it is required to set the filling rate related to each lattices. In our case the lattices are square lattices composed of 30×30 squares. In this case the filling rate is given by the equation (3-3):

$$\eta = \frac{L^2}{c^2} \quad (3-3)$$

where L is the squares size composing the lattice and c is the period (distance center at center between two squares).

Then in order to obtain a relation between the filling rate and the optimal dose, a test sample is realized where lattices with different filling rates are present. To be sure that the relation is valid for any parameters lattices, different square sizes and period are realized, and this for the three angles 0 , 22.5 and 45° . The parameters used and the results related to the dose test are shown in the figure 3-14.

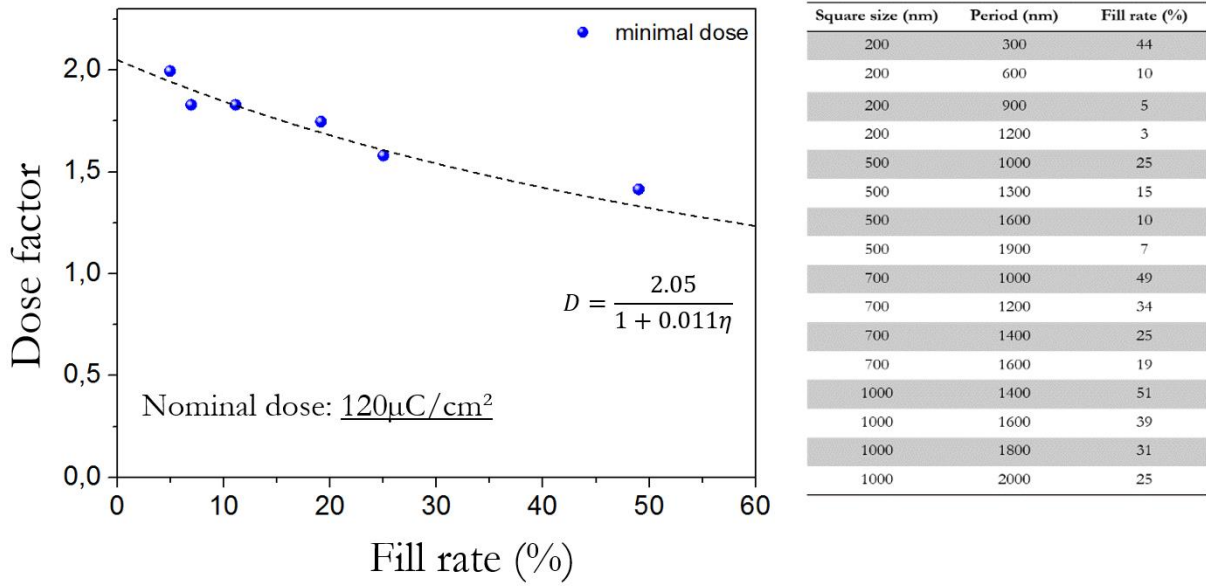


Figure 3-14_ Dose factor as function of the filling rate (in percentage). The blue point correspond to the minimal dose for which the lattices are well defined. The dashed line corresponds to the fit of the blue points and which gives the relation corresponding to ideal dose.

In the figure 3-14, it is represented the minimal factor dose for which the lattices present the parameters expected (square sizes and periods) according to the filling rate. In fitting this curve, a relation between the minimal factor dose corresponding to a well-defined lattice and the filling rate can be extracted:

$$D = \frac{2.05}{1 + 0.011\eta} \quad (3-4)$$

, where D is a dose factor and η is the filling rate.

Thus for our lattices, it is possible to calculate the filling rate and to find the factor dose adapted for the Ebeam lithography.

3.6 Magnetic characterization and tip influence

Now that the optimal conditions for the nano-structuration of our artificial spin system are defined and that the MEB imagery confirms the expected topography for the different lattices, a magnetic characterization is required. Indeed the aim of the realization of these lattices is to compare the fundamental states obtained experimentally with those expected by the spin model. And as part of this problematic, it is essential to have a direct access to the magnetic configurations in the lattices.

In order to do that, the atomic and magnetic force microscopy (AFM, MFM), is commonly chosen as characterization technique for the artificial spin systems. In the nano-materials, nano-scale devices and particularly in the artificial spin systems, this technique has become standard characterization tool [77]. In the following, first we will discuss the magnetic contrast obtained on the nanostructures and we will confirm the monodomain magnetic configurations and its stability.

During the scan with MFM, the tip acts like a magnetic dipole with a leakage field and this field interacts with the nanostructures magnetization. Reference in the literature [78] shows that this interaction can easily disturb the magnetic configurations present in nanomagnets. So a first question is to know if this interaction modifies the magnetic configurations in the nanostructures when the probe is scanning. To that purpose a sample we used square sizes between 100 and 1000 nanometers with periods ranging from 200 nanometers for the smallest squares to 2000 nanometers for the biggest.

3.6.1 Standard tip

First a standard tip is used for the MFM scanning. The magnetic material for the standard tip is made of a CoCr magnetic layer with a thickness of 50 nanometers. In the case of our nanostructures (square), The expected magnetic contrast observed in MFM for monodomain and vortex configurations is represented in the figure 3-15.

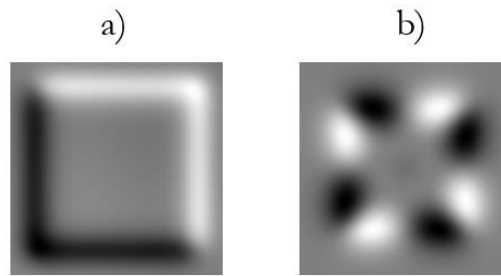


Figure 3-15_ Magnetic contrast expected for two magnetic configurations shown by the MFM for a square. These images are given by micromagnetic simulations obtained from Mumax3. (a) Monodomain along a diagonal characterized by the presence of a white corner and a black corner. (b) Vortex configuration characterized by an alternation between white and black contrast.

As it is observed in the figure 3-15, the magnetic contrast obtained for a monodomain is represented by a black corner and a white corner which describe the monodomain orientation. In MFM, according to the tip magnetization direction, a magnetic configuration in the nanostructure can take two opposites contrasts. Thus for a monodomain, the magnetization direction can be defined as from black corner to white corner or vice versa. For our study the choice is done to keep the same magnetization tip for all the measurements which, for a monodomain, fits a magnetization direction defined from black corner to white corner.

In order to determine if it is possible to observe a magnetic contrast related to monodomain configurations in nanomagnets, the sample is saturated along an anisotropy axis before the MFM measurement, in order to know the initial magnetization direction in the nanomagnets. It has to be noticed here that as the saturation field related to the nanomagnets is not known, the maximum amplitude field available with our electromagnet is used (3600 Oe). It is reasonable to think that this field possesses an amplitude enough to saturate the lattices as the saturation field determined for the full film is only 50 Oe. Then the lattices are observed in MFM and the magnetic contrast obtained is analyzed. In the figure 3-16, the magnetic contrast related to a 45° lattice composed of 300 nanometers squares is represented.

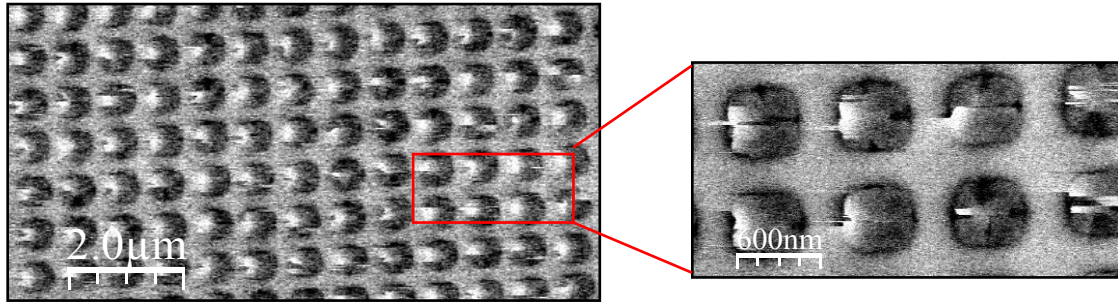


Figure 3-16_ MFM image obtained with a standard tip for a lattice composed of 300 nanometers squares and with a period of 700 nanometers.

This contrast can be compared at the contrast expected for a square relevant a monodomain along a diagonal as shown in the figure 3-15. Thus it appears that the contrast obtained after an MFM measurement is different than that one expected for a monodomain. Moreover, some white trails appear on the MFM images revealing an interaction between the leakage field of the tip and the magnetization in the nanostructures. This result is similar for all the lattices, regardless of the squares size, the period or the angle lattice. Moreover different lift heights are tested and for all the heights, the results obtained are the same as those shown in the figure 3-16. Thus this measurement reveals that the leakage field generated by a standard tip interferes with the magnetization in the nanostructures, and that the magnetic configurations observed in the squares are not monodomains. In order to reduce the leakage field of the tip, a solution is the use of a low moment tip.

3.6.2 Low moment tip

Like for the test with a standard tip, the sample is saturated along an anisotropy axis direction but this time, for the MFM measurement, the tip used is a low moment tip which is made of CoCr with a thickness of 15 nanometers. Thus in decreasing the magnetic layer thickness of the tip, the interaction between the leakage field of the tip and the magnetization in the nanostructures is reduced. We can observe the magnetic contrast obtained with this tip for a lattice composed of 300 nanometers squares with a period of 1.3 micrometers in the figure 3-17.

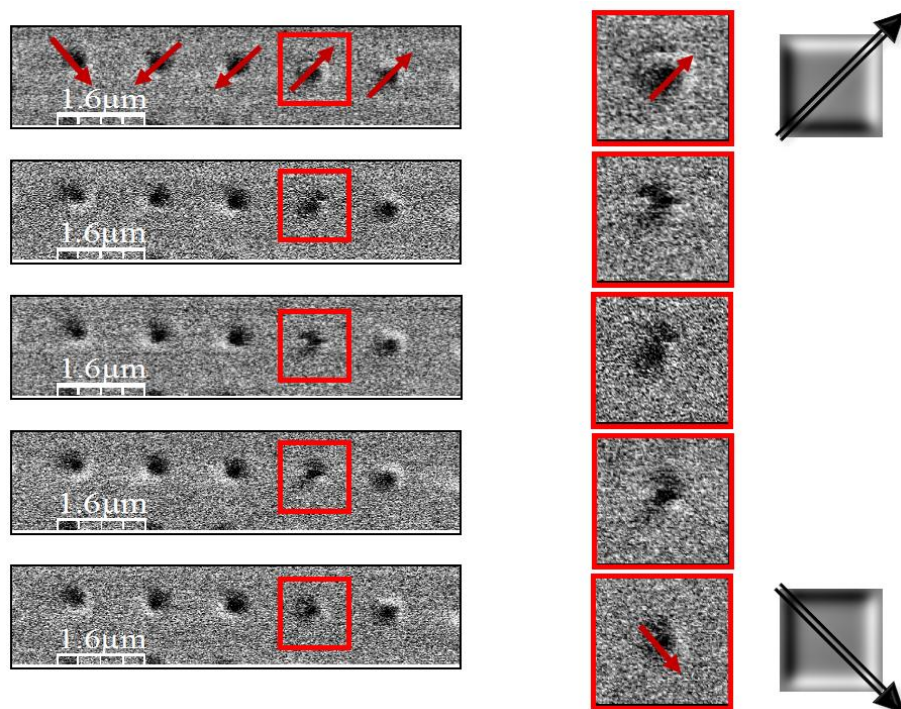


Figure 3-17_ MFM images obtained with a low moment tip: Zoom of a lattice composed of 300 nanometers squares and with a period of $1.3 \mu\text{m}$. This figure shows five consecutive scans of the same region in order to identify a possible perturbation during the measurement. Indeed a first scan present magnetic contrasts consistent with the presence of monodomains in the nanostructures. However the directions for these monodomains are not identical and it is assumed a perturbation of the magnetic configurations due to the leakage field of the tip. This is confirmed thanks to these 5 consecutive scans.

First it appears that for this lattice the magnetic contrast in all the squares represent monodomains. However despite the saturation, the observed magnetic contrasts show different directions for the monodomains. This observation can be made for all the lattices, regardless of the squares size, the period or the angle lattice. It appears also that the larger is the squares size, the larger the number of squares showing magnetization along the saturation direction is. As the monodomain directions are different, two possible explanations can be given. The first is that the saturation field is not large enough to align all spins, and the second is that the leakage field of the tip can perturb the magnetic configurations of the nanomagnets. It turns out that the second hypothesis is the right one. In figure 3-17 several consecutive scan, reveal the tip influence on the magnetization in the squares. Indeed one can observe between the different scans a contrast modification for a same square, even observing a 90 degrees rotation between the first and the fifth scan.

As a conclusion of this part, it is possible with a low moment tip to observe a magnetic contrast which is consistent with a monodomain in nanomagnets and this regardless of the square size, period or angle lattice. But the leakage field of the tip, during AFM scan, remains too strong in order to not disturb the magnetization in the nanomagnets.

3.6.3 Low moment tip combined with spacer layer at surface sample

In order to do a MFM scan, the topography of the surface is firstly recorded in using a tapping mode where the distance between the tip and the surface is imposed by the interaction between the both. Then a second scan is done in following the surface previously recorded at a certain height (lift height) in order to quantify only the magnetic sample-tip interaction. Thus during a scan, it is possible to tune the lift height, but for the first AFM scan in tapping mode the distance between the tip and the surface of the sample is imposed. A solution to limit the tip-sample interaction during the tapping mode consists in increasing the distance between the tip and the magnetic layer by adding a supplementary layer on the sample as represented in the figure 3-18. Several materials were tested as spacer layer.

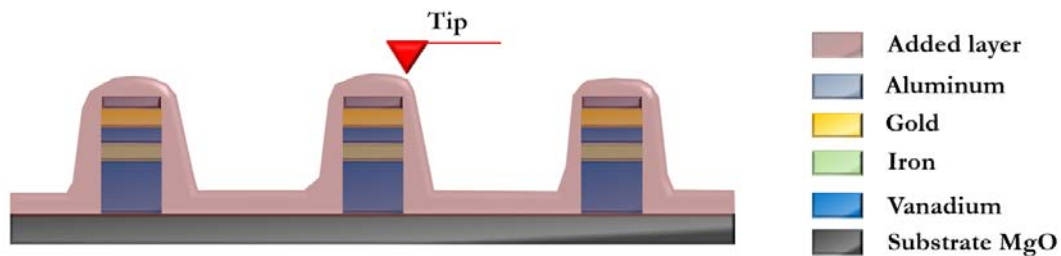


Figure 3-18 During a MFM scan, it is possible to increase the distance during the magnetic measurement in playing with the lift height, but it is not possible to change the distance between the first scan (tapping mode) which gives the topography of the system. However this scan is necessary in order to determine which contribution is related to the topography and which contribution is related to the magnetic interactions. Thus a solution is to increase the distance between the tip and the surface sample with a spacer layer deposited at the top of the sample. This case is represented in this figure.

3.6.3.1 Spacer layer of PMMA

First, PMMA resist used during the Ebeam lithography is used because it is easily removable if needed after AFM/MFM measurements. For PMMA deposition, a thickness of 80 nanometers is selected and a topography study is done with AFM in the aim to compare the nanostructures with and without the spacer layer of PMMA. In the figure 3-19, an AFM height profile for a square of 500 nanometers for the case with PMMA and without PMMA. It appears that with the spacer layer of PMMA, the squares are still identifiable with the AFM but the topography is smoother. This is expected since the resist is deposited by spin coating which is known to provide uniform coverage of thin film sample underneath.

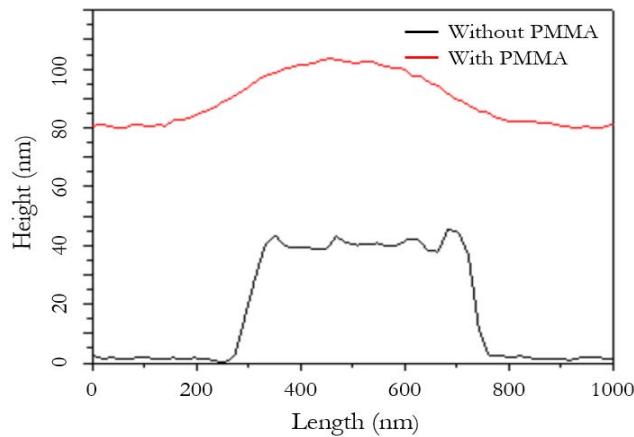


Figure 3-19_ Height profile given by AFM measurement in the case of a square of 500 nanometers for a sample with and without the spacer layer of PMMA.

Let's now verify if it is possible to observe the magnetic contrast with 80 nm PMMA capping layer and if the PMMA layer prohibits the low moment tip influence on the square's magnetic configuration. In order to do that, after the PMMA deposition the sample is saturated along an anisotropy axis with a saturated field of -3000 Oe (same amplitude field as the measurements presented in the section 3.6.1 and 3.6.2).

After the MFM measurement it appears that the contrast obtained is different from the contrast expected for monodomains or vortex. The contrast observed over the nanomagnets corresponds to an out-of-plane magnetization. However, the previous MFM measurements have proven that the magnetization in nanomagnets lays in-plane. So the contrast may not be a magnetic one. To check it, a solution is to magnetize the tip in the opposite direction. The results are presented in the figure 3-20 (a).

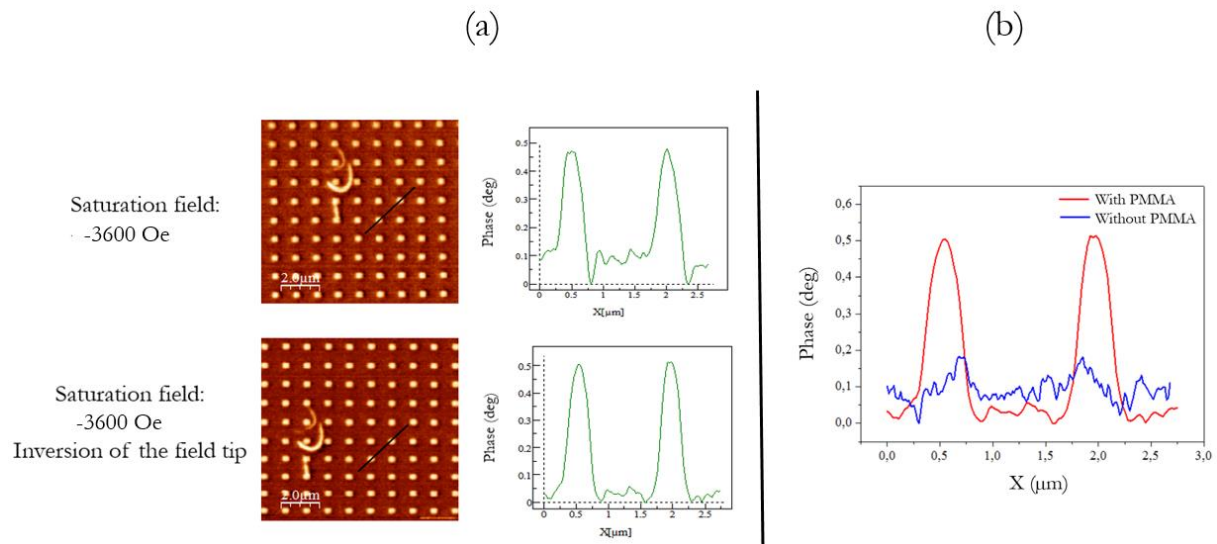


Figure 3-20_ (a) MFM images of a lattice (left image) and phase profiles (right image), related to the black lines present in the MFM images, in the case of a saturation field of -3000 Oe and for a tip magnetized in the opposite direction as usual. These three measurements allow to determine the contrast nature. Indeed if the contrast is magnetic, an inversion of the field tip, gives rise to an inversion of the contrast observed. (b) Comparison between phase profiles obtained for the same nanomagnets with and without the spacer layer of PMMA. The saturation field is the same for the two measurements (-3600 Oe).

After an inversion of the magnetization tip, the contrast obtained stays the same (see figure 3-20 (a)). The fact that the contrast does not change with the tip magnetization shows that the contrast obtained is not a magnetic contrast. To confirm our conclusion on the non-magnetic nature of the contrast, we compare (figure 3-20 (b)) the phase profile for the same squares and same lift height, with and without PMMA, shown in figure 3-20 (b). The magnetic contrast (without PMMA) corresponds to a phase of around 0.2 degrees. With PMMA, the phase is much larger, around 0.5 degrees, although it is expected to be much smaller for the same lift height (the Fe layer being two times further). This comparison confirms that the contrast observed with PMMA is not a magnetic contrast.

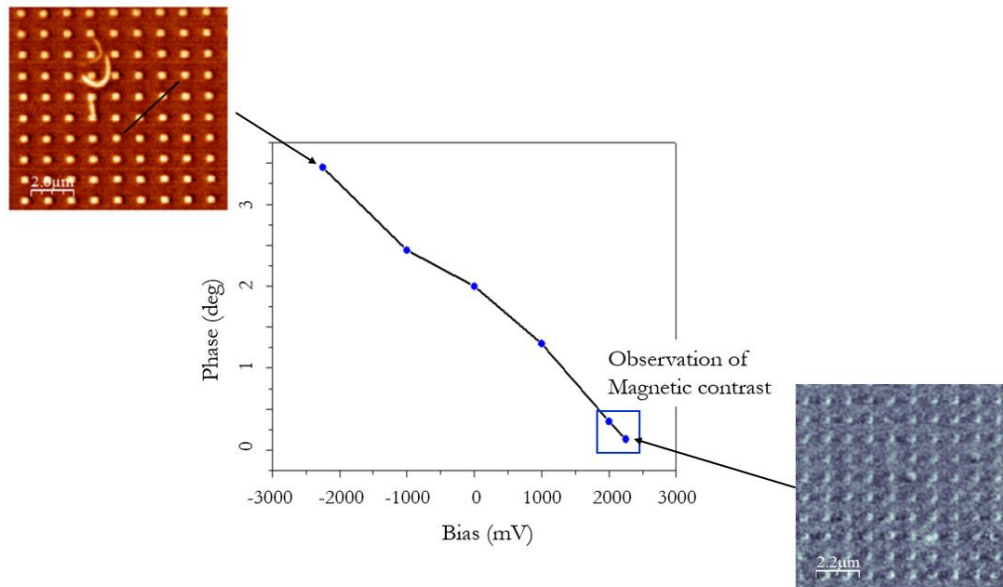


Figure 3-21_ Phase obtained from MFM measurements as a function of the voltage applied on the tip (bias). The results presented here are the average values of the phases for the same lattice.

In order to see if this contrast is a charge contrast, it is possible with the MFM to apply a bias to charge on the tip and thus compensate for eventual charges in the PMMA to have access only to the magnetic contrast. The phase is plotted as a function of the applied bias in Fig 3-21. The phase increases when the applied bias decreases, while the phase changes quasi-linearly from large negative bias to large positive bias. Phase of the order of magnetic contrast phase is obtained for a bias around 2000 mV. Similar results have been obtained for all the lattices, regardless of the square size, of the angle or of the period. We can definitively conclude that the contrast obtained after the PMMA deposition is a charge contrast. For the following experiments, we could apply a tip bias to measure the magnetic contrast. Nevertheless for each PMMA deposition, the bias required to observe the magnetic contrast is different and so for each PMMA depositions, a study as function of the bias would be necessary. This is particularly annoying since PMMA needs to be removed before each thermal demagnetization. So we choose to use another spacer layer.

3.6.3.2 Spacer layer of Aluminum

Aluminum may be a better choice than PMMA as spacer layer. Indeed as mentioned previously aluminum remains on top of nanostructures at the end of the nanofabrication process and it does not seem to disturb the MFM measurements. The first test is made with 20 nm of Aluminum deposited by sputtering. The sample with Aluminum spacer layer is saturated along an anisotropy axis and then installed in the AFM/MFM. The topography of the nanostructures measured by AFM is shown in figure 3-22 (a) and it appears that the nanostructures obtained after the deposition of spacer layer of Aluminum, have the same shape as without the spacer layer but with a difference which is the presence of collars of about 10 nm height (see figure 3-22 (c)). This result is obtained regardless the size squares as well as the periods. The presence of these collars is not a problem for the MFM measurements since Aluminum is not magnetic.

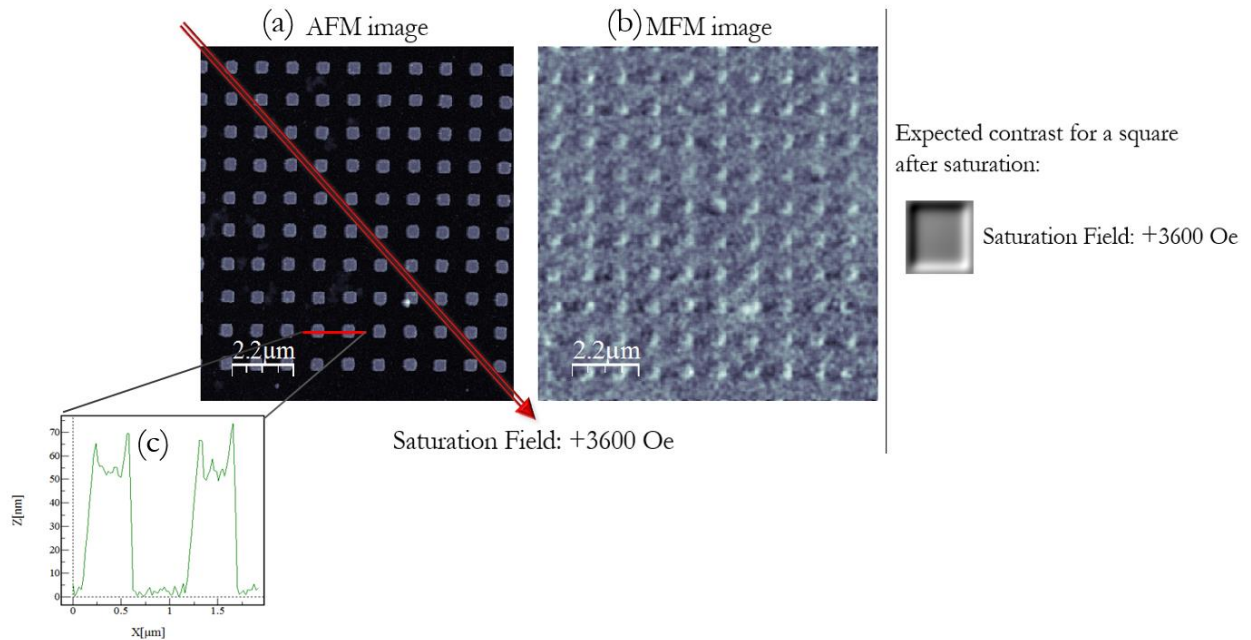


Figure 3-22_ Topographic and magnetic analyzed for a lattice after an aluminum deposition. The AFM (a) and the MFM (b) measurement corresponds to a zoom of a lattice composed of 300 nm squares with a period of 1 μm. The expected contrast according to the saturation direction is also represented at right. (c) Profile representing the height (z axis) as function of the lateral size (x axis) for the red line represented on the AFM image.

Figure 3-22 (b) shows the MFM signal measured on a lattice composed by squares with a length of 300 nanometers and a period of 1 micrometer. Obviously the 20nm aluminium spacer layer lowers the magnetic contrast as compared to the plane sample since the tip is further away from the Fe layer. As a consequence it is now necessary to process the MFM image. The procedure consists in superimposing first the MFM image on the AFM image. Then the transparency is adjusted to obtain the better contrast.

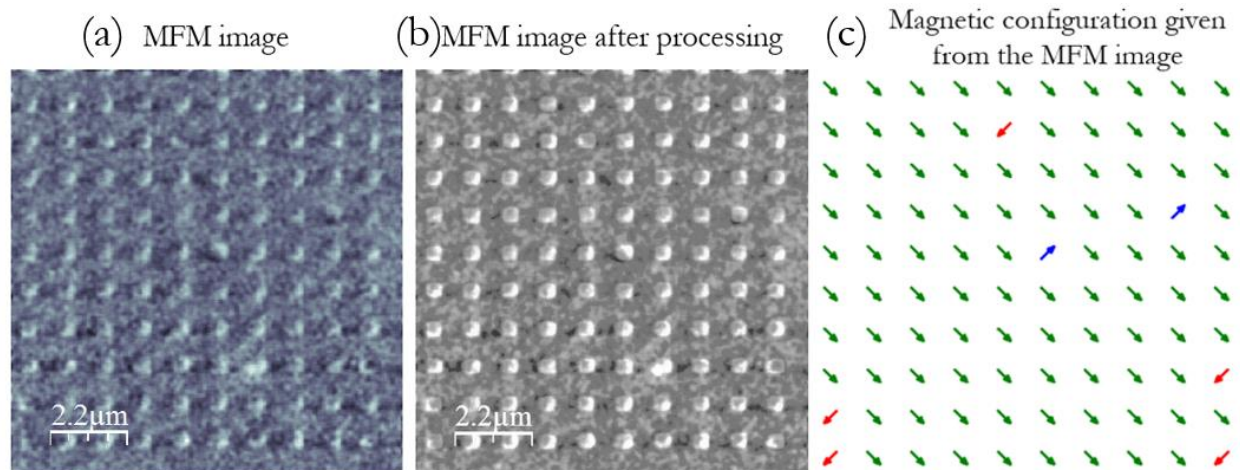


Figure 3-23_ Representation of the MFM image before (a) and after a processing (b). This processing is obtained by superposing the AFM image with the MFM image, then in adjusting the transparency. (c) Magnetic configuration obtained from a MFM measurement (b) and the results given by the Mathematica program (c).

After this image processing, we get a better contrast and so, it is easier to set an orientation for the magnetization in the nanostructures. Thus just by looking at the magnetic contrast shown in the figure 3-23 (b), it seems that the magnetic configurations in the nanostructures fit monodomains. In order to automatically map the orientation of the nanomagnet moments, code has been developed under Mathematica software. The program identifies each square composing a lattice and determines the magnetic contrast in associating to each pixel a value +1 for a black pixel, -1 for a white pixel and 0 when the program can't identify the color of the pixel. Then for each nanomagnet, the program calculates the average value of the contrast for each corner of the squares and determines the difference between the opposite corners. Thus this program can identify the direction of the monodomain in each nanomagnet. Figure 3-23 (c) presents the spin orientation deduced from the MFM image in figure 3-23 (b). Most of the spins are nicely orientated along the saturation field direction.

Approximatively five percent of the spins are not in the saturation field direction, and these spins don't move even after consecutives scans. A hypothesis is that these spins have a coercive field higher than the other spins and larger than the saturation field due to some defects. In order to check that, the sample is saturated several times in different directions, and it appears that these spins, so-called "hard switchers", stay in the same configurations as the one shown in the figure 3-23. Even though this study shows the results for only one lattice, which is a lattice composed of 300 nanometers squares where the angle is 45 degrees and where the period is equal to 1 micrometer, this study is also done for different lattices and it appears that the results observed are similar for all the lattices including different angles, different square sizes and different periods. Indeed it appears a percentage of hard switchers close to 5 percent and this for all the lattices.

The main result of this part is that aluminium spacer layer and image processing allows to identify the direction of the nanomagnet spins. The last point to check before the study of the magnetic behavior of our square lattices composed of artificial Potts spins is the presence of defect in our lattices (lattice distortion) which could affect the physics of our system.

3.7 Lattice distortion

The theoretical considerations of chapter 1 are based on a perfect square lattice with identical elements. But contrary to the natural systems, artificial spin systems made by nanofabrication tools can differ from the ideal desired system. One can distinguish two kinds of differences: fluctuations of individual elements (due to local variations of material properties or fluctuation in the lithography process) or systematic differences. Among the possible systematic differences are distortions of the lattice. These distortions are not so trivial to characterize as the measuring tools can have similar distortions to the fabrication tools (using diffraction is an interesting alternative). The fact that minors distortions in artificial spins lattice can imposed particular configurations is well-known phenomenon.

Since any distortion which transforms the square lattice in an orthorhombic or monoclinic lattice can affect significantly the physics of the system, we have tried to evaluate the distortion. The automatic determination of the element coordinates from the AFM images do not indicate any deviation from the ideal square lattice. This estimation has been determined after proper calibration of the AFM piezoelectric stage and verified by rotating the sample. But the determination of the distortion is limited by the pixel size of our AFM (512 pixels max). In order to increase the precision, the lattices related to the 500 nanometers period are imaged with SEM and we can observe these three images in the figure 4-24. It is important to note that the imaging field has been properly calibrated by displacement of an interferometric stage.

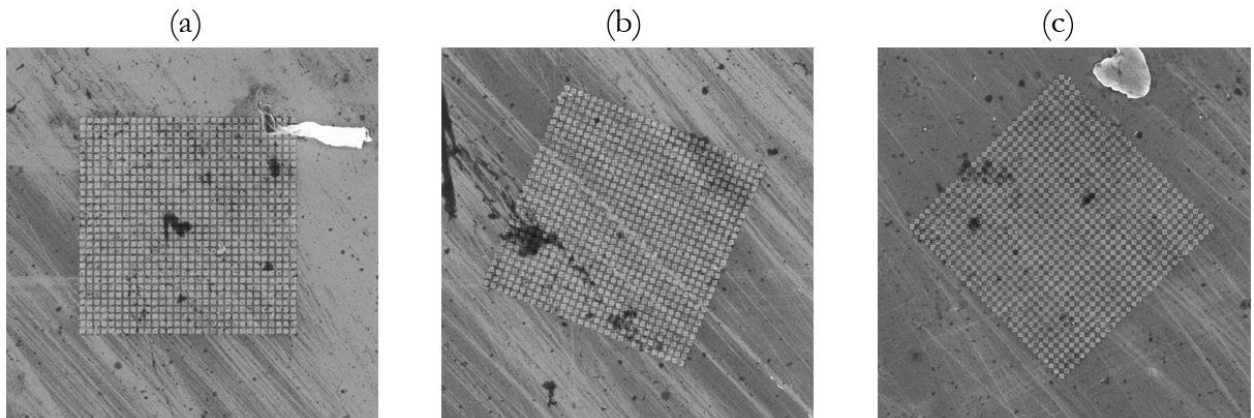


Figure 4-24_ MEB images corresponding to lattices with 500 nm period: (a) 45° lattice, (b) 22.5° lattice and (c) 0° lattice. The field of view used is: $25.6 \mu\text{m}$, and the resolution is equal to 6.4 nm/pixels .

If a distortion exists in these lattices, it should appear a length difference between the lattice edges, for example between horizontal edges and vertical edges for the 45° lattice. Thus in order to confirm or not the presence of distortions for each lattice, the length of two perpendicular edges are measured and the difference between these lengths is calculated. In these SEM images one pixel corresponds to 6.4 nanometers. The difference between different lengths is at maximum of one pixel. We can therefore conclude that the difference between orthogonal lengths is below 0.02%. We have checked that this value has no significant influence on the physics of the system.

Similarly, we have also verified the angle between the borders of the lattice is 90 ± 0.03 degree.

3.8 Summary

In the previous chapter micromagnetic simulations demonstrated that thin square nanomagnets can be used to mimic Potts spin under specific conditions. In the present chapter we tried to make such nanomagnets array. We carefully checked two main aspects: the magnetic properties of the sample selected and the MFM signal from the final nanomagnets. The first important point to take into account for the selection of the sample composition was the thickness imposed on the magnetic layer. To get monodomain nanomagnets, micromagnetic simulations set a maximum thickness of 2.5 nm. In order to avoid a lack of MFM signal, we choose a 2 nm Fe film. We selected the stack MgO/V/Fe (2 nm)/V/Au which shows only a cubic anisotropy and in-plane magnetization. We demonstrated that the interface provide zero surface magnetic anisotropy to the Fe layer [20]. The stack magnetic properties are not by several annealing up to 400°C which is the thermal demagnetization.

We described the lithographic method to obtain lattice of square nanomagnets. First MFM measurements on the nanomagnets reveal the intrusive nature of the tip leakage field which can potentially change the magnetic properties nanomagnets, especially during the AFM scan in tapping mode. Both standard and low moment tip affect the nanomagnets. So we used a spacer layer on the sample to increase the gap between the (low moment) tip and the magnetic layer. PMMA spacer layer has been tested but induces a charge signal that hide the magnetic signal during MFM scan. We have finally selected a 20 nm aluminium layer as spacer layer and could demonstrate no influence of the AFM/MFM low moment tip on the nanomagnet. An image treatment procedure is described that will be used in the following to automatically extract the map of magnetization direction for the array of nanomagnet. Moreover after verification, we have confirmed that any distortions exist in our lattices which could affect the physics of our system.

Bibliography

- [56] M.Sicot, « Des interfaces réelles métal/MgO(001) au transport dans les jonctions tunnel épitaxiées », Thèse de doctorat réalisée à l'université Henry Poincaré, Nancy, France (2006)
- [57] M.Gottwald, « Nouveaux systèmes modèles à aimantation perpendiculaire pour l'étude des effets de transfert de spin », Thèse de doctorat réalisée à l'université Henry Poincaré, Nancy, France (2011)
- [58] H. X. Yang et al, “First-principles investigation of the very large perpendicular magnetic anisotropy at Fe|MgO and Co|MgO interfaces”, *Phys. Rev. B.* **84**, 054401 (2011)
- [59] M.T.Johnson et al, “Magnetic anisotropy in metallic multilayers”, *Rep. Prog. Phys.* **59**, 1434-1438 (1996)
- [60] F. Radu et al, “Magnetic Heterostructures”, Springer Tracts in Modern Physics, 227. Springer-Verlag Berlin Heidelberg (2008)
- [61] T. Hauet et al, “Role of reversal incoherency in reducing switching field and switching field distribution of exchange coupled composite bit patterned media”, *Appl. Phys. Lett.* **95**, 262504 (2009)
- [62] S. Valencia et al, “Interface-induced room-temperature multiferroicity in BaTiO₃”, *Nature Mater.* **10**,753 (2011)
- [63] C.H.Lambert et al, “Quantifying perpendicular magnetic anisotropy at the Fe–MgO(001) interface”, *Appl. Phys. Lett.* **102**, 122410 (2013)
- [64] P. Turban et al, “In-plane lattice spacing oscillations during 2D epitaxy of metals”, *Surf. Sci.* **446**, 241 (2000)
- [65] A. N. Anisimov et al, “Orbital Magnetism and Magnetic Anisotropy Probed with Ferromagnetic Resonance”, *Phys. Rev. Lett.* **82**, 2390 (1999)
- [66] H. Fritzche et al, “Polarized neutron reflectometry study of ultrathin Fe layers on V(1 1 0) and V(1 0 0)”, *Phys. B.* 241–243, 707 (1997)
- [67] A. Broddefalka et al, « In-plane magnetic anisotropy of Fe/V (0 0 1) superlattices », *J. Magn. Magn. Mater.* **241**, 260 (2002)
- [68] P. Turban, « Epitaxie de films minces métalliques : (i) relaxation élastique pendant la croissance pseudomorphe (ii) epitaxie d'hétérostructures NiMnSb/MgO/NiMnSb pour l'électronique de spin », Thèse de doctorat réalisée au Laboratoire de Physique des Matériaux, (2001)
- [69] J. Izquierdo et al, “Origin of dead magnetic Fe overlayers on V(110)”, *Phys. Rev. B.* **64**, 060404(R) (2001)
- [70] F. Dulot et al, “(001) V surface structures analysed by RHEED and STM”, *Surf. Sci.* **473**, 172 (2001)
- [71] P. Pouloupoulos et al, « Magnetic anisotropy and exchange coupling in Fe_nV_m(001) superlattices on MgO(001) », *J. Magn. Magn. Mater.* **170**, 57 (1997)

-
- [72] M. Sicot et al, “Polarization of Fe(001) covered by MgO analyzed by spin-resolved x-ray photoemission spectroscopy”, *Phys. Rev. B.* **68**, 184406 (2003)
- [73] M. Sicot et al, “Electronic properties of Fe, Co, and Mn ultrathin films at the interface with MgO(001)”, *Phys. Rev. B.* **72**, 144414 (2005)
- [74] C. D. Graham, “Magnetocrystalline Anisotropy Constants of Iron at Room Temperature and Below”, *Phys. Rev.* **112**, 1117 (1958)
- [75] D. Sander, “The magnetic anisotropy and spin reorientation of nanostructures and nanoscalefilms”, *J. Phys. Condens. Matter.* **16**, 603 (2004)
- [76] Joel Briones Hernandez, « anisotropie magnétique induite par modulation de surface et étude de la propagation de parois de domaines dans des nanostructures magnétiques ». Thèse de l’Université de Lorraine. (2008)
- [77] B. Bhushan, ed., “Springer Handbook of Nanotechnology”, Berlin, Heidelberg: Springer Berlin Heidelberg (2010)
- [78] A.Thiaville et al, “Measurement of the stray field emanating from magnetic force microscope tips by Hall effect microsensors”, *J. Appl. Phys.* **82**, 3182 (1997)



4. DEMAGNETIZATION OF THE 4-STATE POTTS ARTIFICIAL SPINS

4.1 Pathway to fundamental state : the demagnetization

Artificial array of nanomagnets have been introduced to experimentally mimic the spin ice statistical physic model [11] by a magnetic array of interacting spins. One of the remaining issue in studies dealing with artificial spin systems is the lack of easy and efficient method to drive the system in its fundamental state. In this work and more generally in the artificial spin systems community, the term “demagnetization” does not holds the primary sense of demagnetization, i.e. method to zero the total magnetic moment of the magnetic system. Here demagnetization method means a method able to drive the system towards its energy ground state. This ground state can be a zero magnetization state in the case of non-interacting spins but the ground state for interacting spin can hold various moment values depending of the geometry of the lattice, as shown in our theoretical work in chapter I. Up to now for Ising spins with an in plane magnetization, the main way to demagnetize the samples has been AC field demagnetization [11]. In this protocol it is applied an external magnetic field alternating between a positive and negative field while reducing its amplitude. However, experimentally it is difficult to drive the system in its ground state by using AC field demagnetization. Indeed during the field decay, the nanomagnets with the highest coercive field are the firsts to be frozen, and thereafter can't flip anymore. Moreover energy barrier distribution may strongly affect the state obtained after AC demagnetization [79-81]. Indeed since the spin flips occur for an applied field comparable to the coercive field of nanomagnets, the energy barrier distribution will play a significant role in choosing the pathway during the demagnetization.

As it seems difficult to improve the AC demagnetization protocol, another protocol has to be found in order to drive the system in its ground state. A possibility is to use nanomagnets which can be sensitive to thermal fluctuations. It has been heavily pursued by the community since few years [15, 23, 24, 82-88]. Indeed if the nanomagnets can be thermally activated, the system should gradually minimize its energy in accommodating pairwise interactions. To that purpose, two approaches were conducted: one considering superparamagnetic regime [23] and another one based on an annealing procedure above Curie temperature [15]. In our work, the first approach is selected because diffusion occurs at V/Fe interface around 600°C much below Fe Curie temperature (see section 3.1). The exact thermal demagnetization protocol used in our work is detailed in the section 4.1.2.1. Similarly to results obtained in Ref. [89], we will show in the following chapter that thermal demagnetization allows to reach states closer to the ground state than AC field demagnetization.

4.1.1 AC Field demagnetization

4.1.1.1 Protocol

For the AC field demagnetization, the protocol which is used is identical to the one presented in Wang et al experiment [11]. During AC field demagnetization, the sample is placed on a sample holder turning at a speed of 4000 rpm in the airgap of an electromagnet. The initial field applied is bigger than the system saturation field. Then the field alternates between a positive and negative field while reducing its amplitude as shown in figure 4-1 (a). Since the field amplitude is progressively reduced, the nanomagnets with the highest coercive field are the firsts to be frozen. They emit a magnetic field which is added to the local field senses by the adjacent nanomagnets, and at this step the correlations between elements emerge in the lattice. It is expected that at the end of the AC demagnetization, the system minimizes its dipolar energy.

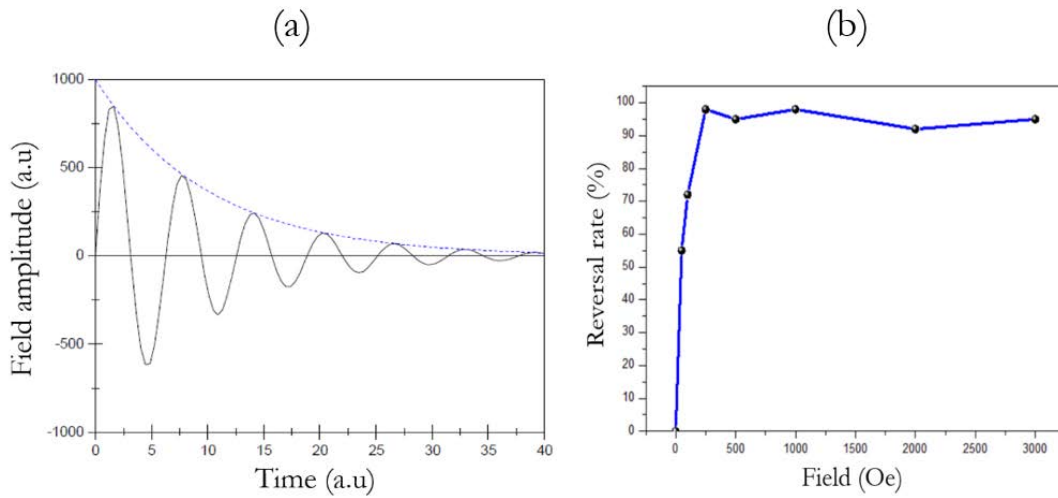


Figure 4-1_ (a) Field amplitude as function of time during the AC field demagnetization protocol. (b) Percentage of spins in the same direction as the saturation field according to the field amplitude. The field is applied along an easy axis in order to impose a particular direction for the spins. This study is carried out on a lattice composed by 300 nanometers squares for an angle of 45° and a period of $1 \mu\text{m}$.

In order to improve the AC demagnetization protocol, one can tune several parameters like rotation speed, initial field, field step and oscillation period. Several studies have studied the influence of these parameters in the case of artificial spins systems [90, 91, 92]. Through these studies, it emerges that the demagnetization is more efficient if it is done slowly with the smallest field step.

To set the AC demagnetization parameters, we performed a first set of experiments in order to quantify the saturation field value. For this study different magnetic fields are applied along one easy axis and then, for each applied field value, the magnetic configuration of the lattice at remanence is imaged by MFM (using the procedure described in chapter 3). The figure 4-1 (b) shows the percentage of the spins aligned along the applied field direction as function of field amplitude. The percentage never perfectly reaches 100% probably because of some perturbations during the MFM scan. Nevertheless, looking at the reversal rate as a function of applied field, the saturation for a lattice composed of 300 nanometers squares with a period of 1 micrometer, is estimated to be around 200 Oe. As expected this value is larger than the one observed for the full film which is around 50 Oe. This fact can be explained by the change in reversal mechanism, the

influence of the defect density as well as the shape anisotropy present in the squared nanostructures.

The value of saturation field of the nanomagnets can vary according to the studied lattice as it depends on nanomagnet volume and nanomagnet to nanomagnet distance. A solution would be to characterize independently all lattices but for obvious reasons of time, another solution is chosen which consists to test a field in particular and to observe if the different lattices are saturated. A field of 500 Oe has been selected and after MFM measurements, the experiments show that this field is adequate to saturate all the lattices. Therefore a field of 500 Oe has always been applied as initial field of any AC demagnetization we did.

Finally, based on previous works of the team [83], the field step has been set at 0.01 Oe and an oscillation period equal to 2 seconds has been used. With these parameters the AC demagnetization time is 1666 minutes (1.5 days).

4.1.1.2 Efficiency

In order to analyze the AC demagnetization efficiency with our selected parameters, we checked the magnetic configuration after demagnetization for a lattice with small dipolar coupling between the nanomagnets. Theoretically, the spins are expected to be equally split between the four preferential directions reachable by each spin. We checked that for the three types of lattice that we are interested in: 0° , 22.5° and 45° lattice. They have been defined in chapter I and the experimental realizations are shown in figure 4-2. It is important to remind here that although the lattice angle changes, the Fe nanomagnets magnetization always points along one of the square diagonals which correspond to the $[100]$ and $[010]$ crystallographic direction for the Fe crystal.

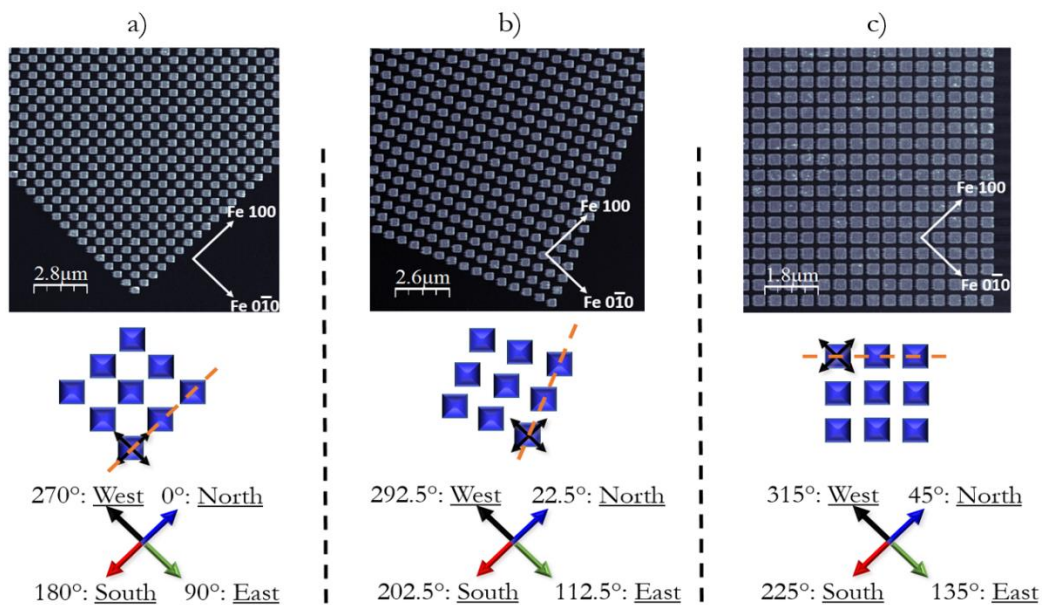


Figure 4-2_Nomenclature of spin directions for three lattices ((a) 0° lattice, (b) 22.5° lattice, (c) 45° lattice). Regardless of the angle lattice, the spin direction is always based on the crystallographic axes of Fe: $[100]$ direction corresponds to North, $[0-10]$ direction corresponds to East, $[-100]$ direction corresponds to South and $[010]$ direction corresponds to West.

To easily identify each spins and its direction, in the three type of lattice, we define the four possible directions and associate them to a color code (north, east, south and west), as described in figure 4-2. We can now observe the spins repartition after field demagnetization.

For this study two nominally identical samples (sample #1 and sample #2 mentioned in the section 3.3), with the same composition and the same lattices, are AC field demagnetized. For one of the sample, the demagnetization and MFM measurements are realized twice in order to increase the statistic, and to see if for a same sample, two independent AC field demagnetizations give the same results or if the results are different. One can observe the results of these demagnetizations in the following table.

Sample	Lattice angle: 0°				Lattice angle: 45°			
	N(%)	E(%)	S(%)	W(%)	N(%)	E(%)	S(%)	W(%)
#1	30	23	18	29	26	17	25	32
#1	22	31	26	21	31	23	21	26
#2	21	33	29	18	20	32	30	18
AVERAGE	24	29	24	23	26	24	25	25

The table represents the results for two different angles lattices which are 0 and 45 degrees where the squares have a size of 300 nanometers and where the period is 700 nanometers. For this period, we have considered the coupling as sufficiently “weak” to observe an equidistribution in the spins directions after demagnetization. Indeed, the experimental results presented in the table show that the spins repartition is distributed around 25%. However, the fluctuations are larger than expected for a totally random process ($25 \pm 3\%$ with a 95% confidence for 900 spins). An example of spin map obtained on sample #1 after AC demagnetization in the case of 0° lattice is presented in figure 4-3. The four colors are represented corresponding to the four directions of the nanomagnet spins. The four directions of spin are spread over the lattice but one can already guess some lines of aligned spin due to the dipolar interactions. Thus a favored local order can be found which shows the importance of the dipolar interactions even for the period of 700 nanometers. This order can explain the fluctuations observed in the spin repartitions.

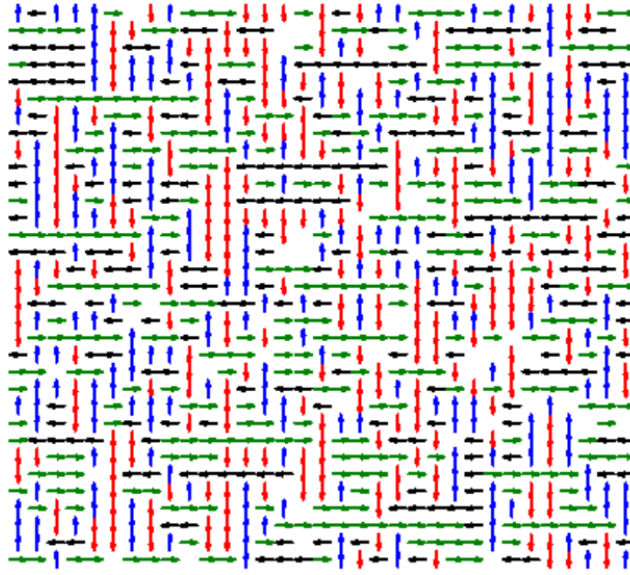


Figure 4-3_Example of magnetic configuration (after processing) of a 0° lattice obtained after a field demagnetization. The lattice observed is composed by 300 nanometers squares and present a period of 700 nanometers.

4.1.2 Thermal demagnetization

4.1.2.1 Protocol

For the thermal demagnetization, two ways are possible. The first used historically [15] consists of anneal the sample above the Curie temperature in order to obtain a true paramagnetic state. Then the sample is cooled up to the dipolar interactions become comparable to the thermal energy in order to drive the system in its fundamental state or at least in a low energy state. This protocol is not the ideal case to drive the system towards its ground state, as this process is irreversible. And we have demonstrated in previous work on Kagome lattices [84] that after this demagnetization protocol the system shows specific characteristic related to an out-equilibrium dynamic of the system. Moreover in our work, this first approach cannot be apply because diffusion occurs at V/Fe interface around 600°C much below Fe Curie temperature (see section 3.1). Moreover the Fe thickness is low and the anisotropy constant (shape anisotropy + magneto-crystalline anisotropy) is presumed weak enough to allow thermally activated reversal of magnetization for temperature much below the Curie temperature.

Therefore we use the second usual thermal demagnetization protocol which is based on the hypothesis that a nanomagnet (with magnetic monodomain configuration) can spontaneously flip for another preferential direction after a certain period of time (so-called Néel relaxation time) [22]. Néel relaxation time is given by the following equation where it appears that this duration increases exponentially with the energy barrier related to the flip between the preferred magnetic orientations:

$$\tau = \tau_0 \cdot \exp\left(\frac{\Delta E}{k_B T}\right) \quad (4-1)$$

where τ is the Néel relaxation time, τ_0 is the characteristic time which depends on the magnetic material, ΔE is the energy barrier and $k_B T$ is related to the thermal energy. In its simplest form

associated to a coherent reversal, the energy barrier equals to the reversed magnetic volume V times the anisotropy constant K ($\Delta E = K.V$, in our case $\Delta E = 8.64 \cdot 10^{-18} J$). Thus, one can play with the temperature, anisotropy constant and nanomagnet volume in order to obtain a time of relaxation around minutes or seconds. In practice, a trade-off needs to be found between the three parameters. Indeed it is easy to change the temperature but the temperature increase can generate a sample destruction or contamination. The reduction of nanomagnet volume is limited by lithographic techniques resolution. Moreover decreasing the nanomagnets volume lowers the dipolar interactions between nanomagnets [93]. Finally the anisotropy constant cannot be tuned on a large range since we chose square shape (with low shape anisotropy anyway) and quadratic anisotropy Fe film (we could have lower it by alloying Fe with Co for instance film). For our sample, thickness of 2 nm, 300 nm square edge size combined with the small square shape anisotropy must favor low barrier height.

In order to have an efficient thermal demagnetization, the choice of the oven is really important because during this demagnetization, it's necessary to avoid any magnetic field. Indeed if an external field is present, the symmetry of the energy barrier between preferential directions for the magnetization will be break and so, one state could be favor. Most of the ovens use resistors with electrical circuits which produce magnetic fields. To avoid this problem, we have used a “home-made” oven (developed by M. Hehn) where the heating system does not create magnetic field. Indeed for this oven, the sample is placed on a sample holder in copper and this sample holder is heated with a halogen bulb puts far away of the sample in order to avoid a magnetic field. Halogen bulb presents the advantage of a very weak magnetic field creation during the heating, but presents the disadvantage of limited annealing temperature. In our case the maximal temperature is 350°C. This temperature is below the Curie temperature of our sample, and so in all the conducted annealing Curie temperature cannot be reached. Furthermore during the annealing, the sample is under vacuum and thus the risk of oxidation by the top or the border of elements is limited.

It is to be mentioned that our “home-made” oven carries an electromagnet without soft iron core, and so we can consider that when there is no electric current in the coil, the remnant field is equal to zero. For all the annealing processes presented in the thesis, the electric current in the coil is fixed at zero, and we checked with a Gauss-meter that the area where the sample is placed presents a magnetic field which is in the order of the earth's magnetic field.

4.1.2.2 Thermally induced magnetization reversal as a function of square size

For this study, the sample is saturated along an easy axis (South direction) in order to set the initial magnetic configurations of the different lattices, and then the sample is heated at a temperature of 300°C during 2 hours (slightly below the oven maximum at 350°C). In figure 4-4 is shown the magnetic configuration measured after heating for two 45° lattices with the same period (1300 nm) with either 300 nanometers squares or 500 nanometers squares. For such large period, the dipolar coupling is considered weak enough to expect equi-distribution of the spins along the four directions after demagnetization.

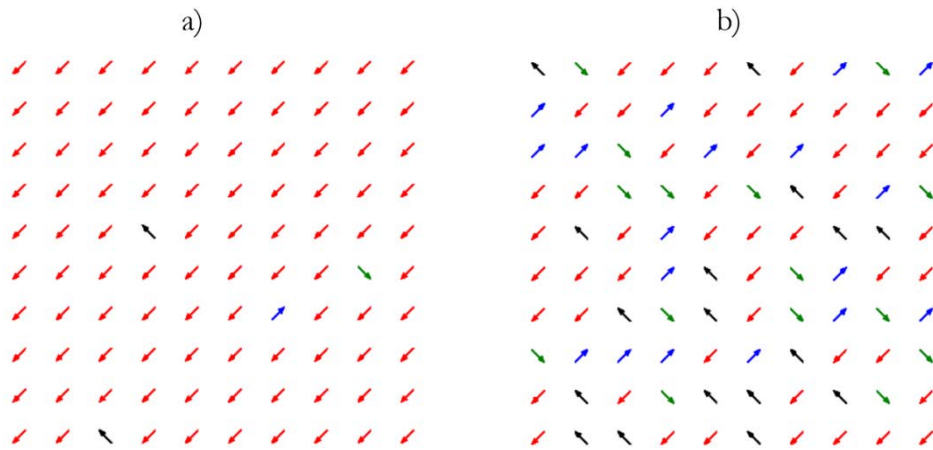


Figure 4-4_ Magnetic configurations of 45° lattices obtained after a heating at 300°C during 2 hours. (a) Lattice composed by **500** nanometers squares and with a period of 1300 nanometers. (b) Lattice composed by **300** nanometers squares and with a period of 1300 nanometers.

Here we studied a 10×10 spins representative portion of the lattice. Figure 4-4 (a) shows that the 500 nanometers squares nanomagnets moments do not switch after 2 hours annealing at 300°C . 96% of the spins still point along the saturation field direction, in the **south** direction (red arrow), instead of only 25 % as expected. Most probably, the energy barrier inhibits temperature activation. The other 4% of spins can be either “hard switchers” which have not been affected by the saturation field, or nanomagnets with lower energy barrier which have switch during the heating process. Unfortunately the initial configuration (after saturation) has not been recorded with MFM.

In the case of 300 nanometers squares, as shown in figure 4-5(b), much more spins are dispatched in the North, East and West direction after annealing. It is in line with the decrease of the magnetic volume and of the energy barrier as compare to 500 nm. Nevertheless we must point out that a large number of spins, around 50%, remain in same direction as the saturation field. As only a part of the lattice is studied, it's not possible to conclude about the efficiency of this demagnetization with a temperature of 300°C , but this experiment clearly demonstrates that 300 nanometers squares are thermally activated at 300°C annealing. We tested others lattices and we observed that for a square size superior at 300 nanometers, a temperature of 300°C is too low to allow magnetization reversal thermally activated regardless of the angle or of the period.

In the following, only studies of 30×30 squares with a length of 300 nanometers are reported.

4.1.2.3 Efficiency

Now that the proper nanomagnet size has been identified, one must do a similar study for the annealing parameters (time, temperature, temperature ramp) to optimize the demagnetization process. Unlike field demagnetization, no previous study of thermal demagnetization (below the Curie temperature) has been done in our team. Moreover, for thermal demagnetization, parameters are strongly correlated with the material used and the nanostructures patterned. To tune the annealing parameters, we use a lattice of 30×30 spins lattice with a period of 700 nanometers and an angle α equal to 45° . Again the period is large enough to consider the dipolar interaction as weak and equi-distribution of spins repartition is mostly expected after demagnetization process.

4.1.2.3.1 Heating time influence

The first parameter which is checked is the heating time, and this study is done with the sample #1 mentioned in the section 3.3. For this study the temperature used for the heating is fixed at 300°C and the ramp temperature, which is the same for the temperature rise and for the temperature drop, is fixed at 10°C/min. Actually as it does not exist a cooling system in the oven, the fastest ramp for the temperature drop will be given by the thermic inertia of the oven. The sample is saturated along an anisotropy axis, in order to set the initial state before annealing. The summary of the different heating is represented in the following table.

Initial state	Heating Time (hours)
North saturated	0.5
South saturated	0.5
South saturated	1
South saturated	1
North saturated	2
North saturated	2
North saturated	5
West saturated	5

The spins repartition at remanence after thermal demagnetization is plotted as a function of the heating time in the figure 4-5 (a). Since we change the saturation direction between heating, in the figure 4-5 (a) and (b), the spins are not identified by their directions against the sample (N, E, S, W), but by their directions against the saturation direction used to obtain the initial state. Thus the black points represent the spins which stay in the same direction as the saturation field, the red and blue points represent the spins which have rotated 90° clockwise and counterclockwise, and the green points represent the spins which are opposite to the saturation direction. In this study, each heating time is done twice and the figure 4-5 (a) shows the average value for each heating time with the standard deviation. This spins repartition does not bring to light a difference according to the heating time for time larger than 1 hour. Only half hour shows a weak difference. After demagnetization a majority of spins (around 40%) stays in the saturation field direction, a minority of spins point in the opposite direction to the saturation (around 10%) and an equi-distribution is observed for the two directions transverses (around 25% each). Considering the fact that the heating time does not change the spins repartition obtained after the demagnetization, the average percentage of spins repartition is calculated including all the heating time (see figure 4-5 (b)). The same “40%, 25%, 25%, 10%” repartition is obtained.

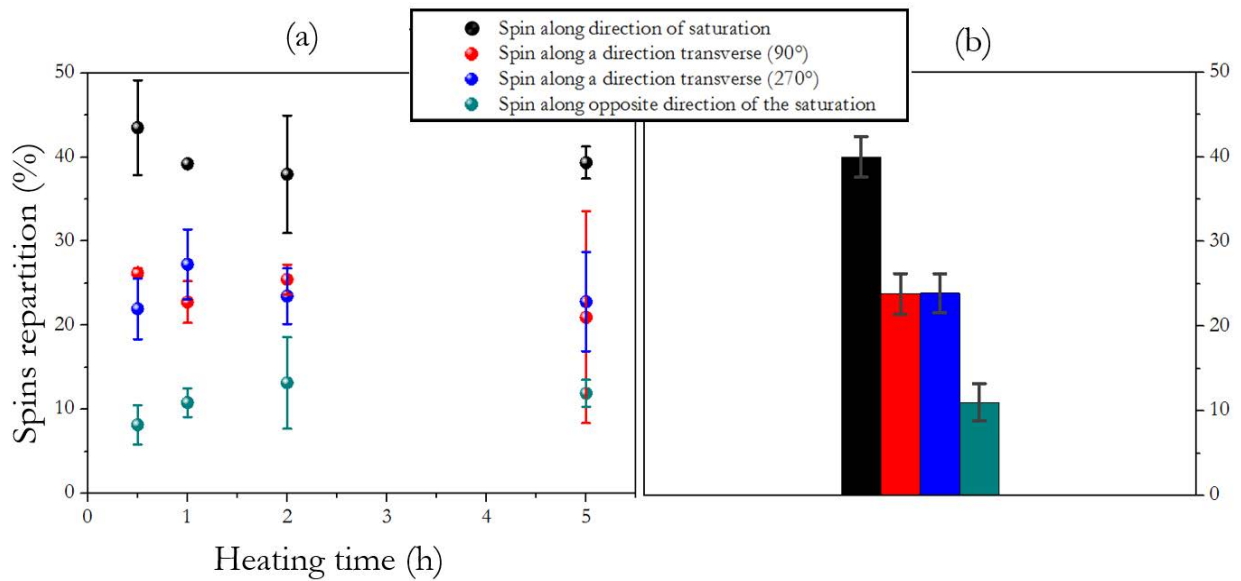


Figure 4-5_ (a) Spins repartition obtained after thermal demagnetization as a function of the heating time. (b) Average spins repartition independently of the heating time. For these two graphics the spins are identified against the direction of the saturation imposed to obtain the initial state.

The fact that we do not obtained an equi-distribution of the spins in the four direction can be explained by a distribution of energy barrier for the nanostructures. Indeed as the heating time has not or very weak effect from the point of view of the spins repartition, it is possible that only a part of the nanostructures are sensitive to this temperature while the others, so called “thermal hard switcher” or just “hard switcher”, are insensitive to it. The imbalance between the number of spins in different directions may also originate by a specific reversal process.

In order to interpret the experimental results, it is useful to apprehend with a simple model the expected dynamic. Considering a single element (with no coupling nor applied field), it has four stable states, North, East, South, West, of equal energy. These states are separated by energy barriers which determine the transition rate between them. The characteristic time τ is simply related to the barrier height E_b by $\tau = \tau_0 \cdot \exp(E_b/k \cdot T)$. In our system we can consider two different processes: 90 degree reversal (associated to characteristic time τ) and 180 degree reversal (associated to characteristic time τ'). These processes are graphically represented in figure 4-6.

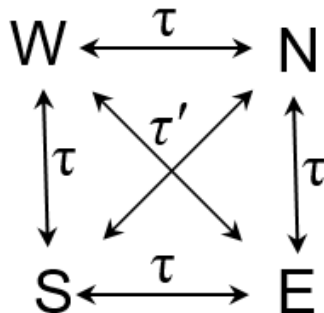


Figure 4-6_ Characteristic times as function of the reversal process

Considering the proportion of spin (or the probability for a spin to be) in state N, it is therefore ruled by the following differential equation:

$$\frac{dP_N}{dt} = -\frac{2}{\tau}P_N + \frac{1}{\tau}P_W + \frac{1}{\tau}P_E - \frac{1}{\tau'}P_N + \frac{1}{\tau'}P_S \quad (4-2)$$

The set of equation for all the states can be conveniently written in a matrix form by introducing the vector $\mathbf{P} = (P_N, P_E, P_S, P_W)$:

$$\frac{d\mathbf{P}}{dt} = \begin{pmatrix} -\frac{2}{\tau} - \frac{1}{\tau'} & \frac{1}{\tau} & \frac{1}{\tau'} & \frac{1}{\tau} \\ \frac{1}{\tau} & -\frac{2}{\tau} - \frac{1}{\tau'} & \frac{1}{\tau} & \frac{1}{\tau'} \\ \frac{1}{\tau'} & \frac{1}{\tau} & -\frac{2}{\tau} - \frac{1}{\tau'} & \frac{1}{\tau} \\ \frac{1}{\tau} & \frac{1}{\tau'} & \frac{1}{\tau} & -\frac{2}{\tau} - \frac{1}{\tau'} \end{pmatrix} \mathbf{P} \quad (4-3)$$

This matrix has a zero determinant and therefore it exists a non-zero solution in the permanent regime ($d\mathbf{P}/dt = 0$) which is $\mathbf{P}(\infty) = \left(\frac{1}{4}, \frac{1}{4}, \frac{1}{4}, \frac{1}{4}\right)$.

The matrix possesses three eigenvalues: 0, $-\frac{4}{\tau}$ and $-2\frac{\tau+\tau'}{\tau\tau'}$ (2 times degenerated) and therefore the general solution writes:

$$\mathbf{P}(\infty) = \left(\frac{1}{4}, \frac{1}{4}, \frac{1}{4}, \frac{1}{4}\right) + \mathbf{A} \exp\left(-\frac{4t}{\tau}\right) + \mathbf{B} \exp\left(-2\frac{\tau+\tau'}{\tau\tau'}t\right) \quad (4-4)$$

For a system initially saturated in the North direction, its evolution is simply given by:

$$\begin{aligned} \mathbf{P}(\infty) = & \left(\frac{1}{4}, \frac{1}{4}, \frac{1}{4}, \frac{1}{4}\right) + \left(\frac{1}{4}, -\frac{1}{4}, \frac{1}{4}, -\frac{1}{4}\right) \exp\left(-\frac{4t}{\tau}\right) \\ & + \left(\frac{1}{2}, 0, -\frac{1}{2}, 0\right) \exp\left(-2\frac{\tau+\tau'}{\tau\tau'}t\right) \end{aligned} \quad (4-5)$$

We can consider two limiting cases which are relevant for our system:

- Equal probability for 90 and 180 degree reversal ($\tau = \tau'$). In that case, the time evolution of states East, South and West is the same and governed by an unique time constant, $\tau/4$ (figure 4-7 (a))

- No direct 180 degree reversal ($\tau \ll \tau'$). This situation is the one predicted by the micromagnetic simulations. In that case, the system first evolves toward states East and West and later towards state South. The two time constants associated with these phenomena are $\tau/4$ and $\tau/2$ (figure 4-7 (b)).

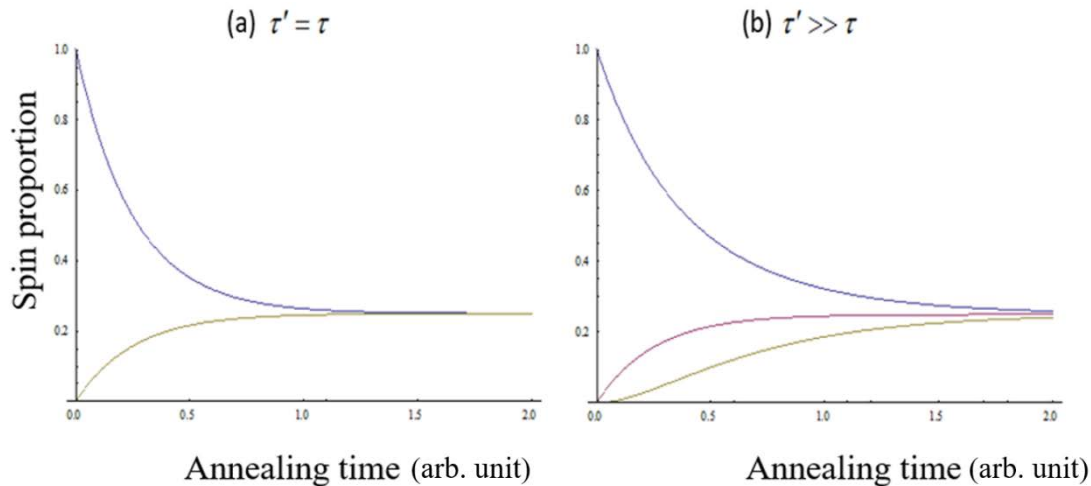


Figure 4-7_ Time evolution of states North (blue curve), East (pink curve), South (yellow curve) and West (pink curve) in the case of: (a) two equal probability for 90 and 180 degree reversal: the time evolution is the same for the spin proportion in the East, West and South directions. (b) No direct 180 degree reversal: the time evolution is the same for the spin repartition in East and West directions (90° reversal) but is slower for the spin repartition in South direction (180° reversal).

Are our experimental results well explained by this model? Obviously no. As a matter of facts, as the proportion of state is not dependent of the annealing time, one can expect that we have reached the permanent regime. But in the permanent regime we expect an equal repartition between the states. A simple way to explain this discrepancy is to consider that all the elements do not have the same energy barrier. The elements with a higher energy barrier, called hard switchers, cannot switch in the considered temperature range and the repartition observed would be a combination between "easy switchers" (equiprobable repartition) and "hard switchers" staying in the North direction.

But such a scenario cannot explain the unbalance between East-West and South states. Considering that the system has actually reached the permanent regime, the unbalance can only be explained if some elements can switch from North to East (or West) but not from East (or West) to South. As there is no reason that the energy of South and North states are different (time reversal symmetry), we therefore have to consider non-reciprocal transition rate between North-South and East-West states.

This non-reciprocal transition rate can be explained by a small energy difference between North-South and East-West states du to symmetry breaking. Figure 4-8 shows such an example: a defect in an element corner lift the degeneracy between North-South and East-West directions. In this example, the difference in energy is $1.2 \cdot 10^{-19}$ J (29 kT at room temperature).

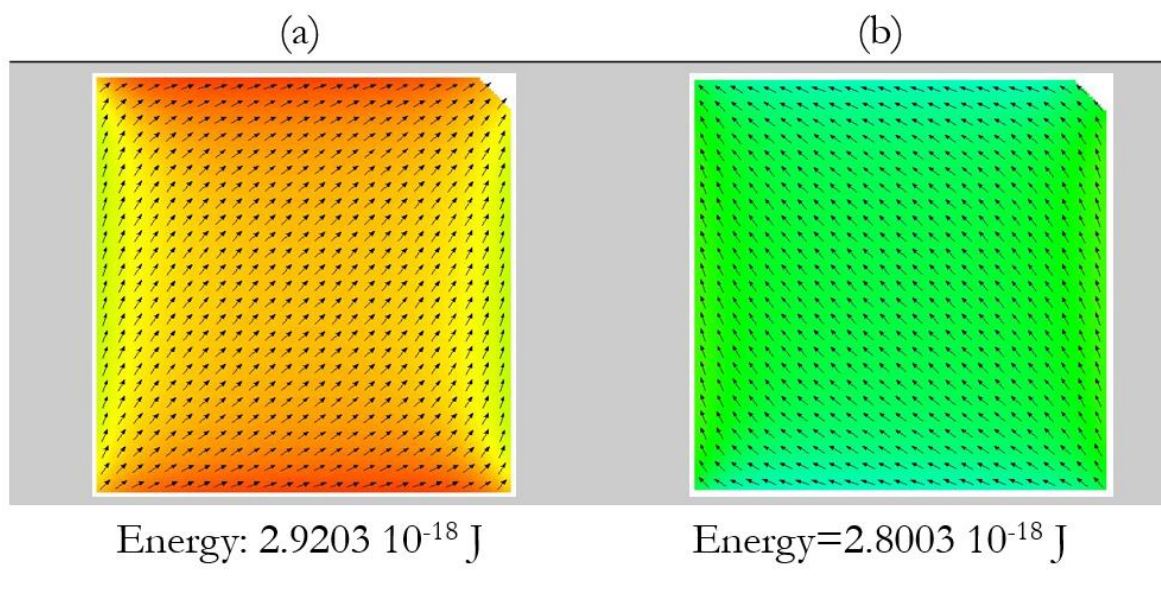


Figure 4-8 Micro-magnetic configuration and related energy for square with a defect in a corner as function of the magnetization direction: (a) North direction, (b) West direction.

This difference in energy, resulting in an effective uniaxial anisotropy, is far from negligible despite the small size of the defect. In real sample, it is possible that such defects are present and randomly distributed favoring one or the other direction from element to element. Another aspect, not easy to integrate in our simple picture, is that considering the reversal initiates in one of the element corner, a reversing from one direction to the other does not occur in the same corner of the element than the reciprocal reversing.

4.1.2.3.2 Temperature influence

As mentioned previously, it's reasonable to think that in our lattices, it exists a potential barrier distribution for the nanostructures. Yet if it is the case, the number of "hard switchers" found after the heating should decrease by increasing temperature. Therefore, the same sample and the same protocol as for the previous study is used with now the highest temperature possible with our oven, i.e. 350°C. The sample is saturated along an anisotropy axis and then heated at a temperature of 350°C with a ramp temperature fixed at 10°C/min. For this study two heating are performed (on the same sample) with these parameters. The resulting spin repartition is shown in figure 4-6 and compared with 300°C annealing.

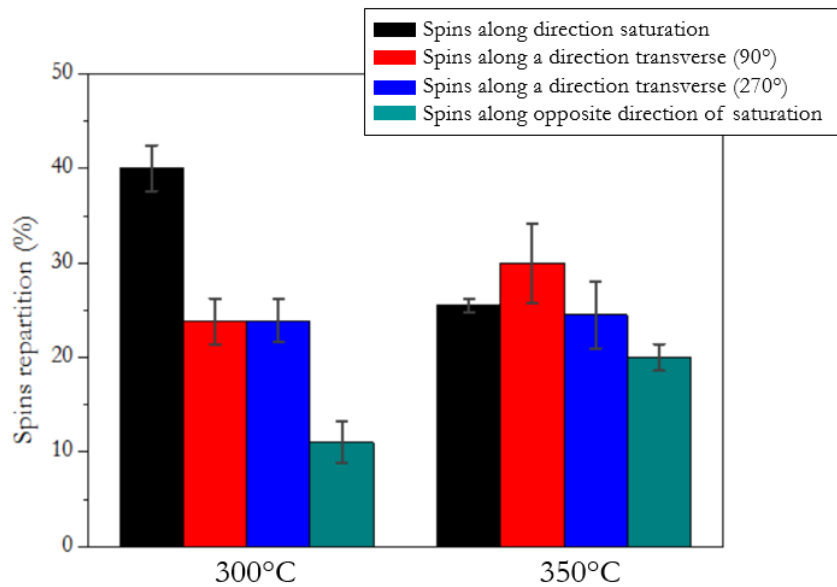


Figure 4-6_ Spins repartition for the same lattice (30x30 spins, square size: 300 nm, period 700 nm and alpha angle: 45°) related to two heating temperatures: 300°C and 350°C. The spins are identified against the direction of saturation used to obtain the initial saturated state.

It turns out that increasing annealing temperature from 300°C to 350°C leads towards a much better equi-distribution of the spins directions. The proportions after 350°C annealing are very close of the expected 25% each. This result is in accordance with the presence of a potential barrier distribution for the nanostructures composing the lattice. While increasing the temperature, much more spins are thermally activated and can be reoriented. It would be good to further increase temperature to insure excitation of all spins in the lattice. Unfortunately with our oven, 350°C is the maximum temperature that we can reach and so it has not been possible to check higher temperature.

Another parameter can be considered: the ramp temperature. If we consider that after the heating at 350°C the system is abruptly cooled down (quench), the spins will be frozen and the influence of the dipolar interactions should be significantly reduced. On the contrary, the longest dropping time should favor the best rearrangement of the spins (via dipolar interactions) and therefore favors the obtaining of ground state configuration. Unfortunately, for time reasons this parameter has not been checked for our demagnetization and the choice is done to select the slowest possible ramp with our equipment: 0.1°C/min.



5. EXPERIMENTAL DEMONSTRATION OF DIPOLAR 4-STATE POTTS MODEL: COUPLED POTTS SPIN LATTICE

Up to now we only focus on weakly coupled spins repartition in order to optimize demagnetization efficiency. Let's now observe the magnetic configurations obtained after demagnetization in the case of strongly coupled nanomagnets, and compare with our theoretical predictions detailed in chapter I. 2D dipolar Potts system is expected to possess very different ground state magnetic configuration depending on the angle between spins and lattice. Here we study only three angles which are 0, 22.5 and 45 degrees where the lowest energies states are respectively: antiferromagnetic state, spin ice state (by analogy with the square ice introduced by Wang et al: 2in-2out) and ferromagnetic state.

For this chapter, only sample #3 is measured (see section 3.3). On this sample, finite (30x30) square lattices with different orientations for spin direction and different periods are studied as summarized in the following table.

Lattice angle (°)	Square size (nm)	Periods (nm)
0	300	500_600_700
22.5	300	500_600_700
45	300	500_600_700

All the demagnetizations discussed in this chapter are shown in the following table.

Initial state	Demagnetization	Parameters	Name
Est saturated	Thermal	350°C; 5h	Sat/T _{demag} #1
Est saturated	Thermal	350°C; 5h	Sat/T _{demag} #2
"Est saturated"	AC Field	H:500 Oe; ΔH:0.01 Oe; Δt: 2s	H _{demag}
AC Field demagnetization (upper line)	Thermal	350°C; 5h	H _{demag} /T _{demag}

Where: - Sat/T_{demag} is related to thermal demagnetization performed from a saturated initial state.

-H_{demag} is related to AC field demagnetization.

-H_{demag}/T_{demag} is related to thermal demagnetization performed after AC field demagnetization.

The same protocol is used for Sat/T_{demag}#1 and Sat/T_{demag}#2, but the orientation of the sample in the oven is different (90° rotation between them). This rotation will be discussed in the section 5.2.

5.1 Coupled Potts spin lattice: qualitative study

5.1.1 Magnetic configurations measured after AC field demagnetization

In this section, the magnetic configurations shown are obtained after an AC field demagnetization with the same optimized parameters as defined previously: saturation field of 500 Oe, a field step of 0.01 Oe and an oscillation period of 2 seconds. In figure 4-7 are presented the magnetic configurations extracted from MFM images for lattice periods of 500, 600 and 700 nanometers and for the three lattice angles 0, 22.5 and 45 degree. Missing spins are located when the contrast is not good enough to determine the spin direction.

The figure 5-1 (a) to (c), show the configurations resulting from the AC field demagnetization for the 0° lattices for three lattice period. The lowest energy state for a theoretical system composed by spins with only dipole-dipole interactions is an antiferromagnetic state. In our case a perfect antiferromagnetic state should be represented by alternate lines which would be red and blue if it is North and South or green and black if it is West and East. The experimental results of figure 5-1 (a) to (c) are far away from a perfect antiferromagnetic state. Nevertheless small antiferromagnetic domains in the North-South and East-West directions are distributed over the whole lattice. It suggests the possibility to observe the behavior expected for the 0° lattice with a more efficient demagnetization procedure. The configuration of the three lattices (with 500, 600 and 700 nm period) show similar areas cover by anti-ferromagnetic domains.

Figure 5-1 (d) to (f) show the three lattices (with 500, 600 and 700nm period) for the 22.5° case. From our calculation, the fundamental state must be a ferromagnetic phase. The experimental maps do not show this behavior over the whole maps. Some ferromagnetic domains appear for the three periods but these domains are really small.

The configuration expected for 45° lattice with only dipole-dipole interactions between spins is a spin ice state which in our case, for a perfect ground state, is represented exclusively by two spins in and two spins out for each vertex. In terms of graphic representation, this configuration is reflected by the presence of 4 different arrows (North, South, East and West) at each vertex, which must lead to the creation of succession of “North, South, East, West loops” in the lattice. Experimental spin maps presented in figure 5-1 (g) to (i) show some “loops” which were never observed in the other lattice angles.

As a conclusion at this section, AC field demagnetization locally drives the system in its ground state, for the three angles 0, 22.5 and 45 degrees. But the number of the ground state domains is small and their sizes very restricted. As we already tuned the AC demagnetization as much as we could, it is unlikely that we can ever reach the ground state with AC field demagnetization. As a consequence, as of now, we will focus on our optimized process of thermal demagnetization.

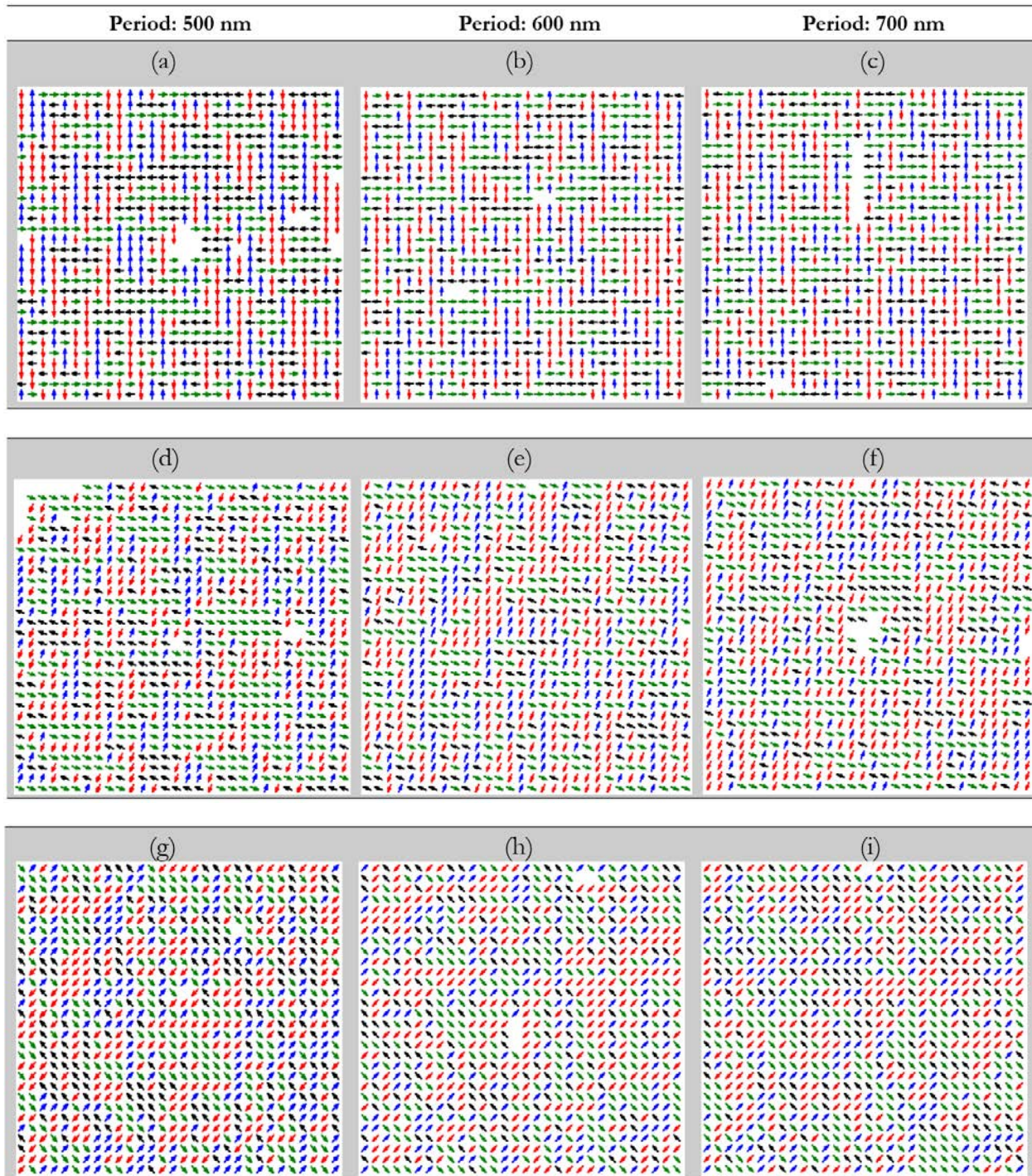


Figure 5-1_ Magnetic configurations extracted from MFM measurement for (a) to (c) 0° , (d) to (f) 22.5° and (g) to (i) 45° lattices as a function of the period (500, 600, 700 nm) obtained after AC field demagnetization.

5.1.2 Magnetic configurations measured after thermal demagnetization

The magnetic configurations, which are shown in the figure 5-2, are related to the demagnetization $Sat/T_{demag}\#1$. After an initial saturation along an anisotropy axis, the lattices are submitted to a five hour heating at a temperature of 350°C, then the sample is cooled down following a temperature ramp of 0.1°C/min. After demagnetization, magnetic configurations of the different lattices are imaged by MFM and these MFM images are processed by the “home program” Mathematica (mentioned in section 3.6.3.2), in order to represent directly the spin maps of nanomagnets lattices. Note that in the next paragraphs, the lattices have always been saturated in the **East** direction.

As mentioned previously, the configuration expected for 0° lattice with only dipolar interactions between spins is an antiferromagnetic state. In figure 5-2 (a) to (c) are presented the spins maps extract from MFM measurement on 500, 600 and 700 nm period for the 0° lattice. First, it is obvious that the perfect ground state does not appear in any of these experimental spin maps regardless of the period. Nevertheless some zones of the map are covered with antiferromagnetic lines configurations. This result is not surprising as a perfect ground state can only be obtained when only one spin is fixed at the beginning of the cooling down procedure while the others are still free to switch. From there dipolar interactions will force the neighboring nanomagnets to minimize the dipolar energy. Thus an antiferromagnetic domain is formed which grows until the entire lattice is covered. In real life, and even with a thermal barrier distribution, there are no reasons why only one spin should be frozen at the first place. Therefore few anti-ferromagnetic domains independently grow without coherency leading to multiple domains, with various sizes and shapes, at the end of the demagnetization process. These antiferromagnetic domains seem more numerous along one direction which is **North/South**, i.e. at 90° from the initial saturation. This fact is especially prominent for the lattice with 500 nm period. For the periods 600 and 700 nanometers, the antiferromagnetic domains, in **North/South** majority, are numerous but with small sizes. However for the period of 500 nanometers, these antiferromagnetic domains are less numerous but their sizes are clearly bigger than for the others periods. Another clear difference between the 500 nm period lattice and the two others, is the presence of big ferromagnetic domains whose spins point in the saturation direction (**East**). As the ferromagnetic state energy is just above the antiferromagnetic state in our calculations (see chapter I) some thermal hard-switchers may stay in the saturation direction and promote ferromagnetic ordering of the neighboring nanomagnets. The reminiscence of the saturated state is discussed in details in sections 5.2 and 5.5.

The configuration expected for 22.5° lattice with only dipolar interactions between spins is a ferromagnetic phase. For the three periods, ferromagnetic domains exist. Lots of small ferromagnetic domains can be seen for 600 and 700 nm period, while for 500 nm period they are less numerous but much bigger. These configurations seem to have been significantly driven by the dipolar interactions between nanomagnets and clearly different from the 0° lattice configurations. In the case of 500 nm, where the ferromagnetic domains are the biggest, only **East** and **South** directions cover most of the map and the **East** direction is the most extended one. It can be due, as discussed above, to the presence of thermal hard switchers. The prominence of these two directions is discussed quantitatively in details further in this manuscript.

The configuration expected for 45° lattice with only dipolar interactions between spins is a spin ice state which in our case, for a perfect ground state, is represented exclusively by loops in the lattice.

Thus a first ground state indicator should be the number of “loops” present in the lattice. Figure 5-2 (g) to (i) show the spin maps for 45° degree lattices with 500 up to 700 nm period. The numbers of loops are 71, 125 and 137 for 700, 600, 500 nm period respectively. So we can conclude that thermally demagnetized magnetic configurations depend on the dipolar interaction intensity. The good comparison with our theoretical calculations could also have been made on the argument of vertexes. Indeed, the perfect ground state is also represented by vertex composed by two-in/ two-out spins.

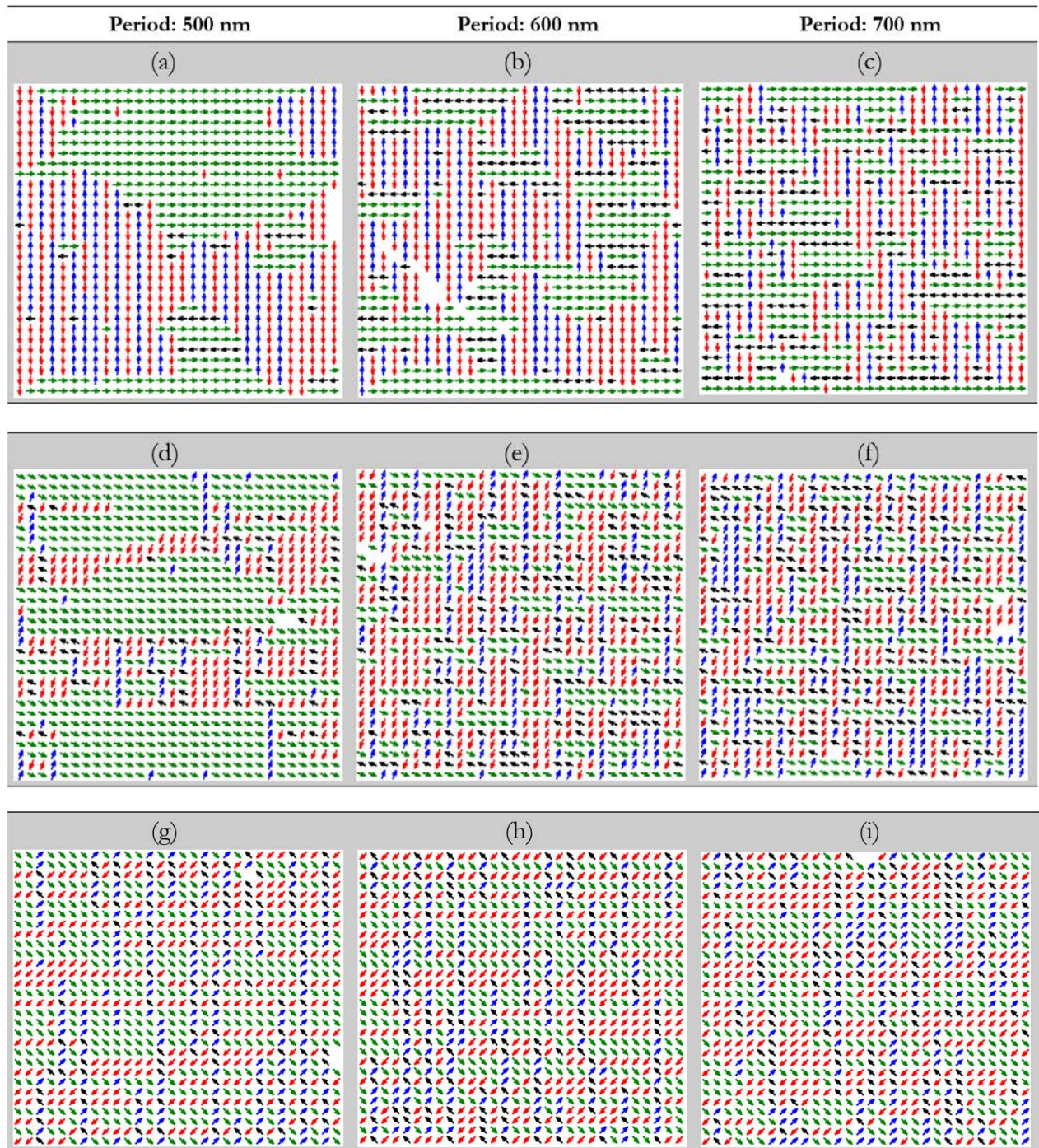


Figure 5-2_ Magnetic configurations extracted from MFM measurement for (a) to (c) 0°, (d) to (f) 22.5° and (g) to (i) 45° lattices as a function of the period (500, 600, 700 nm) obtained after thermal demagnetization (heating at 350°C) performed from an initial saturated state in the East direction (green arrows).

The configurations presented in the figure 5-2 are related to the $Sat/T_{demag}\#1$. And the results show different magnetic behavior for our system according to the spins directions, as expected from our theoretical calculations. In order to confirm these results, the magnetic configurations obtained from $Sat/T_{demag}\#1$ are compared with those obtain from the $Sat/T_{demag}\#2$ (identical demagnetization protocol). The results for lattices with a period equal to 500 nm are presented in the figure 5-3.

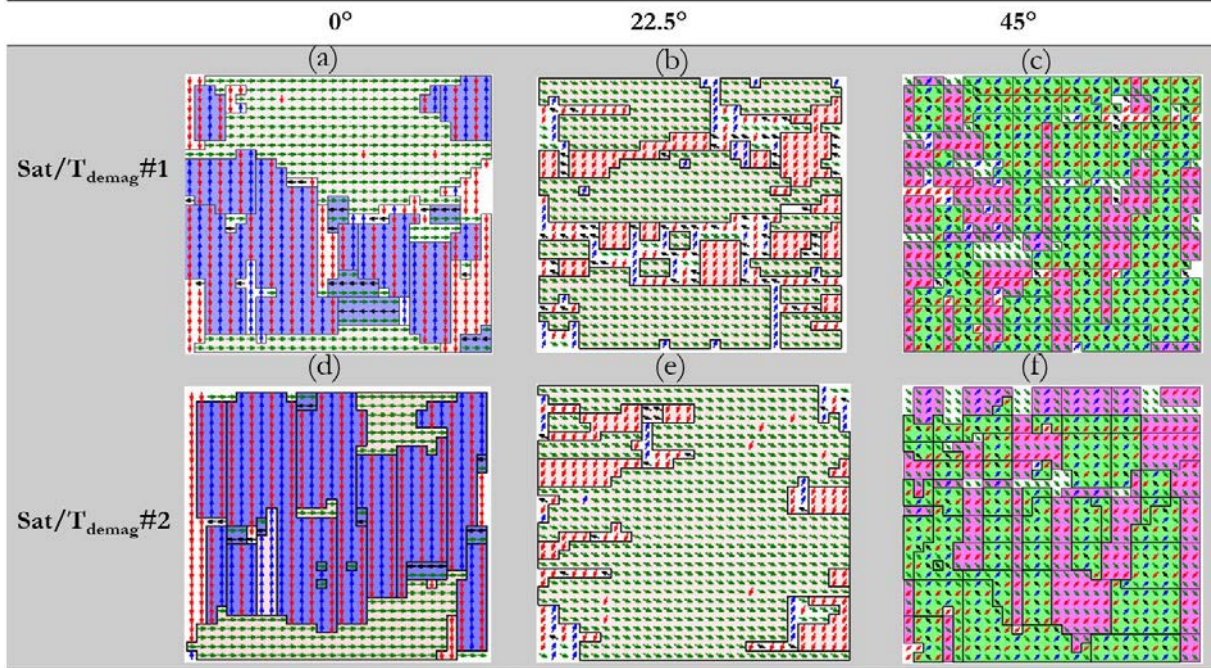


Figure 5-3_ Magnetic configurations extracted from MFM measurement for (a) to (c) $Sat/T_{demag}\#1$, (d) to (f) $Sat/T_{demag}\#2$ as a function of the angle (0° , 22.5° , 45°). The two demagnetizations correspond to a thermal demagnetization (beating at 350°C) performed from an initial saturated state in the East direction (green arrows). The spins maps are represented as well as particular domains. For 0° the antiferromagnetic domains (blue) and the ferromagnetic domains (beige) are represented. For 22.5° the ferromagnetic domains are represented (beige). For 45° the spin ice domains (green) and the wave domains (pink) are represented.

In the figure 5-3, the label (color as a function of the direction) for the spins is the same as previous spins maps, and the domains present in the different lattices are highlighted in order to make easier the comparison between the two thermal demagnetizations. For 0° lattices (Figure 5-3 (a), (d)), the antiferromagnetic domains (blue) and the ferromagnetic domains (beige) are represented. For 22.5° lattices (Figure 5-3 (b), (e)), the ferromagnetic domains (beige) are represented. And for 45° lattices (Figure 5-3 (c), (f)), the spin ice domains (green) and the wave domains (pink) are represented. Through the observation of the figure 5-3, we conclude that the results for the both thermal demagnetizations are really close.

For the three lattices angles, the magnetic configurations are a combination of the lowest energy states determined in the section 1.5: for 0° lattices the magnetic configurations are composed of ferromagnetic and antiferromagnetic domains, for 22.5° lattices the magnetic configurations are composed of ferromagnetic domains and for 45° lattices the magnetic configurations are composed of spin ice domains, waves domains and ferromagnetic domains. Thus we conclude that two thermal demagnetizations performed with the same protocol give similar magnetic configurations which show different magnetic behavior according to the spins directions as expected from our theoretical calculations.

5.1.3 Thermal demagnetization performed after field demagnetization

In the previous part, it has been shown that large ferromagnetic domains with spins pointing in the saturation direction remain after thermal demagnetization for the three lattice angle, although ferromagnetic state is not the ground state for 0° and 45° . It is therefore of interest to check the influence of thermal demagnetization on an AC field demagnetized lattice. For this analysis, only the results for the lattices with a period of 500 nanometers obtained from the $H_{\text{demag}}/T_{\text{demag}}$ are shown in this section. The initial state of the sample which is selected is the same as the configurations present in the section 4.2.1 for AC field demagnetization. Thus the system first undergoes AC field demagnetization, then is heated at a temperature of 350°C during 5 hours and finally is cooled down with a ramp temperature equal to $0.1^\circ\text{C}/\text{min}$.

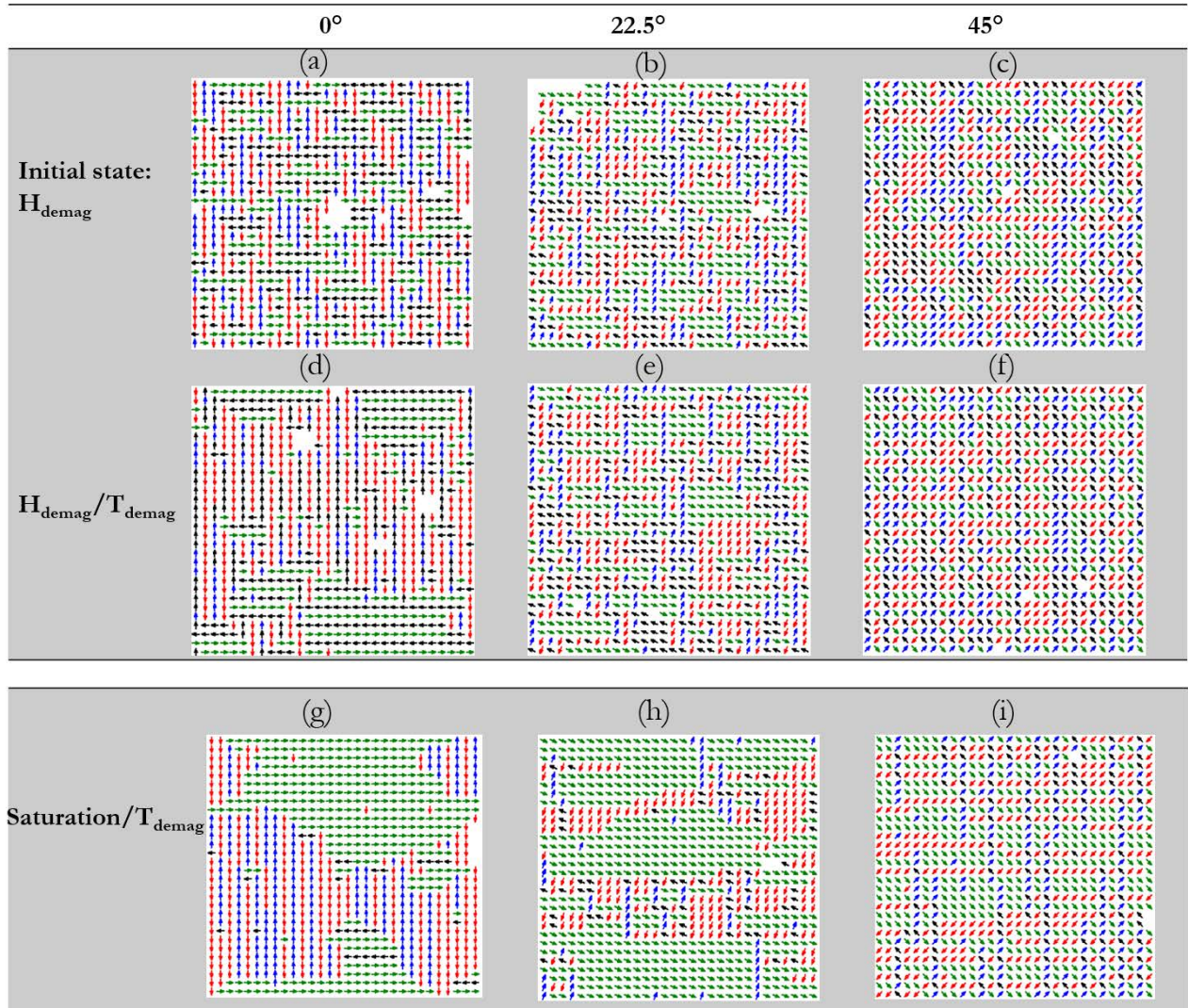


Figure 5-4_ Magnetic configurations (corresponding to lattices with a period of 500 nm) obtained after a field demagnetization (H_{demag} : from (a) to (c)) followed by a thermal demagnetization ($H_{\text{demag}}/T_{\text{demag}}$: from (d) to (f)). The configurations from (d) to (f) are compared with magnetic configurations induced by thermal demagnetization after saturation (Saturation/ T_{demag} : from (g) to (i)).

Comparison between spins map before and after thermal demagnetization (the initial state being an AC demagnetized state) is shown in figure 5-4. For the three angles, the configurations are closer to their fundamentals states after the thermal demagnetization. As an example, in the 45° case, the number of loops increases from 60 to 145 with thermal demagnetization. Mostly it seems that the ground state domains present in the initial state extend during the thermal demagnetization.

Let's now compare configurations induced by thermal demagnetization after saturation (figure 5-4 (g) to (i)), so-called Saturation/ T_{demag} , and after AC demagnetization (figure 5-4 (d) to (f)), so-called $H_{\text{demag}}/T_{\text{demag}}$. For the 0° lattice, the antiferromagnetic domains are bigger for Saturation/ T_{demag} , but these domains are only along one direction which is **North-South**. For the configuration $H_{\text{demag}}/T_{\text{demag}}$, antiferromagnetic domains don't show a preferential direction. Moreover the ferromagnetic domains present after the demagnetization Saturation/ T_{demag} are no longer visible in $H_{\text{demag}}/T_{\text{demag}}$. It confirms that these ferromagnetic domains originate from the saturation. They most probably remain in Saturation/ T_{demag} because of the weak energy difference between antiferromagnetic state energy and ferromagnetic state energy or because a large energy barrier to pass from one to the other. For the 22.5° lattice, since the initial state is already the expected ground state in Saturation/ T_{demag} it is not surprising that Saturation/ T_{demag} presents much larger ferromagnetic domains than $H_{\text{demag}}/T_{\text{demag}}$. Finally for the 45° lattice, the difference between the two demagnetizations is less evident. Saturation/ T_{demag} (137 loops) and $H_{\text{demag}}/T_{\text{demag}}$ (145 loops) have similar number of loops. The main difference between Saturation/ T_{demag} and $H_{\text{demag}}/T_{\text{demag}}$ consists, as in the 0° case, in the existence in Saturation/ T_{demag} of ferromagnetic domains with spins pointing along saturation field (**East**) and in the **South** direction. Nevertheless, as for the 0° lattice, it is not so simple to determine the best demagnetization process for the 45° lattice. One needs to quantify the energy of the final states.

As a conclusion of this part devoted to the first observation of spin maps obtained after thermal demagnetization, different magnetic behaviors for 0° lattice, 22.5° lattice and 45° lattice, are clearly demonstrated, as expected from our theoretical calculations. After the thermal demagnetization, we observe antiferromagnetic domains, ferromagnetic domains and spin ice type domains which are supposed to be the ground state for 0° , 22.5° , 45° respectively. These experimental results confirm that thermal demagnetization is efficient to reach low energy state, at least for the tested Potts spin lattice system. In the following we will compare in a more quantitative manner the experimental results and the theoretical predictions.

5.2 Discussion: Spins repartition and broken symmetry

Our above qualitative studies have shed a light on the impact of the initial state on the thermal demagnetization to drive the system toward its ground state. It means that the sample history matters and so that the temperature is not strong enough to completely excite the system over all the thermal energy barriers.

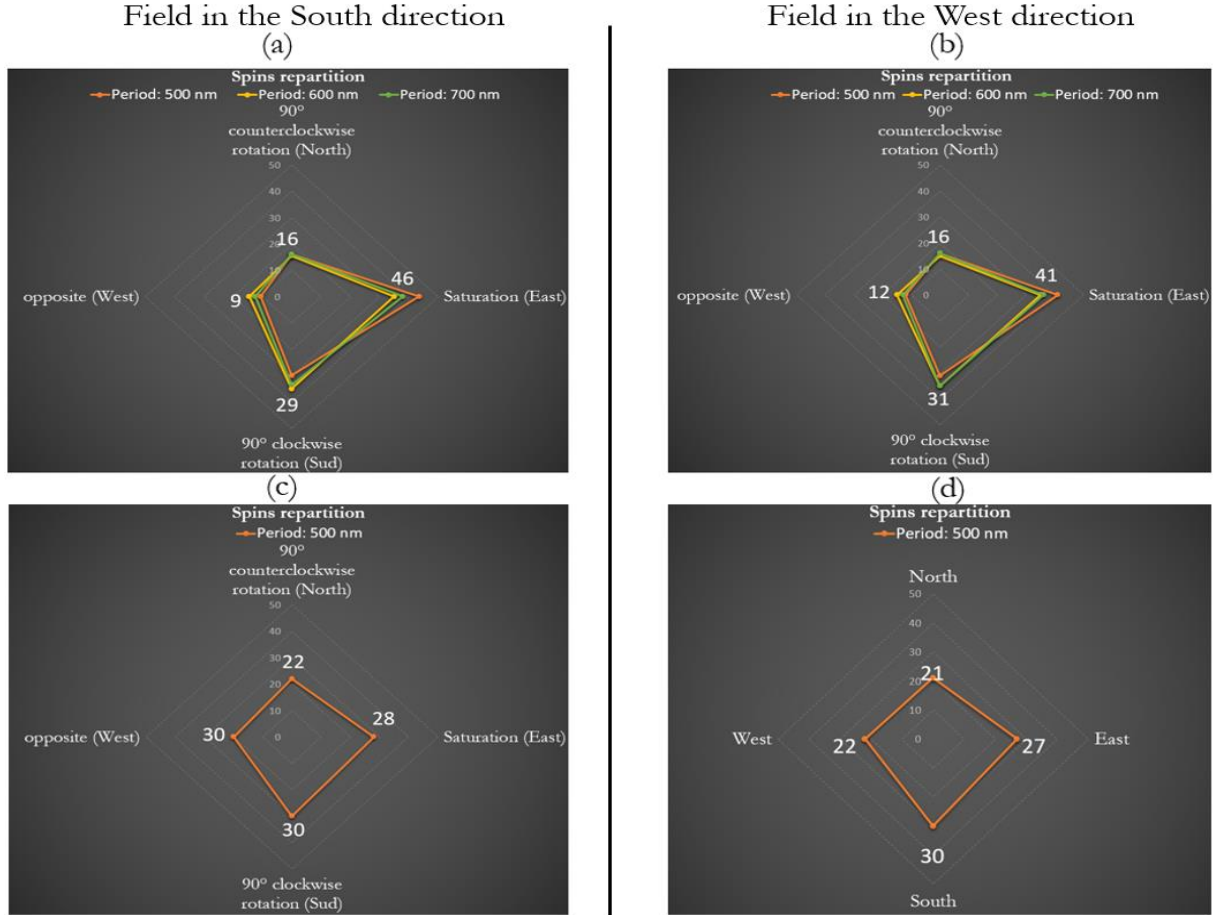


Figure 5-5_ Spins repartition (in percentage) for 45° lattices obtained after Sat/Tdemag#1 (a), Sat/Tdemag#2 (b), Hdemag (c) and Hdemag/Tdemag (d). For (a), (b), (c) the spins are identified according to their directions against the saturation direction related to the initial state (East). For (d), as the configuration is obtained after a thermal demagnetization performed from Hdemag, the spins are identified according to their nominal directions (East, West, North, South).

Now it remains a point to check that we have not used yet which is the imbalance between the four directions obtained after demagnetization for sample studied in section 5.1. In section 4.1, we used one sample hosting 700 nm period lattices. We used the weak coupling between the spins to demonstrate the good balance between the four directions found after demagnetization (almost 25% of spins per direction). For the section 5.1, we used a second sample which is nominally the same but which host 500 nm, 600 nm and 700 nm period lattices. Surprisingly, in this second sample (supposed to be identical) the same demagnetization protocol leads to an unidirectional imbalance of the 4 directions. This Spin imbalance is highlighted in figure 5-5, which represents the spins repartition in 45° lattices for all the demagnetization protocols performed on the sample. For (a), (b) related to the thermal demagnetizations performed from an initial state saturated, the three periods 500, 600 and 700 nm are represented. And for (c), (d) related to AC field demagnetization and thermal demagnetization performed after the AC field demagnetization

(respectively), the period of 500 nm is represented. Labels in the figure 5-5 (a, b, c) (opposite, 90° clockwise, etc.) refer to the direction of spins compared with the saturation field direction, as described in section 4.1.2.3.

For this 45° lattice in both strongly coupled (500nm) and weakly coupled (700 nm) case, we theoretically expect spins equi-distribution for the ground state (each loop must contain the 4 spin directions in the strongly coupled case). Nevertheless for Sat/T_{demag} (figure 5-5 (a) and (b)), a large number of spins are along the direction of the saturation field. This has been already discussed and originates from the choice of setting the system in a saturated state before the thermal demagnetization. In addition we observe an imbalance between the 90° counterclockwise spin and 90° clockwise spin. This imbalance is certainly not expected neither explained at this stage. For H_{demag} and H_{demag}/T_{demag} (figure 5-5 (c), (d)) a weak imbalance is also observed in favor of the direction East and South, as for the Sat/T_{demag}.

On this sample, we found that similar unidirectional imbalance exists for all the lattices regardless of the angle or of the period. Besides, it is especially pronounced for the Sat/T_{demag} protocol. Three potential sources of the broken symmetry can be mentioned: presence of a remaining magnetic field during the heating, existence of an exchange bias in our sample, and influence of the MFM tip during the scan.

Two independent annealing are performed (Sat/T_{demag}#1 and Sat/T_{demag}#2) and allow to check the presence of a magnetic field in the oven which could explain the two predominant directions. Indeed for these two thermal demagnetizations, the sample is saturated in the East direction then it is placed at the same position in the oven, except that the sample is rotated by 90° around the perpendicular direction to the sample. In figure 5-5 (a), (b) is shown the results related to these two thermal demagnetizations. In the figure 5-5 (a) the spins points mostly along the saturation direction (East direction) and toward the south direction. So maybe the oven contain a field pointing in the South direction. Figure 5-5 (b) shows similar diagram measured on the same sample, also saturated East but rotated by 90° in the oven during the thermal demagnetization. Comparison between figure 5-5(a) and 5-5(b) shows that the North-South asymmetry is identical whatever is the placement of the sample in the oven. Therefore we can conclude that the North-South asymmetry does not originate from a remanent magnetic field in the oven. This conclusion is also confirmed through the imbalance observed for AC field demagnetization, which is similar as this one for the thermal demagnetization.

Unfortunately for time reasons, the hypotheses of exchange bias and the tip influence have not been checked. In order to determine the presence of an exchange bias in our sample, magneto-optical Kerr effect (MOKE) measurements could be done. However in the chapter III, the magnetometric study of the sample has not revealed this exchange bias, and if this supplementary anisotropy exists, this one is maybe appeared in our sample due to the heating. If the tip during the MFM scan induced this imbalance in the spins repartition, the inversion of the magnetization direction of the tip (against this one used for all the results presented in this chapter) should show an inversion in the imbalance (North favored).

Nevertheless it remains that despite this not expected imbalance in the results, magnetic behaviors for 0° lattice, 22.5° lattice and 45° lattice are clearly different as expected from our theoretical calculations. We can now investigate more qualitatively the results obtained after demagnetizations.

5.3 Dipolar coupling effect

The parameter that can be used to probe the demagnetization efficiency and verify our dipolar Potts model is the lattice energy. For non-interacting spins, the spins direction repartition should be 25% for the four possible directions, and the energy resulting of such lattice should be equal to 0. For dipolarly coupled spins, the efficient demagnetization should lead to states with energies calculated in the section 1.5 for a 30x30 spin lattice. The experimental dipolar energies discussed in the next sections are extracted from the magnetic configurations shown in the section 5.1, in considering only dipolar interactions between nanomagnets.

In this section the influence of the intensity of the dipolar coupling between elements (through the period) is probed, for AC field demagnetization and thermal demagnetization.

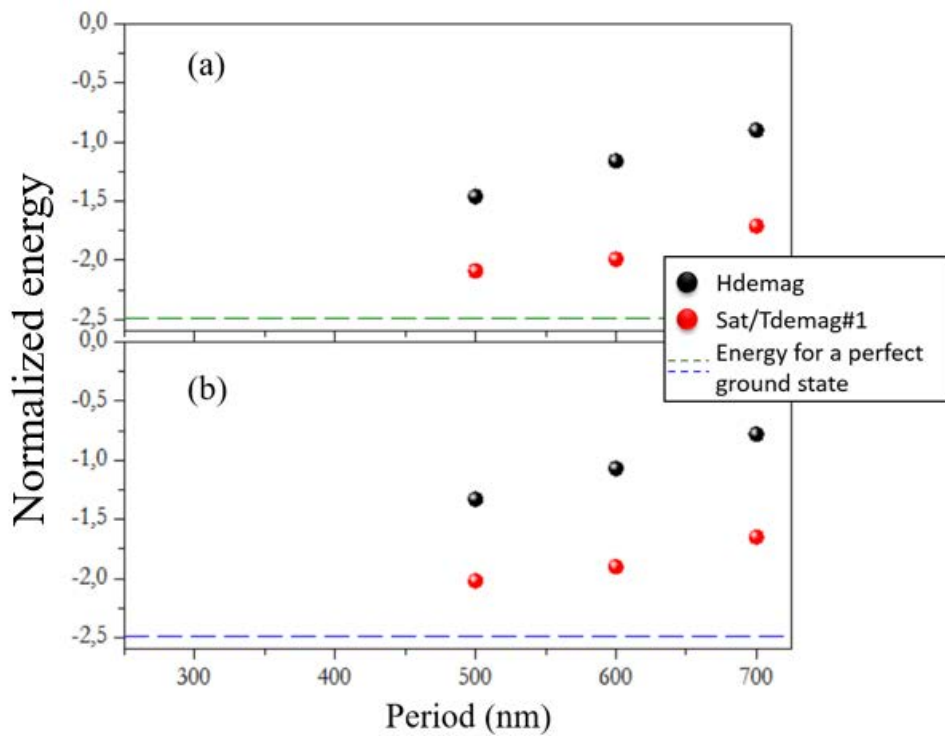


Figure 5-6_ Experimental configurations energies obtained after two demagnetization protocols (AC field demagnetization and thermal demagnetization) according to the period of lattices for two angles lattices: (a) 45° and (b) 0°. The black points are related to the configurations obtained after AC field demagnetization (H_{demag}) and the red points are related to the configurations obtained after thermal demagnetization (Sat/T_{demag}#1). The dashed lines (green and blue) represent the dipolar energies for the perfect ground state (spin ice state and antiferromagnetic state) calculated for a lattice 30x30 spins.

In the figure 5-6, the points represent the energies corresponding to the experimental spin maps extracted from MFM measurements for the three periods and two angles: (a) 45° lattice and (b) 0° lattice. The black points correspond to the results obtained after an AC field demagnetization (H_{demag}) and the red points correspond to the results obtained after a thermal demagnetization (Sat/T_{demag}#1). The green and blue dashed lines represent the energies given by the calculation for a 30x30 spins lattice where the magnetic configurations are spin ice state and antiferromagnetic state respectively. Although the dependence of the magnetic configuration on the lattice period for the AC field demagnetization was unclear from the eye, one can observe that the energy clearly

decreases when the period decreases for the two demagnetizations. This analysis in terms of energy confirms that the dipolar fields play a significant role during the demagnetizations (field or thermal). Moreover the magnetic configurations obtained by thermal demagnetization are much lower in energy than the ones obtained by AC demagnetization, as suspected in the observations of the magnetic configurations shown in the section 5.1. These results presented for 0° lattices and 45° lattices are also valid for the 22.5° lattices. As the figure 5-7 shows that the best efficiency for the demagnetizations is obtained for the smallest period (500 nm), we can now compare the different demagnetization protocols mentioned in the section 5.1 in term of dipolar energies in focusing the study on the smallest period.

5.4 Comparison between demagnetization protocols

The results shown in this section correspond to the energies linked with the configurations represented in the section 5.1, for only lattices with a period of 500 nanometers. The energies extracted from spin maps given by MFM images (see figure 5-4) are presented in the figure 5-7 and compared with theoretical energy values.

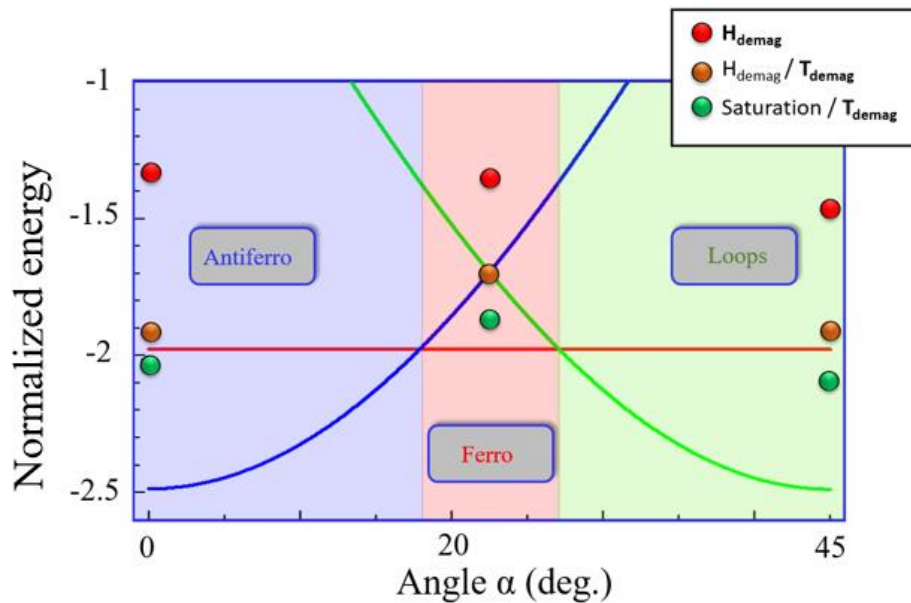


Figure 5-7_ Experimental configurations energies obtained after several demagnetization protocols for lattices with a period of 500 nm, layered on the theoretical energies determined in the section 1.4.2. Three protocols are presented which are field demagnetization (H_{demag}), thermal demagnetization with a ferromagnetic initial state (Saturation/ T_{demag}) and thermal demagnetization with an initial state obtained from field demagnetization ($H_{\text{demag}}/T_{\text{demag}}$).

These three demagnetization protocols are the same as mentioned in the section 5.1: field demagnetization (red points, H_{demag}), field demagnetization followed by thermal demagnetization (brown points, $H_{\text{demag}}/T_{\text{demag}}$) and saturation followed by thermal demagnetization (green points, Saturation/ T_{demag} #1). The results for Saturation/ T_{demag} #2 are really close to those observed for Saturation/ T_{demag} #1 and so are not represented to make the figure easier to read. In the following the label Saturation/ T_{demag} makes reference to Saturation/ T_{demag} #1.

Interestingly, comparison of AC demagnetization (H_{demag}) and thermal demagnetization after AC demagnetization ($H_{\text{demag}}/T_{\text{demag}}$) provides a direct quantification of the gain in energy induced by thermal demagnetization. So thermal demagnetization allows to form configurations closer from the ground state. In fact, figure 5-7 shows that lowest energies are always provided by the saturation then thermal demagnetization process (Saturation/ T_{demag}). Although it was difficult to deduce it from simple observation of the magnetic configuration in the case 0° and 45° lattice in section 5.1, it is now clear that performing thermal demagnetization on a saturated state is more efficient than on a AC demagnetized state. In the case of 22.5° lattice, it was intuitively expected. Indeed starting from a saturated state is the simplest way to get the ferromagnetic phase.

For 0 degree, antiferromagnetic domains are theoretically lower in energy than the ferromagnetic domains (see red and blue curves in figure 5-7). Saturation/ T_{demag} shows large **North-South** antiferromagnetic domains and two large ferromagnetic domains in the saturation direction, i.e. at 90° compared to the antiferromagnetic domains. Whereas $H_{\text{demag}}/T_{\text{demag}}$, shows antiferromagnetic domains in the two possible directions (**North-South** and **East-West**) and no ferromagnetic domains. It is therefore surprising that Saturation/ T_{demag} has lower energy than $H_{\text{demag}}/T_{\text{demag}}$, and domain walls between the domains may have a significant impact on this discrepancy.

In order to confirm this hypothesis, we determine the energy of each spin and represent in figure 5-8 a histogram showing the number of spins as a function of their energies, for a perfect antiferromagnetic state, a perfect ferromagnetic state, and for both Saturation/ T_{demag} and $H_{\text{demag}}/T_{\text{demag}}$ cases.

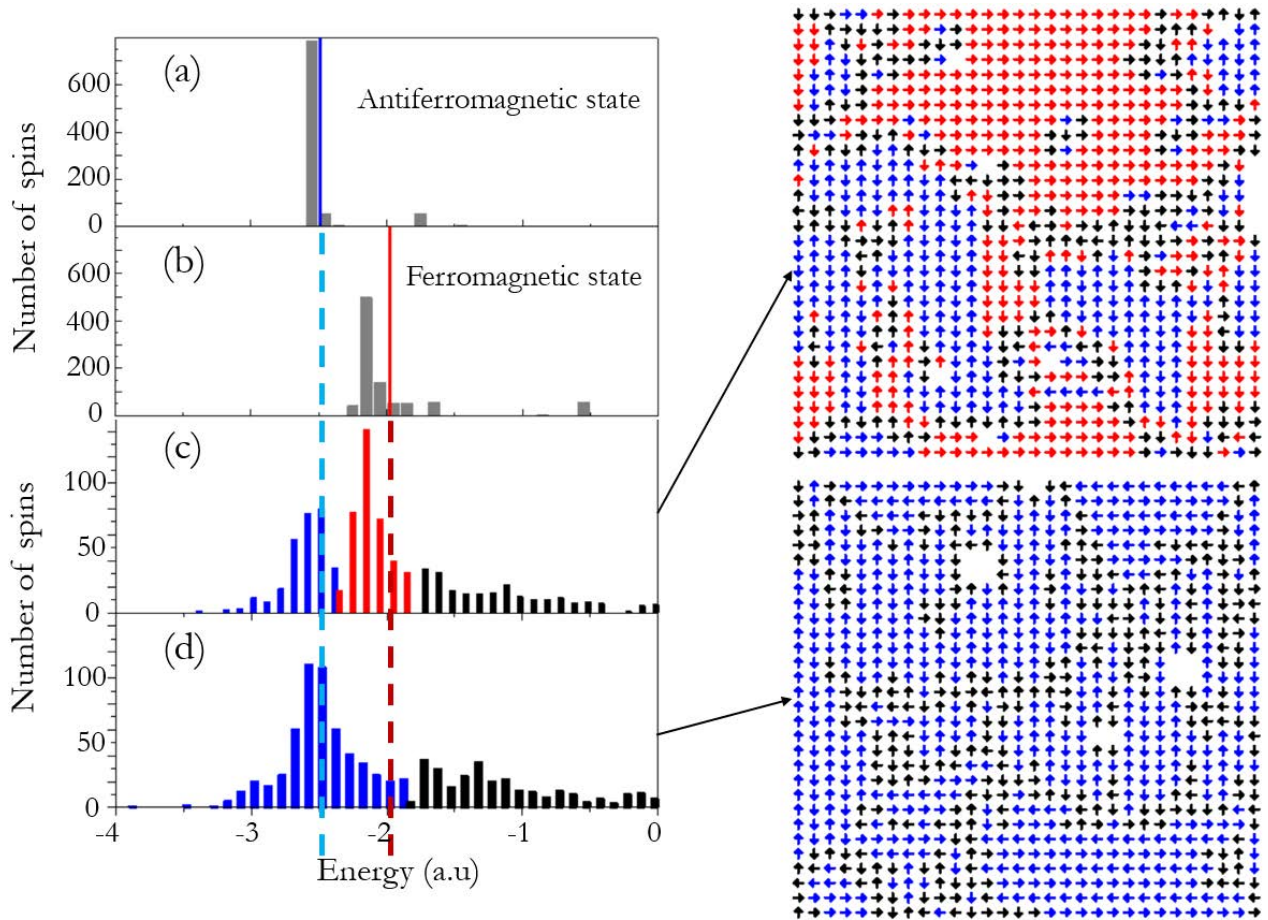


Figure 5-8_ Histograms representing the number of spins as function of the energy for (a) antiferromagnetic state for a 30×30 spins lattice, (b) ferromagnetic state for a 30×30 spins lattice, and for configurations obtained after two thermal demagnetizations with different initial states: (c) initial state: saturated, (d) initial state: state obtained from field demagnetization. The blue bars correspond to the spins composing the antiferromagnetic domains (blue spins in maps). The red bars correspond to the spins composing the ferromagnetic domains (red spins in maps). The Black bars correspond to the spins composing domain walls (black spins in map). The blue dashed line represents the energy for a perfect antiferromagnetic state in a 30×30 spins lattice and the red dashed line represents the energy for a perfect ferromagnetic state in a 30×30 spins lattice.

In the figure 5-8, in both histogram and map, spins in antiferromagnetic domains are colored in blue, the spins in ferromagnetic domains in red and the others spins in black. Blue, resp. red dashed line in the histogram represents the calculated energy for a perfect antiferromagnetic state, resp. ferromagnetic state, in a 30×30 spins lattice. The diagram highlights the high energy of the black spins which are located between magnetically ordered domains (i.e. they constitute domain walls).

In $\text{Saturation}/T_{\text{demag}}$, where the initial state is a saturated state, the histogram shows two main peaks. The spins are mostly either in the antiferromagnetic state or in ferromagnetic state. In $H_{\text{demag}}/T_{\text{demag}}$, only one antiferromagnetic (blue) spins peak appears, above in energy a continuum of domain wall (black) spins exists up to positive energies. The average energy for the domain wall (black spins) evolves from -1.178 in $\text{Saturation}/T_{\text{demag}}$ to -0.959 for in $H_{\text{demag}}/T_{\text{demag}}$. As a consequence, when summing the energies of all blue, red and black spins, although $H_{\text{demag}}/T_{\text{demag}}$ has more antiferromagnetically ordered spins, it has larger energy than $\text{Saturation}/T_{\text{demag}}$ because it holds more (and more energetic) black spins. This experience reveals the importance of the domain walls on the total energy of the system.

Besides, one can notice that, for the two demagnetizations, the energies corresponding to the spins composing the ferromagnetic state or antiferromagnetic state are in average lower than the energies expected for perfect ferromagnetic or antiferromagnetic states. This difference is not surprising and is explained by the small size of the domains observed which strengthens the side effects on the energies.

For the lattice 45° , our previous qualitative study indicated that $H_{\text{demag}}/T_{\text{demag}}$ (AC demagnetization, then thermal demagnetization) seemed more efficient than $\text{Saturation}/T_{\text{demag}}$ (saturation then thermal demagnetization). In particular the number of loops (revealing existence of ground state spin ice domain), is larger in $H_{\text{demag}}/T_{\text{demag}}$ than in $\text{Saturation}/T_{\text{demag}}$ (see figure 5-4). Counter-intuitively, the figure 5-7 shows that total energy of $\text{Saturation}/T_{\text{demag}}$ is lower than total energy of $H_{\text{demag}}/T_{\text{demag}}$. Similarly to the 0° case, this surprising result originates from the energy of spins between magnetically ordered zones of the lattice. Indeed in $\text{Saturation}/T_{\text{demag}}$, the spins between the spin ice domains present in majority two domains types which are ferromagnetic domains and wave domains (simple configuration mentioned in the section 1.4.2) as shown in the figure 5-3. The ferromagnetic domains are along two directions which are **East** (in majority) and **South** in minority, hence wave domains follow **East-South** direction. In $H_{\text{demag}}/T_{\text{demag}}$, the spins between the spin ice domains are more “disordered”, i.e. no specific order is found like ferromagnetic domains, wave domains or antiferromagnetic domains. Since ferromagnetic domains or waves domains have a much low energy than a disordered assembly of spins, and although the spin ice domains are more numerous in $H_{\text{demag}}/T_{\text{demag}}$, the total energy of $\text{Saturation}/T_{\text{demag}}$ is lower than the total energy of $H_{\text{demag}}/T_{\text{demag}}$. This confirms the important energy cost of domain wall in our demagnetized magnetic configuration.

The qualitative study of the configurations combined with the quantitative study of the energies have shed light on the ability of thermal demagnetization to locally drive our experimental Potts spins system towards its fundamental state. Moreover the experimental system well reproduced our theoretical model presented in section 1.5. The spin lattice magnetic behavior strongly depends on the lattice angle α . We were able to demonstrate experimentally that, in a specific case (22.5° lattice) dipolar field can force a ferromagnetic order in a 2D system, which is a quite remarkable behavior.

5.5 Some insights in the demagnetization process

A major limitation of our approach is that we only observe the final state of a complicated demagnetization process. However understanding and controlling this process is essential in order to decrease the gap between an artificial spin system and statistical physics. In the following lines, we will discuss some issues related to the phenomena which can occur during the demagnetization process.

A first very simple observation is that our process is able to "heat" the system. This is clearly seen for the thermal demagnetization starting from a saturated state. The energy of the final state is lowered for 0 and 45 degree but increased at 22.5 degree (this is the case for the 500 nm period, for 600 and 700 nm the energy is increased for any angle). However, the effective heating is not high enough to reach a highly fluctuating high temperature state. As a matter of fact, the nature of the initial state clearly influences the final state. This has been discussed in detail in the section 5.4. The importance of the initial state during the thermal demagnetization is revealed through the number of spins which are modified (and not) by the thermal demagnetization after the AC field demagnetization: 50% in the same state as the initial state, 34% which have rotated by 90° and 16% which have rotated by 180°. The maximum effective temperature during the demagnetization is therefore not high enough to make all the spins flip. This is the notion of hard switchers already mention in the section 4.1.2.3.

It is interesting to count the number of thermal hard switchers and to locate them on the spins maps in order to understand their impact on thermally demagnetized magnetic configurations. It is possible that this remanence of the saturation imposed the directions of the others spins, and in particular for the nearest neighbors, in order to minimize the dipolar energy between nanomagnets.

In order to identify the thermal hard switchers, we look for the spins which keep the same direction before and after a thermal demagnetization (for $Sat/T_{demag}\#1$, $Sat/T_{demag}\#2$ and H_{demag}/T_{demag}) for 500 nm period lattices. We count the number of unchanged spins and find the following percentage according to the lattice angle: 7% for 0° lattice, 29% for 22.5° lattice and 18% for 45° lattice. The fact that the proportion of hard switchers changes drastically according to the lattice angle is not expected for a point of view of single elements. The determination of the hard switchers is overestimated due to the demagnetization protocol where the initial state is saturated (2 out of 3 of the demagnetizations used), and it is necessary to consider that within these unchanged spins most of them (in particular for 22.5°) may not be hard switchers.

Nevertheless the hard switchers are identified in the spins maps related to the smallest lattice period (500 nm) for $Sat/T_{demag}\#1$ and H_{demag}/T_{demag} and represented for 45° lattices in the figure 5-14.

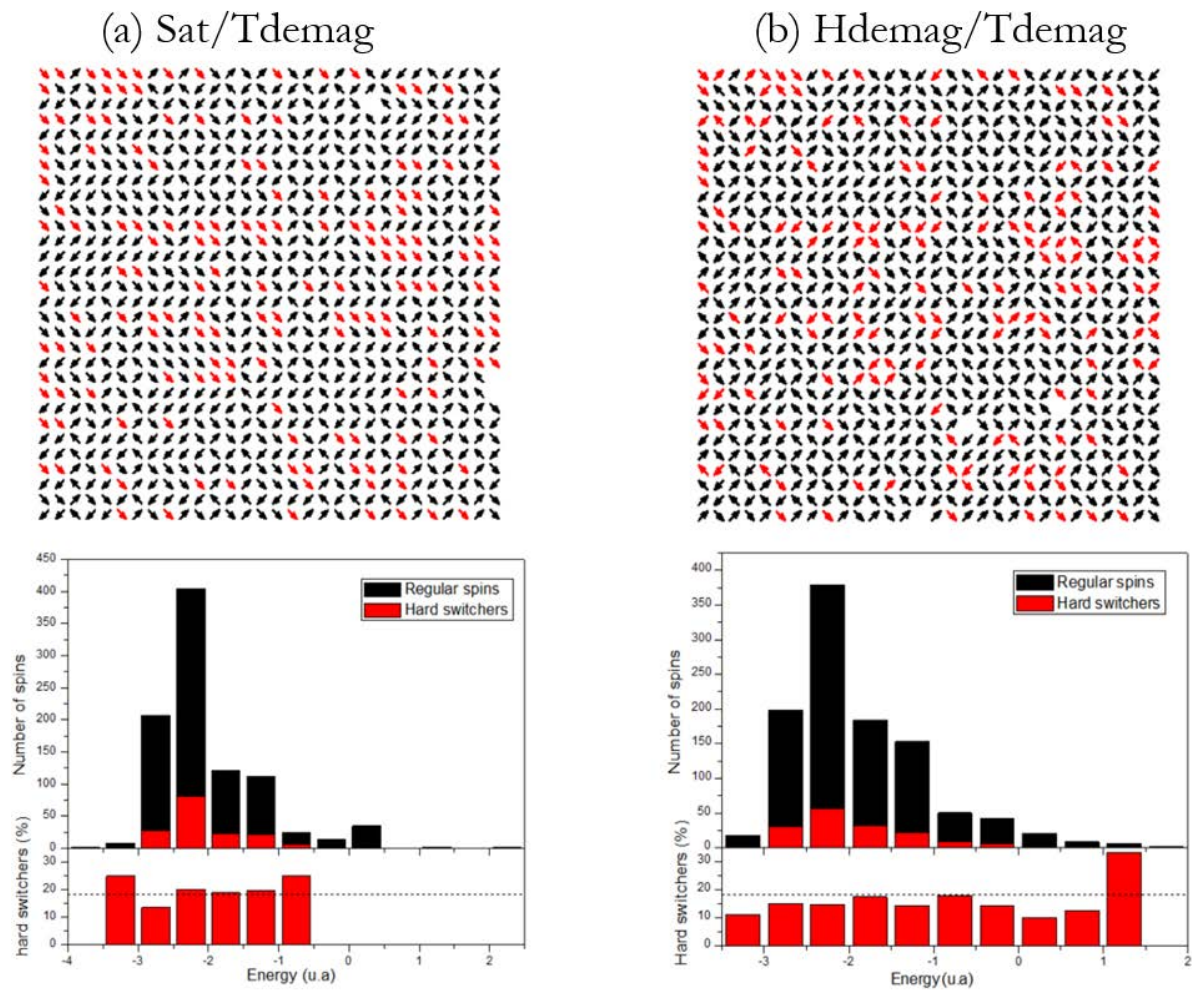


Figure 5-14_ Spins maps of the 45° lattices representing the regular spins (in black) which move before and after the thermal demagnetization and the thermal hard switchers (in red) for two thermal demagnetization protocols: (a) Sat/T_{demag} and (b) H_{demag}/T_{demag} . The histograms show the number of spins according to their energies for regular spins and hard switchers and also the proportion of hard switchers in the lattices according to the considered energies. The dashed lines represent the proportion of hard switchers in the entire lattice (regardless of the energy).

The hard switchers should favor the creation of ground state domains (loop domains for the figure 5-14) around them and so present a low energy. This fact should be especially the case for thermal demagnetization performed after the AC field demagnetization (H_{demag}/T_{demag}) where the spins are more disordered than for the ferromagnetic state (Sat/T_{demag}) where the spins are already in a low energy state. The observation of the spins maps seems confirm this hypothesis: the hard switchers in the configuration obtained after Sat/T_{demag} are all in waves or ferromagnetic domains which are low in energy, but not in loop domains which are the lowest in energy. While the hard switchers in the configuration obtained after H_{demag}/T_{demag} seem be in majority in loop domains. But a detailed analysis of the energy shows through the histograms of the figure 5-14 that the hard switchers in the configuration obtained after H_{demag}/T_{demag} (figure 5-14 (b)) present all the possible energies in equivalent proportion, while the hard switchers in configuration obtained after Sat/T_{demag} (figure 5-14 (a)) are part of the low energy spins. It emerges that it is difficult to determine a local order given by the hard switchers. But it is important to keep in mind that the determination of the hard switchers is overestimated, and so it is possible that this local order induced by the “true” hard switchers is hidden.

Another issue is the "thermalization" of the system. It is clear that the system does not reach its ground state but does the final corresponds to any effective temperature? To answer this question, we can consider the energy as an indicator directly related to the effective temperature. To do so we compare the energy determined for the 500nm period for three angles with Monte-Carlo results (already presented in section 1.5). It is clear that in the case of thermal demagnetization, it is not possible to affect a shared effective temperature for different angles. In particular, the angular dependence is less pronounced in experimental data than for equilibrium Monte-Carlo simulations. For a more quantitative analysis, we represent in figure 5-15, the direct correspondence with the effective temperature for the different configurations. For a thermalized process, the effective temperature should be the same for any angle.

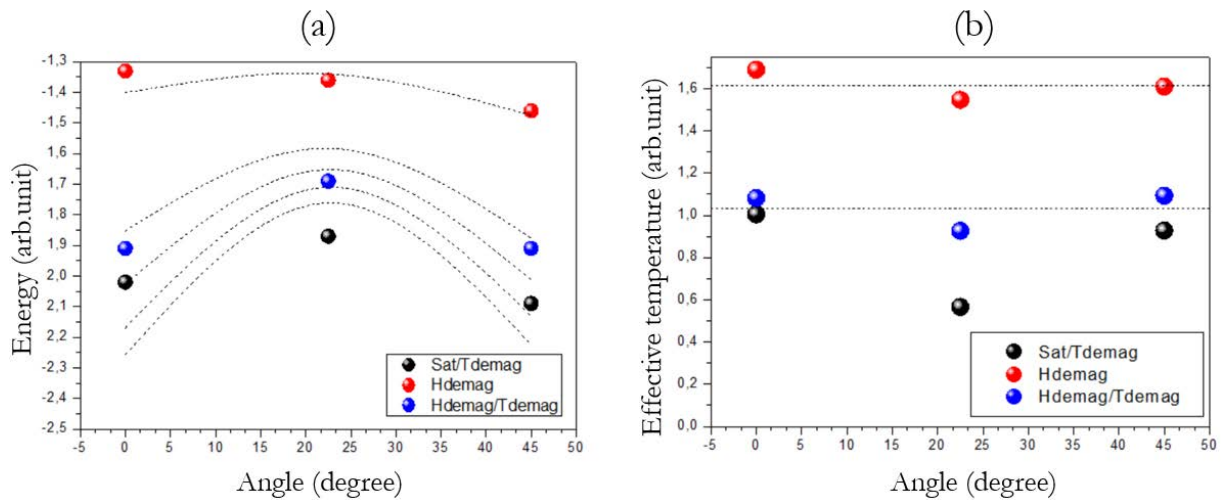


Figure 5-15_ The dotted lines are guides to the eyes. They are computed from the energies at 0, 22.5 and 45 degrees. (a) Experimental energies related to a lattice period of 500 nm obtained after three demagnetization protocols according to the lattice angle. (b) Effective temperature related to the energies given in the figure 5-15 (a), which are expressed in reduced units.

The comparison between the different angles relies on the fact that the coupling is the same, independently of the lattice angle. The micromagnetic simulations (section 2.3) have shown that is not exactly the case and that for a period of 500 nm, the coupling (expressed as the difference of energy between the two lowest energy states) is increased by quasi 50% at 0 degree compared to 45 degree. This would induce a lowering of the effective temperature in the same proportion. This is not observed here.

From the data, it is clear that the thermal demagnetization from the saturated state is the less coherent with a single effective temperature. This is not surprising as we already realized that these low energy states are achieved by keeping unchanged large domains of the initial saturated state. The corresponding configurations do not therefore correspond to thermal equilibrium states. For the two other protocols (field demagnetization and thermal demagnetization from a non-saturated state), the conclusion is less clear. The three configurations can be associated with a single temperature range, respectively 1.62 ± 0.07 and 1.01 ± 0.08 . This is a strong indication but beyond energy to assess the validity of the effective temperature all other properties have to be mapped and moreover more configurations should be determined to increase the statistical relevance of the data. The effective thermalization of the artificial dipolar Potts system thus remains an open question.

5.6 Summary of chapters 4 and 5

“Historically” the artificial spin systems have been introduced to realize experimentally models of the statistical physics. And one of the main issue of these systems is to find the best way to allow the system to explore its phase space, in order to compare the experimental behavior to this one expected by the spin model. In the community of artificial spin systems two main ways (called demagnetizations) have been explored in order to drive the system towards its ground state. The first, exposed historically by Wang et al [11], is the AC demagnetization. And the second exposed more recently [15, 23] is the thermal demagnetization. For this second protocol, two approaches are possible, one considering superparamagnetic regime [23] and another proposed by Zhang et al. [15] involving an annealing procedure above the Curie temperature. In this chapter, the AC demagnetization and the thermal demagnetization considering superparamagnetic regime were used, and their efficiencies were compared.

One of the first questions of this chapter, was to know if the thermal demagnetization is possible for our experimental system described in the chapter III. Indeed one of the challenge for the community [23, 24] is to design nanomagnets which can be sensitive to thermal fluctuations. Thus the lattices were firstly heated at a temperature of 300°C, and it appears that according to the size of the nanomagnets, it can occur a magnetization reversal in the nanomagnets. Indeed for a size below 500 nanometers, the thermally activated reversal is possible. This means that for a size of nanomagnets around 300 nanometers, a temperature of 300°C is large enough to give a thermal energy higher than the intrinsic energetic barrier that separates two preferential directions for the magnetization. Thus in this chapter, only squares with a length of 300 nanometers were selected. Then the optimal parameters for the heating were determined and in particular the heating time (5 hours), the ramp temperature (0.1°C/min) and the temperature (350°C).

As the aim is to drive the system towards its ground state thanks to the demagnetization, the AC demagnetization and the thermal demagnetization were performed, and the magnetic configurations given by these two protocols were compared. The first chapter reveals that according to the angle between spin and the lattice axis (alpha angle), the dipolar 4-state Potts model shows different properties for its ground state, and in particular three configurations related to three angle ranges. Thus three angle lattices were designed which are 0°, 22.5° and 45° lattices. In order to characterize the configurations obtained after the demagnetizations, two parameters were recorded which are the direct observation of the magnetic configurations (spins map) and the dipolar energies related to these spins maps. Moreover these parameters were recorded for three periods of lattices which are 500, 600 and 700 nanometers in order to demonstrate that the demagnetization protocols were just a way to let the system gradually minimize its energy in accommodating pairwise interactions via the dipolar interactions.

A first conclusion emerges regarding the results obtained according to the periods of the lattices. Indeed the results for the two demagnetization protocols show a reduction of the dipolar energy when the period of the lattice is reduced. This observation reveals that the demagnetizations performed (field and thermal) let effectively the system minimize its energy via the dipolar interactions between nanomagnets. However with the direct observation of the magnetic configurations (qualitative characterization), a significant difference according to the period appears only for the thermal demagnetization. Nevertheless regarding the results obtained with the two demagnetization protocols for the smallest period (500 nanometers), the results show for the both that the configurations obtained present a signature of the ground state shown by the dipolar

4-state Potts model. Indeed according to the alpha angle, the configurations present really different properties: for alpha equal to 0° antiferromagnetic domains appeared, for alpha equal to 22.5° ferromagnetic domains appeared, and for alpha equal to 45° loop crystal domains appeared.

In observing the dipolar energies related to the magnetic configurations obtained after different demagnetization protocols (Sat/T_{demag} , H_{demag} , $H_{\text{demag}}/T_{\text{demag}}$) for the smallest period, it emerges clearly that the thermal demagnetization drives the system in a lower energy state than the AC field demagnetization. So the thermal demagnetization turns out to be, in our case, the best way to drive the system towards its fundamental.

However the results obtained after Sat/T_{demag} reveal a remanence of the initial state imposed in our system which is a saturated state. Moreover this remanence is in part responsible of the low energy states observed after the demagnetization. Thus the origin of this remanence was determined, and after a detailed observation it emerges that this remanence is due to a distribution of the energy barrier that separates the preferential states for the magnetization, which gives rise to the presence of hard switchers. So a thermal demagnetization was directly performed after a field demagnetization, in order to determine the influence of the initial state for the thermal demagnetization. And the thermal demagnetization performed from the saturated initial state gives configurations closer to the ground state expected by the spin model than the other thermal demagnetization. And thus it can be concluded that as the thermal demagnetization is not optimal, the ferromagnetic domains induced by the hard switchers, which are not so far in term of energy from the expected ground state for the three angle lattices, induce a low energy state. However it is important to keep in mind that if the efficiency of the thermal demagnetization can be improve, these hard switchers could be a limitation to drive the system towards its ground state.

Bibliography

- [11] R.F.Wang et al, “Artificial ‘spin ice’ in a geometrically frustrated lattice of nanoscale ferromagnetic islands,” *Nature*. **439**, 303–306 (2006)
- [15] S.Zhang et al, “Crystallites of magnetic charges in artificial spin ice”, *Nature*. **500**, 553-557 (2013)
- [17] S.Zhang et al, “Perpendicular Magnetization and Generic Realization of the Ising Model in Artificial Spin Ice”, *Phys. Rev. Lett.* **109**, 087201 (2012)
- [22] L.Néel, “Théorie du trainage magnétique des ferromagnétiques au grains fin avec applications aux terres cuites. *Ann. Géophys.* 5 (1949), pp. 99–136”, *Annals de Géophysique*. **5**, 99–109 (1949)
- [23] V.Kapaklis et al, “Melting artificial spin ice”, *New J. Phys.* **14**, 035009 (2012)
- [24] A.Farhan et al, “Direct Observation of Thermal Relaxation in Artificial Spin Ice”, *Phys. Rev. Lett.* **111**, 057204 (2013)
- [79] Z.Budrikis et al, “Disorder regimes and equivalence of disorder types in artificial spin ice”, *J. Appl. Phys.* **111**, 07E109 (2012)
- [80] Z.Budrikis et al, “Disorder Strength and Field-Driven Ground State Domain Formation in Artificial Spin Ice: Experiment, Simulation, and Theory”, *Phys. Rev. Lett.* **109**, 037203 (2012)
- [81] Z.Budrikis et al, “Diversity Enabling Equilibration: Disorder and the Ground State in Artificial Spin Ice,” *Phys. Rev. Lett.* **107**, 217204 (2011)
- [82] J.P.Morgan et al, “Thermal ground-state ordering and elementary excitations in artificial magnetic square ice,” *Nat. Phys.* **7**, 75–79 (2011)
- [83] A.Farhan et al, “Exploring hyper-cubic energy landscapes in thermally active finite artificial spin-ice systems,” *Nat. Phys.* **9**, 375–382 (2013)
- [84] F.Montaigne et al, “Size distribution of magnetic charge domains in thermally activated but out-of-equilibrium artificial spin ice”, *Sci. Rep.* **4** (2014)
- [85] I.A.Chioar et al, “Kinetic pathways to the magnetic charge crystal in artificial dipolar spin ice”, *Phys. Rev. B.* **90**, 220407 (2014)
- [86] J.Drisko et al, “FePd₃ as a material for studying thermally active artificial spin ice systems”, *Phys. Rev. B.* **91**, 224406 (2015)
- [87] A.Farhan et al, “Thermally induced magnetic relaxation in building blocks of artificial kagome spin ice”, *Phys. Rev. B.* **89**, 214405 (2014)
- [88] I.Gilbert et al, “Emergent ice rule and magnetic charge screening from vertex frustration in artificial spin ice”, *Nat. Phys.* **10**, 670–675 (2014)
- [89] H.Riahi, «Propriétés du réseau kagomé artificiel : micromagnétisme, chiralités et cristaux de charges émergents», Thèse de doctorat réalisée à l’université Henry Poincaré, Nancy, France (2013)
- [90] R.F.Wang et al, “Demagnetization protocols for frustrated interacting nanomagnet arrays, *J. Appl. Phys.* **101** (2007)

[91] X.Ke et al, “Energy minimization and ac demagnetization in a nanomagnet array, Phys. Rev. Lett. **101**, 037205 (2008)

[92] J.P.Morgan et al, “Linear field demagnetization of artificial magnetic square ice, Frontiers in Physics. **1** (2013)

[93] J.M.Porro et al, “Exploring thermally induced states in square artificial spin-ice arrays”, New J. Phys. **15**, 055012 (2013)

6. Conclusions and Perspectives

6.1 Conclusions

Since 2006 [11], the lithographically-patterned arrays of nanomagnets have been a strong surge of interest as it has been demonstrated that these systems can be count as toy-spin models. Indeed the artificial spin systems propose quasi-limitless possibilities for the design of spins or arrays, and allow an observation in the direct space of the magnetic degrees of freedom. Generally, the nanomagnets interact with each-other in a magnetostatic framework, and through demagnetization protocols, like AC field demagnetization [11] or more recently thermal demagnetization [15], it is possible to visualize the phase spaces of these artificial spin systems.

Up to know in the artificial spin systems, lots of topologies for the arrays have been designed [12, 11, 16] but all the nanomagnets designed in these arrays present themselves as classical Ising spins where the magnetization (in-plane or out-of-plane) has two preferential orientations. This particularity was one of the main motivation of this thesis, where the idea was to designed in playing with the anisotropy (shape and crystalline), a new system where the spin is not a 2-states spin but a 4-state spin. Indeed historically, in the 1920's, lots of spin models have been described and in particular two well-known models which are the Ising model [18] and the Potts model [19]. Thus during this thesis, the purpose was to design an artificial spin system which is no longer linked to the Ising model (as up to know in the artificial spin systems) but linked to the Potts model.

In this context, the present thesis has described briefly the “classical” Potts model with the general definition of the Hamiltonian related to this model, then a particular case was detailed which was the dipolar 4-state Potts model. In this model it is considered spins with 4 states confined in a plane which interact between each-other via dipolar interactions. Thus a first comparison between two Ising spins and two Potts spins reveals that the introduction of 2 supplementary states for the spins, induced a more complex behavior for the system, as the introduction of two supplementary states for the spins induced new possible configurations and so new energy levels. Moreover the study of two Potts spins brings to light that the energy levels depend on the angle between the spin and the axis between the two spins (called alpha angle), and so that according to this angle, the ground state present in the system is different. Then the study was extended to the case of an infinite 1D chain then to the case of an infinite 2D lattice, both composed of Potts spins and a particular attention was given to the identification of the ground state for the infinite 2D lattice. In this aim, simple configurations were observed (like ferromagnetic state or antiferromagnetic state), then more complex configurations were observed (lattice formed by the replication of unit meshes composed of 2x2 spins) and finally configurations formed by the replication of unit meshes composed of 30x30 spins. The observation of the dipolar energies related to the different configurations demonstrates that the ground state related to the infinite lattice composed of Potts spins is strongly related to the angle between the spins directions and the lattice axis. Indeed it appears that the lowest energy state determined take three different configurations according to the alpha angle: the antiferromagnetic state (for spin directions close to the lattices directions), the spin ice state (for spin directions close to 45 degrees from the lattices directions) and the ferromagnetic state (for intermediate spin directions). Moreover even if the ground state was not exactly determined, the indications given by the lowest energy states determined (and confirmed by Monte Carlo

simulations) reveal that the 2D lattice composed of Potts spins is a very versatile system as the simple rotation between spins and the lattice axis gives rise to very different properties for the ground state. These interesting properties have motivated the experimental realization of the dipolar 4-state Potts system. It was decided to design 30x30 lattices because of a compromise between time measurements and accuracy measurements. For this size lattice, Monte Carlo simulations have shown a similar ground state as the one observed for the infinite lattice except for 22.5° , where the lowest energy state determined is a Landau state composed of ferromagnetic domains which follow the edges.

As it was the first time that an artificial 4-state spin system was designed, a preliminary study was realized, through micromagnetic simulations (via Mumax3 [49]), in order to determine the conditions for this realization. And it emerges that the realization of a 4-state spin is possible in taking a shape with cubic symmetry and in selecting for the magnetic layer a thin film with a cubic anisotropy. Thus the monodomain stabilization in several shapes was studied and a square designed in a thin film of iron with cubic anisotropy axes aligned with the diagonals of the square appears as the best candidate to obtain a uniform magnetization which can take 4 preferential directions. Moreover the simulations have also confirmed the validity of the dipolar approximation in showing that, in the case of two nanomagnets, the coupling present the same behavior (energy levels according to the configurations) as this one revealed by the spin model.

The material selected for the experimental realization was a multilayer sample with the following composition: MgO/V (20 nm)/Fe (2 nm)/V (2 nm)/Au (20 nm), which reveals only a cubic anisotropy with a magnetization in-plane no disturbed by the interfaces V/Fe or after an annealing up to 400°C . Then some artificial 4-state spin lattices were designed in this sample and the magnetic configurations were probed in using a standard characterization technique: the magnetic force microscopy (MFM). Several tests have confirmed the intrusive nature of this technique, as it was shown in this thesis that the MFM scans (with standard tip and low moment tip) disturb the magnetic configurations in our lattices. And a solution was given, which consists in adding a nonmagnetic layer at the sample surface in order to increase the distance between the tip and the magnetic layer during the MFM scans. This solution is efficient but induces a reduction of the magnetic contrast observed in our lattices.

One of the main issue of this thesis was to find a way to allow the system to explore its phase space, in order to compare the experimental behavior to this one expected by the spin model. In this aim two demagnetization protocols were used: the AC field demagnetization [11] and the thermal demagnetization [23]. Several sizes (200, 300, 500, 700, 1000 nm) for the nanomagnets were designed and after the two demagnetization protocols the results demonstrate that the best compromise between demagnetization efficiency and MFM measurements accuracy is obtained for a size of 300 nanometers. Thus only lattices composed of squares with a length of 300 nanometers and with three periods (500, 600 and 700 nm) were selected and their magnetic configurations given by the two demagnetization protocols were recorded. And as the dipolar 4-state Potts model reveals different properties according to the angle between spins direction and lattice direction (α angle), three lattices angles were designed: 0° , 22.5° and 45° .

The dipolar energies related to the magnetic configurations given by the two demagnetization protocols, according to the lattices period, demonstrate the influence of the dipolar coupling. Indeed the results of the two demagnetization protocols show a reduction of the dipolar energy when the period of the lattices is reduced. This observation confirms that in our artificial spin

system, the demagnetizations are just a way to let the system gradually minimize its energy via the dipolar interactions.

A detailed study of the magnetic configurations (and the related energies) obtained after the both demagnetizations for the lattices with a period of 500 nanometers reveals different properties according to the lattices angles which are in good agreement with the spin model. Indeed according to the lattice angle, different domains appears which represent the signature of the ground state given by the dipolar 4-state Potts model: for 0° lattice antiferromagnetic domains appear, for the 22.5° lattice ferromagnetic domains appear and for 45° lattice spin ice domains appear. Nevertheless this study shows clearly that our system reaches a state closer to the ground state expected by the spin model after a thermal demagnetization than after an AC field demagnetization.

6.2 Perspectives

This PhD has presented the principle of the dipolar 4-state Potts model and proposed an experimental realization of the model. But the subject is far from being closed and different points remain to be studied and new aspects can also be considered. The biggest question mark is certainly about the dynamic of the system. Our results show that it exists a distribution of barrier height for the reversal and that the barrier height can even depend on the direction. But these conclusions are drawn from final frozen configurations and a "real-time" characterization of the high temperature behavior is clearly missing. This characterization could be obtained with XMCD-PEEM imaging. Even for an individual element such a dynamic study would be interesting as, to the best of our knowledge, up to now only 2 state systems have been studied. The impact of this dynamic on the ordering of the dipolar 4-state Potts model would be the ultimate goal.

The understanding of the dynamic should lead to the optimization of the demagnetization protocol and so opening the way to more quantitative analysis. For example, in this work, we focused only on the 0, 22.5 and 45 degree lattices. It would be interesting to investigate intermediate angles and particularly the transition angles at which antiferromagnetic or loop state have the same energy than the ferromagnetic state (uniform or multidomain). The next step can also be to study other systems than the square lattice. We already showed that the 1D chain is an interesting system with a (small) angular range in which complex magnetic patterns can occur. Thanks to the versatility of lithography any other lattice can be considered (hexagonal lattice for instance or more exotic forms like Shakti lattices).

Another aspect is the potential use of this "artificial spins" as element of nanomagnet logic. A lot of work has been devoted to magnetic logic using nanomagnet coupled by dipolar interactions [94, 95, 96]. An appropriate arrangement of the elements is able to realize some Boolean logic function. As we are able to make these 4-state nanomagnets and to control the interactions between them, there is maybe a possibility to build some 4 states logic gates!

Bibliography

- [11] R.F.Wang et al, “Artificial ‘spin ice’ in a geometrically frustrated lattice of nanoscale ferromagnetic islands,” *Nature*. **439**, 303–306 (2006)
- [12] M.Tanaka et al, “Domain structures and magnetic ice-order in NiFe nano-network with honeycomb structure”, *J. App. Phys.* **97**, 10J710 (2005)
- [15] S.Zhang et al, “Crystallites of magnetic charges in artificial spin ice”, *Nature*. **500**, 553-557 (2013)
- [16] I.A Choar et al, « Nonuniversality of artificial frustated spin systems », *Phys. Rev. B*. **90**, 064411 (2014)
- [18] E.Ising, “Beitrag zur Theorie des Ferromagnetismus”, *Z. Phys.* **31**, 253-258 (1925)
- [19] Potts, “Some generalized order-disorder transformations”, *Proc. Comb. Phil. Soc.* **48**, 106 (1952)
- [23] V.Kapaklis et al, “Melting artificial spin ice”, *New J. Phys.* **14**, 035009 (2012)
- [49] A.Vansteenkiste et al, « The design and verification of Mumax3 », *AIP Advances* (2014)
- [94] J.Jaworowicz et al, “Magnetic logic using nanowires with perpendicular anisotropy”, *Nanotechnology*. **20**, 21 (2009)
- [95] D.A.Alwood et al, “Magnetic domain wall logic”, *Science*. **309**, 5741, 1688-1692 (2005)
- [96] J.H.Franken et al, “Magnetic domain wall ratchets with perpendicular anisotropy”, *Nature Nano-Technology*. **7**, 499-503 (2012)



Vers un nouveau système de spins artificiels: le modèle de Potts dipolaire à 4 états

Depuis la proposition en 2006 d'utiliser des nano aimants réalisés par des techniques top-down pour reproduire des « spins artificiels », l'étude des systèmes de spins artificiels a suscité un large intérêt. En effet la possibilité de pouvoir réaliser arbitrairement tous types de réseaux de spins artificiels et de pouvoir imager les configurations magnétiques de ceux-ci dans l'espace direct, offre un large terrain de jeu dans le domaine de la physique statistique. Jusqu'à présent seuls des réseaux de spins d'Ising, multi axes (réseaux kagomé ou carré avec une aimantation planaire) ou plus récemment uni axes (avec une anisotropie perpendiculaire), ont été étudiés. Cependant en physique statistique d'autres modèles de spins sont étudiés et notamment les modèles de Potts à q -états. Au cours de cette thèse nous avons étudié le cas d'un modèle de Potts à 4 états, ayant la particularité de posséder uniquement des interactions dipolaires entre les spins: le modèle de Potts dipolaire. Nous avons tout d'abord réalisé une étude théorique, montrant que sur un réseau carré, en fonction de l'angle entre les spins et ce réseau, le système possède des états fondamentaux très différents : un ordre antiferromagnétique, un ordre respectant les règles de la glace (2 in- 2 out) ou un ordre ferromagnétique. Dans une deuxième partie, nous avons exposé l'étude expérimentale du modèle de Potts dipolaire. Des réseaux formés d'aimants carrés ayant 300 nm de côté ont été réalisés par lithographie électronique, à partir d'une couche épitaxiée de Fer possédant une anisotropie quadratique. A température ambiante, ces plots possèdent une configuration magnétique monodomaine pouvant prendre 4 directions équivalentes, comme recherché pour le modèle de Potts dipolaire à 4 états. Un passage à 350°C (inférieure à la température de Curie) sous champ nul permet d'activer thermiquement la réorientation des spins afin qu'ils se rapprochent de l'état fondamental de l'assemblée de spins. Les configurations magnétiques observées après recuit, à l'aide d'un microscope à force magnétique, montrent l'importance du couplage dipolaire sur les états obtenus, ainsi que l'influence de l'angle entre les spins et l'axe du réseau. Les différentes configurations prédites théoriquement sont bien observées.

Mots-clés : spin artificiel, interaction dipolaire, modèle de Potts.

Towards a new artificial spin system: the dipolar 4-state Potts model

Since the proposal in 2006 to use nanomagnets patterned by top-down techniques to mimic "artificial spins", the studies of artificial spin systems has attracted wide interest. As a matter of facts, the possibility to design "upon request" arbitrary network and the possibility to determine completely the "spin" configuration with magnetic imaging offer a wide playground for statistical physics. Up to now only Ising spin systems, multi axes with planar magnetization (on square or Kagome lattice) or more recently, single axis with perpendicular anisotropy, have been studied. However, beyond Ising spins, statistical physics and condensed matter physics have shown the interest of other spin models like q -state Potts models. In this thesis, we introduce the dipolar 4-state Potts model. It is shown that on a square lattice, depending on the angle between spins and lattice, the system present very different properties like antiferromagnetic order, spin ice state (2 in-2 out ice rule) and even dipolar ferromagnetism. This model has been realized experimentally. 300 nm square magnets are patterned from a 2 nm thick Fe layer with cubic anisotropy. At room temperature, the magnets present a uniform state with 4 equivalent directions. Upon heating at 350 °C the magnets switch from one direction to another. It is therefore possible to simply drive the system toward its ground state. The magnetic configurations determined by magnetic force microscopy reveals the importance of the dipolar coupling as the different expected ground states (antiferromagnetic, spin ice and ferromagnetic) are indeed observed. It is noticeable that these very different properties are obtained with the same "spins" (magnetic elements) and same lattice.

Key words : artificial spin, dipolar interaction, Potts model.